Laboratory-Scale Analysis of Energy-Efficient Froth Flotation Rotor Design

Christopher Aaron Noble

Thesis submitted to the Faculty of the
Virginia Polytechnic Institute and State University
in partial fulfillment of the requirements for the degree of

Master of Science
in
Mining and Minerals Engineering

Gerald H. Luttrell, Chair
Roe-Hoan Yoon, Co-Chair
Gregory T. Adel

October 5, 2012
Blacksburg, Virginia

Keywords: Froth Flotation, Flotation Machines, Rotor Design, Power Consumption

Laboratory-Scale Analysis of Energy-Efficient Froth Flotation Rotor Design

Christopher Aaron Noble

(ABSTRACT)

Froth Flotation is an industrial separation process commonly used in the primary enrichment of run-of-mine mineral material. Over the past 100 years, much of the process's development has come from empirical evolution, rather than fundamental understanding. While many of the governing sub-processes are still poorly understood, the primary influential factors lie within the chemical, equipment, and operational variables unique to each flotation system. This investigation focuses on the phenomenological investigation of the equipment variables, particularly the rotor design, at the laboratory scale.

During this study, several small-scale flotation systems were developed, including various rotor and stator designs, tank sizes, and flow conditions. Experimental techniques were also developed to identify operational performance in four criteria: power consumption, gas dispersion, operational robustness, and flotation kinetics. Evaluation of the various rotors was conducted in two campaigns: (1) an exploratory campaign which featured 14 rotors in limited operational conditions (2) a detailed campaign which featured three rotors in an exhaustive set of conditions.

The results show that different rotors exhibited varying degrees of performance when judged by the aforementioned performance criteria. In general, excessive fluid pumping leads to an increase range of stable operation at the expense of greater power consumption. However, this increased power consumption does not necessarily correspond to increased flotation performance, as the data generally confirms the linearly proportional relationship of flotation rate and bubble surface area flux. Consequently, enhanced flotation kinetics can be achieved by rotors which disperse high rates of gas while retaining a small bubble size.

This work received financial support from FLSmidth Minerals.

Acknowledgments

The preparation of this thesis has been a rewarding undertaking. I would like to first thank the LORD for the many blessings I have experienced.

I cannot understate the role of my research advisor Dr. Gerald Luttrell in motivating me to compile this document. He has been a constant friend and mentor throughout this time. Additionally, I owe my original interest in flotation to Dr. Roe-Hoan Yoon. His unquenchable thirst for understanding is both a silent and, at times, vocal motivator for continued success. My final committee member, Dr. Greg Adel, has been a constant source of solidarity and direction.

I also express considerable gratitude to FLSmidth for the genesis and continued funding of this project. I also cannot understate the help and knowledge I have received from individuals at this company. Asa Weber, Don Foreman, Ronney Silva as well as many other have constantly challenged me to be pragmatic and creative in my research methods.

Many other current and former graduate students have assisted with this project. My colleague, Dr. Sanja Miskovic, was instrumental in the initial design of this project. I would like to thank her for the long hours and heated discussions we shared concerning the initial direction of this project. Also, I thank Michael Kiser and Erich Dohm for their assistance in the lab.

I want to thank my family and close friends for their love and support during this process. Finally, I thank my 여자 친구 Alice Lee (이 현아) for being a constant source of joy and hope.

Contents

List of Figures

List of Tables

List of Abbreviations

d_b	Bubble size
h_g	Height of air holdup
h_t	Total tank height
J_g	Superficial gas velocity
k	Flotation rate constant
t	Flotation time
D	Rotor diameter
DDA	Dodecylamine
F	Fraction of material in class
Fr	Froude number
MIBC	Methyl isobutyl carbinol
N	Rotational speed
N	Number concentration
N_A	Aeration number
P	Flotation probability, (i.e. $k = P_{Sb}$)
P	Power
P_{gassed}	Power draw under gassed condition
P_N	Power number/dimensionless power
$P_{ungassed}$	Power draw in the absence of gas
Pe	Peclet Number
PPG	Polypropylene glycol
Q	Volumetric gas flow rate
R	Recovery
R_f	Froth recovery
R_p	Pulp recovery
Re	Reynolds number
RT	Round tank

S_b	Bubble surface area flux: $6J_g/d_{32}$
t	Flotation rime
T	Torque
V_d	Displaced volume (air holdup)
V_t	Total volume
We	Weber number
ε	Global air hold-up
θ	Contact angle
μ	Fluid viscosity
ρ	Density
τ	Residence time

Chapter 1

Introduction & Background

1.1 Preface

Froth flotation is a chemio-physical separation process commonly used to enrich mining products. Run-of-mine material usually consists of one or more valuable components, designated as ore minerals, mixed with a significant portion of waste components, designated gangue minerals. Initial processing of the run-of-mine material seeks to physically separate these components, so that the valuable minerals may be retained for further processing, while the gangue may be properly disposed. Froth flotation is a common unit operation which separates constituents based on differences in surface wettability. Since nearly all minerals exhibit some distinction in surface characteristics, froth flotation can, in theory, selectively separate any mixture of liberated particles. This theoretical anticipation is pragmatically corroborated in the diversity and magnitude of mineral separation circuits that incorporate flotation operations. Froth flotation is commonly found in separation plants that process copper, lead, zinc, tin, gold, silver, iron ore, silica, molybdenum, platinum group elements, rare earth elements, phosphates, fluorite clays, and fine coal (Wills & Napier-Munn, 2006). Outside of the minerals industry, flotation has witnessed recent alternative uses in waste water treatment (Wang, Fahey, & Wu, 2005), algae harvesting (Phoochinda, White, & Briscoe, 2004; Lynch, Watt, Finch, & Harbort, 2007), and paper recycling (Bloom & Heindel, 1997; Kemper, 1999; Gomez, Watson, & Finch, 1995).

The modern froth flotation process or the chemically-aided separation of minerals via air bubbles was originally patented in 1905 (Sulman, Picard, & Ballot, 1905). This technique was not the first to exploit contrasts in surface properties; however, earlier attempts proved

prohibitively expensive and useful in only a few applications (Lynch et al., 2007; D. Fuerstenau, 2007). Most prominently, the Bessel brothers of Germany developed processes to clean graphite by adding oil to the slurry run-of-mine slurry and generating air bubbles by boiling (Bessel, 1877). A later patent described the use of CO_2 bubbles generated by the reaction of lime rather than air bubbles (Bessel, 1886). Nevertheless, by 1905, most base-metals and porphyry copper deposits were processed via simple gravity separation. The poor separation performance and the ever-increasing ore complexity lead to substantial milling deficiencies and lost revenue (Lynch et al., 2007). A large capacity, highly selective industrial process was needed to ensure the survival of the world-wide base metal industry.

Given its inherent strengths, the froth flotation process fulfilled this role and quickly grew to one of the most crucial metallurgical processes. With the development of selective reagents by the 1930s, processing plants were beginning to use froth flotation as the sole separation process (Wills & Atkinson, 1991). Since then, the froth flotation process has become in itself an interdisciplinary art and science, with pragmatic and fundamental research efforts addressing chemistry, equipment, mathematical modeling, applied mineralogy, economics, and separation metallurgy. Given its prominence in the economic production of base metals, several authors have defended the froth flotation process as one of the most significant technological innovations of the 20th century (Klassen & Mokrousov, 1963; Napier-Munn, 1997; M. Fuerstenau, 1999; Lynch et al., 2007). Despite the apparent industrial success of froth flotation, many aspects of the process are not well understood. Even today, much of the development is driven by evolutionary adaptation driven from empirical success rather than revolutionary innovation driven from fundamental insight.

1.2 Literature Review

1.2.1 Fundamentals of Flotation

Froth flotation is a physical separation process founded on select principles of applied surface chemistry, namely surface wettability. As a result of unique chemical structures and characteristics, every surface in nature exhibits a definable degree of surface wettability. Wettable surfaces, labeled hydrophilic, exhibit strong intermolecular cohesive forces between water and the material at the interface. From the macroscopic viewpoint, this property is characterized by water droplets naturally spreading across the surface, attempting to maximize the interfacial area. Contrastingly, non-wettable surfaces, labeled hydrophobic, exhibit weak cohesive forces, and potentially disjoining forces at the interface (Wills & Napier-

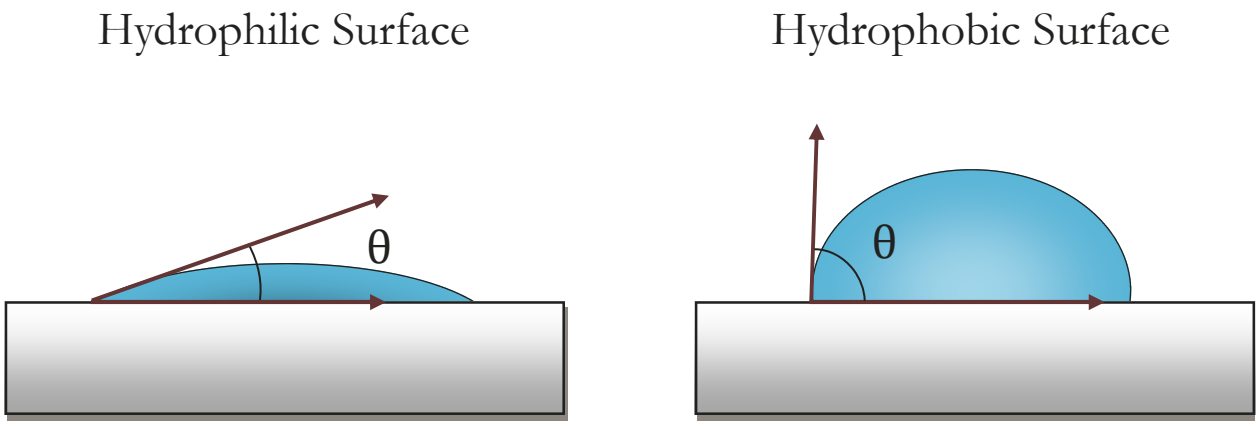

Figure 1.1: Depiction of hydrophobic and hydrophilic surface. θ = contact angle.

Munn, 2006; Berg, 2009; Pan, Jung, & Yoon, 2011). This property is characterized by water droplets beading up at the surface, attempting to minimize the interfacial area. The degree of wettability is described by the *contact angle* (θ). The contact angle measures the physical angle formed when a liquid droplet rests on a solid surface. The angle is measured between the solid and gaseous phases, through the liquid phase. Large contact angles indicate greater degrees of hydrophobicity. Figure 1.1 depicts the contact angles of a hydrophilic surface and hydrophobic surface.

Froth flotation uniquely exploits these contrasts in surface wettability. In a typical operation, a mixture of gangue and mineral components are suspended in water as a slurry and introduced into a stirred vessel. Concurrently, air is sparged into the vessel, creating a highly turbulent, three phase environment of air, water, and solid particles. This environment produces collisions between the particles and the air. Particles that have been rendered hydrophobic will selectively attach to the air bubbles (in an attempt to minimize interfacial solid-liquid area), while the hydrophilic particles will remain suspended in the water. The attachment of air bubbles to the hydrophobic particles causes a reduction in the apparent density of the bubble-particle aggregates. Eventually the aggregates will attain positive buoyancy and float to the top of the vessel. The rapid accumulation of the bubble-particle aggregates at the vessel's surface generates a mineralized foam, or *froth*. This froth is removed (either by mechanical or natural flow mechanisms) producing a mineral rich concentrate. At the bottom of the vessel, the processed slurry is removed, producing a gangue-rich tailings. In industrial practice, this process is carried out in a continuous-flow state, with constant feed addition, and continual concentrate and tailings removal.

In addition to concentrate recovery as a result of bubble-particle attachment (aka *true flotation*), recovery also occurs by a secondary, non-selective process known as *entrainment* (King, 2001; Wills & Napier-Munn, 2006). Fundamentally, entrainment occurs as fine particles (both valuable and gangue material) are carried into the froth with water. The degree of entrainment has been shown to strongly correlate with the particle size and the volume of water recovered, with finer particles and higher water flow rates correlating to increased entrainment. Other factors, such as the froth structure, particle shape, and froth residence time, also influence entrainment; however, these factors are less prominent. In practice, entrainment is perceived as a necessary deficiency that is to be minimized if possible (Vianna, 2011).

Other authors have also described a third, also non-selective, recovery mechanism, known as *entrapment* (Gaudin, 1957; Wills & Napier-Munn, 2006; Vianna, 2011). Here, particles are physically retained in the froth phase between valuable particles which are attached to bubbles. Few authors comment on the portion of material recovered by this mechanism, and few mathematical models explicitly include it.

1.2.2 Factors Influencing Flotation Performance

Macroscopically, flotation performance is controlled by many factors, which are broadly classified in three categories: chemical, equipment, and operational (Klimpel, Hansen, & Fee, 1986; Gorain, 2007). Chemical factors encompass variables pertaining to the solution chemistry unique to each flotation system. The reagents used in flotation fall into several distinct categories: collectors, frothers, pH modifiers, depressants, and activators.

While some minerals are naturally hydrophobic, most flotation systems can benefit from carefully controlled chemical addition. Collectors are chemicals which enhance the hydrophobicity of hydrophilic or mildly hydrophobic mineral surfaces. These chemicals are usually organic molecules which commonly fall into the chemical families of monothiophosphates, dithiophosphates, xanthates, and others (Wills & Napier-Munn, 2006). Collectors are usually classified by the type of ion (anion or cation) which provides the hydrophobicity, and the degree of hydrophobicity is strongly related to the length of the hydrocarbon chain (Bulatovic, 2007). Aside from cost purposes, collectors are usually dosed in low concentrations, though typically sufficient to produce a monolayer on the surface. Additionally collector addition usually decreases selectivity, as the collector absorbs onto unwanted minerals. Further addition may actually reduce the recovery of valuable minerals, as multilayers of collector form on the mineral surface (Wills & Napier-Munn, 2006).

Since mineral surface chemistry and consequently, collector absorption is strongly dependent on pH, acid or base modifiers are used to maintain desired levels of acidity/alkalinity. Fundamentally, most minerals retain a positive surface charge in acidic conditions and a negative charge in alkaline conditions. Furthermore, many minerals have a unique iso-electric pH. Through pH control and appropriate collector selection, selective separation of many simple mineral systems is possible. Typically, price and availability determine the selection of a modifier; lime is a fairly common choice.

Activators and depressants are other reagents which respectively promote or inhibit the flotation of select minerals by altering the degree of collector absorption. These chemicals are common in sulfide flotation which usually involves selective flotation of several valuable components.

Frothers are usually long chain surfactants which absorb to the air water interface. These reagents reduce the air-water interfacial tension in order to promote smaller bubble sizes and froth stability (Bulatovic, 2007). As many flotation models indicate, reduced bubble size enhances flotation performance (Yoon & Luttrell, 1989; Gorain, Franzidis, & Manlapig, 1995a). The reduced interfacial tension resulting from surfactant absorption mitigates bubble coalescence and allows the generation of a froth phase. Up to a designated concentration, increased frother addition will enhance the effects (i.e. continued bubble size reduction). However, once all the available interfacial area is saturated with surfactant, increased frother addition will not result in increased performance. High frother dosages may produce highly stable or metastable froth, which can adversely affect handling and downstream processing.

In addition to the reagent type and dosage, other chemical factors which influence flotation performance include process water quality, solution temperature, and reagent conditioning time. In general, the chemical condition of the flotation system has a pronounced effect on the attainable separation performance of a flotation unit. Consequently, chemical variables become more crucial as more complex separations are desired.

Equipment factors include the details of the flotation cell and the separation circuit design. Many researchers have indicated that the hydrodynamic environment of the flotation cell strongly influences the rate at which material floats (Luttrell & Yoon, 1991, 1992). Consequently, the cell geometry, size, sparging mechanism, and power input all contribute to overall flotation performance. Since this thesis is explicitly focused on specific details of flotation machine design, these factors have been researched separately (Section 1.2.4) to accommodate a more thorough analysis.

Operational factors include details of the flotation system which are unique to the daily

operation of each plant. These factors are generally associated with variable characteristics of the ore, such as particle size, feed grade, and degree of feed oxidation. Additionally, operational factors may include those which are to the discretion of the plant operator, such as feed flow rate, residence time, and pulp density. In general, operational factors provide interdependent and complex influences on the flotation performance. In example, the feed particle size has a dramatic influence on the flotation efficiency. The classic curve shows a substantial drop off in recovery for particles generally less than 20 microns and greater than 200 microns (Jowett, 1980), with the larger size limit being a function of particle density (Jameson, Nguyen, & Ata, 2007). In general, smaller particles lack the inertia necessary to penetrate the liquid film surrounding the bubble, while larger, heavier particles are more susceptible to detachment and froth drop back (Mao & Yoon, 1997; Sherrell, 2004; Do, 2010). Furthermore, the nature of the particle distribution (such as the presence or absence of fine particles) may have a marked influence on froth stability and thus recovery of material from the froth.

1.2.3 Modeling Approaches

Given the multitude of contributing factors, comprehensive and purely theoretical flotation models are still immature. Instead, empirical and partially phenomenological models have been well vetted and used extensively for many simulation purposes. From a microscopic perspective, the complex mechanics of froth flotation may be described by several transport mechanisms. The most recent studies include the rate of pulp to froth transport by bubble attachment, the rate of material drop back from the froth, the rate of water drainage from the froth, and/or the rate of entrainment. Most modeling approaches attempt to quantify the specific rates and interaction of these mechanisms.

Most simply, many researchers have empirically witnessed the kinetic behavior of bulk flotation recovery as a function of time. This evidence has prompted many to model flotation as a first-order rate process analogous to a chemical reaction (Sutherland, 1948; Tomlinson & Fleming, 1965; Fichera & Chudacek, 1992). Other order rate models have been postulated, but few have gained as much widespread applicability as the first-order model. The first-order rate model defines a constant proportionality between the depletion of mineral particles (dN/dt) and the number of particle in the system (N):

$$dN/dt = kN \tag{1.1}$$

where k is a proportionality or *rate* constant.

From the first-order assumption, Equation 1.1 may be solved at various boundary condition to determine the recovery (R) as a function of flotation time (t) or *retention* time (τ) for both a plug-flow reactor (Equation 1.2) and a perfectly-mixed reactor (Equation 1.3) (Levenspiel, 1998). These equations have been used to model the flotation process in scaling from a laboratory to an industrial flotation unit:

$$R = 1 - e^{-kt} \tag{1.2}$$

$$R = \frac{k\tau}{1 + k\tau}. \tag{1.3}$$

Several modifications to these models have been proposed to incorporate a theoretical maximum recovery and a flotation delay time (Dowling, Klimpel, & Aplan, 1985; Gorain, Franzidis, Manlapig, Ward, & Johnson, 2000; Sripriya, Rao, & Choudhury, 2003) . Additionally, some researchers have suggested that industrial cells (especially column cells) substantially deviate from the perfectly-mixed assumption (Dobby & Finch, 1988; Luttrell & Yoon, 1991). Coinciding with the aforementioned chemical reaction analogy, an expression for recovery is proposed which incorporates the degree of axial mixing, via the Peclet Number (Pe) (Levenspiel, 1998):

$$R = 1 - \frac{4A \exp(Pe/2)}{(1+A)^2 \exp[(A/2)Pe] - (1-A)^2 exp[(-A/2)Pe]}$$

$$A = \sqrt{1 + 4k\tau/Pe}.$$

While the general rate-based approach to flotation modeling has substantial empirical justification, researchers and practitioners have realized that not all particles of a given mineral in a flotation system exhibit the same kinetics. This observation has led to the development of distributed parameter rate models (Fichera & Chudacek, 1992). Various researchers have identified properties to justify the distribution, with one of the more prevalent parameters being particle size. Gaudin, Schuhmann Jr, and Schlechten (1942) first experimentally measured the dependence of flotation rate on particle size, noting the substantial degradation in flotation rate for large particles. This observation was later given a more thorough theoretical consideration which investigated the streamline hydrodynamics for given bubble and particle sizes (Sutherland, 1948).

A more general approach to model parameterization was conducted by Imaizumi and Inoue (1965). This modeling approach considers distributed floatability classes which lump together the combined effects of particle size, shape, and other surface properties. Most

contemporary flotation models include distributed flotation classes, often in the form of a double distributed model which includes size and flotability (Fichera & Chudacek, 1992).

Further attempts to add fundamental insight to the empirical first-order observation have led many to propose analytical expressions for the flotation rate constant. These expressions generally suggest a strong dependence of gas dispersion on the flotation rate. One such model suggests that the rate constant is proportional to the bubble surface area flux (S_b) and a generic probability or collection efficiency term (P) (Jameson, Nam, & Young, 1977; Yoon & Mao, 1996; Gorain, Franzidis, & Manlapig, 1997; Gorain, Napier-Munn, Franzidis, & Manlapig, 1998):

$$k = 0.25PS_b.$$

Here, S_b is a derived term which defines the degree of aeration present in the cell (Finch & Dobby, 1990; Gorain et al., 1997; Gorain, Napier-Munn, et al., 1998). S_b balances the superficial gas velocity (J_g) and the mean bubble size (d_b):

$$S_b = \frac{6J_g}{d_b}.$$

This model has been very successful at normalizing flotation performance when the gas dispersion variables are known. The linear $k-S_b$ relationship has been experimentally verified for various minerals and at various scales (Gorain, Napier-Munn, et al., 1998; Hernandez-Aguilar, Rao, & Finch, 2005). The overall acceptance in this model has several comprehensive studies in characterizing and quantifying gas dispersion in flotation cells (Finch, Xiao, Hardie, & Gomez, 2000; Tavera, Escudero, & Finch, 2001; Kracht, Vallebuona, & Casali, 2005; Schwarz & Alexander, 2006; Miskovic, 2011).

Other models have proposed a purely theoretical expression for k, based on surface chemistry and hydrodynamic variables (Luttrell & Yoon, 1992, 1991; Mao & Yoon, 1997; Sherrell, 2004; Do, 2010). These models were originally applicable for predicting rate constants under quiescent conditions, such as in column cells. More recently, the fundamental models have addressed the turbulent hydrodynamic conditions found in conventional cells. Additionally, these models have added fundamental or semi-empirical models to describe material drop back and fluid drainage from the froth. All of these fundamental models are based on a compartment model which independently defines the flotation rate constant as a combination of probabilities of collision (P_c), attachment(P_a), and detachment (P_d):

$$k = PS_b = (P_cP_a(1 - P_d))S_b$$

In these models, the probability terms have been analytically defined using fundamental hydrodynamic variables (such as turbulent kinetic energy) and surface energies calculated

from the Van Der Waals, electrostatic, and hydrophobic force components. The extended DLVO theory was invoked to define the composite interaction of these forces (Yoon & Wang, 2007; Kelley, Noble, Luttrell, & Yoon, 2012). Ultimately these models will predict flotation performance as a function of intensive mineral properties and machine characteristics which are either well known or do not change with scale (Kelley et al., 2012).

In addition to the aggregate recovery models, other recent studies have focused on the inclusions of other transport mechanisms, such as froth recovery and entrainment. Such models consider flotation to be a two stage process, modeling the pulp and the froth as independent reactors. Most of the pure pulp recovery models invoke analytical forms similar to the rate models presented above with some empirical correction to negate the ever-present froth effects (Gorain, Harris, Franzidis, & Manlapig, 1998; Vera et al., 2002).

Similar to pulp recovery, froth drop back has been identified as a rate process which can be modeled as a plug-flow reactor considering the interaction of a rate constant and residence time (Equation 1.2) (Gorain, Harris, et al., 1998). When the independent froth (R_f) and pulp (R_p) recoveries are known, the overall recovery may be calculated by (Finch & Dobby, 1990):

$$R = \frac{R_f R_p}{1 - (1 - R_f)R_p}.$$

Since the identification of the two compartment flotation modeling approach and the kinetics of froth drop back, researchers have attempted to gain further fundamental understanding, especially with regard to froth residence time (Vera et al., 2002). Most simply, froth residence time can be determined by dividing the froth height by the superficial gas rate for the cell ($\tau_f = h/J_g$) ((Mathe, Harris, O'Connor, & Franzidis, 1998). Since this calculation does not accommodate for different cell geometries and froth travel distances, many have proposed revisions to the initial calculation, while retaining the kinetic plug-flow model. Gorain, Harris, et al. (1998) suggest the inclusion of the distance from the center of the flotation cell to the launder, while Lynch, Johnson, Manlapig, and Thorne (1981) base the calculation on the volumetric slurry flow through the froth.

1.2.4 Flotation Equipment

Equipment variables which influence flotation performance include many aspects of the flotation cell design including: the type of cell, the cell dimensions, the cell geometry, the rotor and stator design, various clearances and rotor dimensions, rotor speed, specific power input, state of air dispersion, the froth removal mechanism, and the circuit design.

Modern flotation machines are most generally classified into two types: conventional cells and column cells. Conventional cells are mechanical agitated vessels which are aerated by air introduction in the rotor region. Such aeration may occur due to the natural pressure difference created by the rotor (self-aspirated or sub-aeration designation) or by the supplementary action of a blower (forced-air designation). Column flotation cells are generally not mechanically agitated vessels, exhibiting high aspect ratios in the vertical direction. Rather than attempting to suspend slurry in the cell, new slurry is introduced near the top of the vessel and flows downward to the tailings discharge located at the vessel's bottom. Air is typically sparged at the bottom of the vessel and travels upward to the froth phase. This counter-current flow of slurry and air propagates bubble particle collisions. Additionally, column cells are generally characterized by deep froths and the inclusion of froth washing. In this action, fresh water is sprayed onto the top of the froth in an effort to reduce the entrainment of unattached gangue particles traveling with the water in the froth phase (Wills & Napier-Munn, 2006; Finch, Cilliers, & Yianatos, 2007). Figure 1.2 compares conventional and column cell designs.

The most prevalent manufacturers of flotation technology today include the major mineral processing providers, FLsmidth, Outotec, and Metso (Peaker, 2007; Weber & Tracyzk, 2007; Oravainen & Allenius, 2007). Each manufacturer features several unique machine designs applicable for a variety of mineral industries. Across all manufacturers, the size of flotation cells has grown exponentially since the 1960s. Figure 1.3 shows the increase of the average flotation cell size reported in literature over the past century. As shown, common sizes for industrial units today span up to 600 cubic meters, with the trends favoring larger units in attempt to capitalize on economy of scale. According to the exponential fit of the data, the size of large flotation cells doubles every 8.9 years.

Given the rapid increase in flotation cell size, one of the most challenging aspects of machine design is scale-up from the laboratory and pilot-plant sizes to the industrial sizes. Traditionally, process scale-up has been driven by operator experience and empirical "scaling" factors (Tatterson, 1991, 1994). By the 1960s, dimensionless numbers and simple chemical reactor analysis replaced purely heuristic scaling parameters. Table 1.1 lists several dimensionless numbers commonly used in flotation scale-up.

While these criteria were able to appropriately scale solid suspension and mechanical agitation, they proved only marginally effective for predicting scaled metallurgical performance since they do not account for crucial parameters, such as bubble size (Gorain, 2007). Currently, additional hydrodynamic expressions (Table 1.2), along with the common dimensionless numbers are used in flotation scale-up (Weber & Tracyzk, 2007). Furthermore,

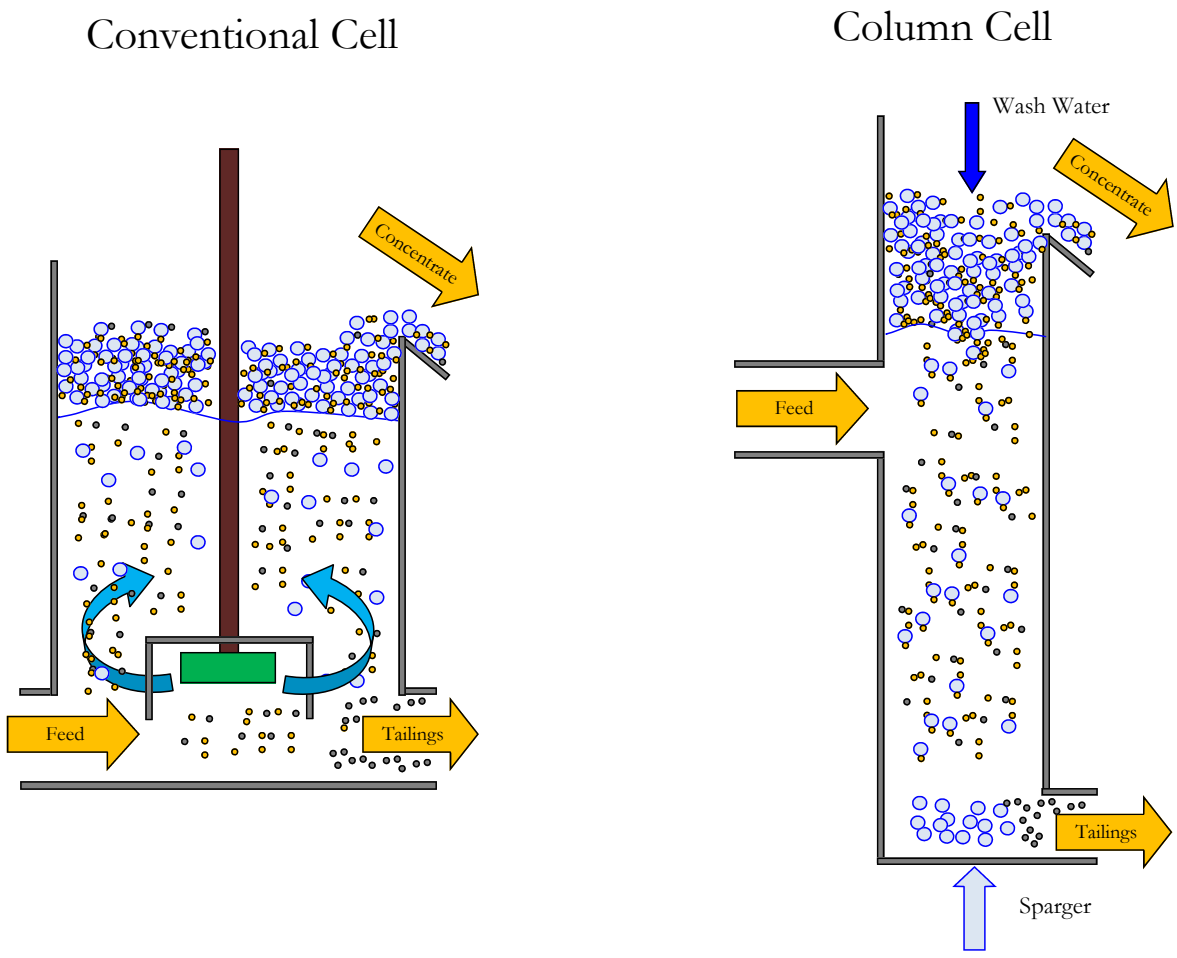

Figure 1.2: Comparison of conventional and column cell design.

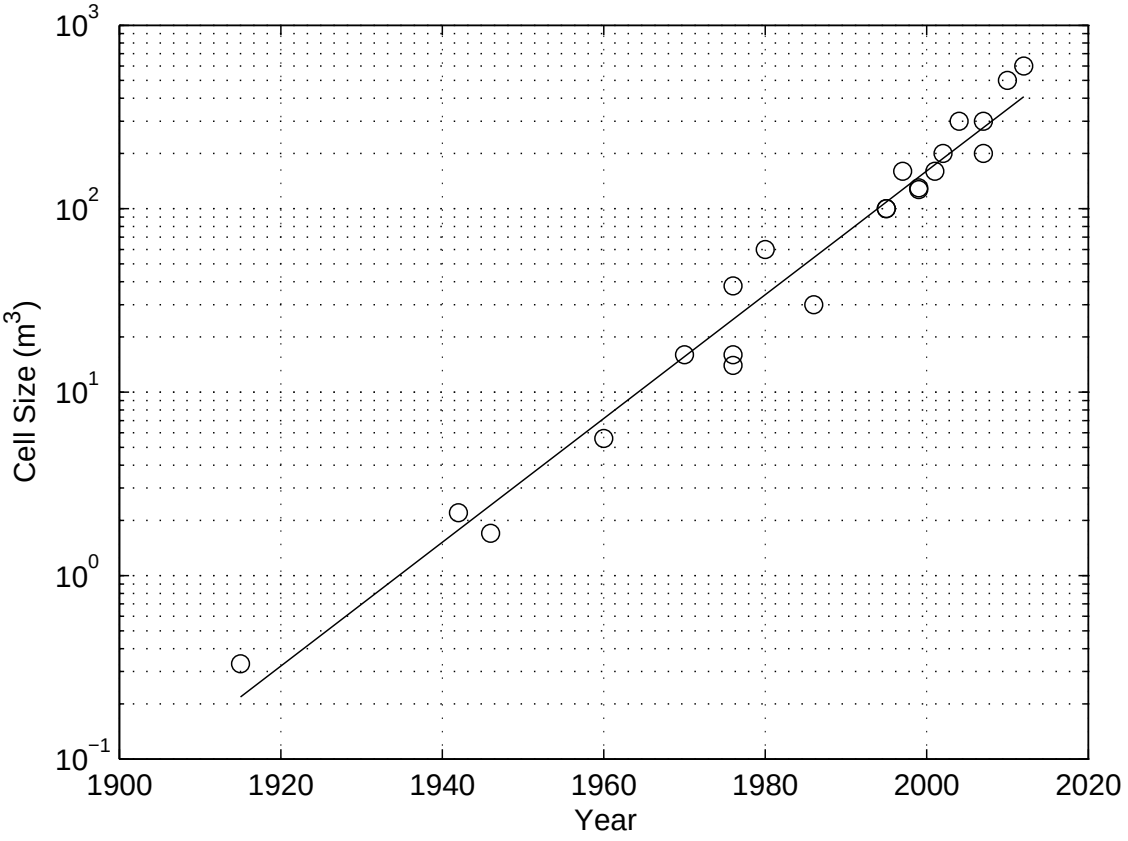

Figure 1.3: Size of large flotation cell sizes reported in literature since 1917. Data after (Taggart et al., 1945; Hanna et al., 1976; Weber et al., 1999; Meenan, 1999; Lynch et al., 2007; Gorain, 2007; Weber & Tracyzk, 2007; Oravainen & Allenius, 2007).

Table 1.1: Common Dimensionless Numbers Used in Flotation Scale-up, after (Gorain, 2007; Young et al., 2010).

Name	**Expression**	**Description**	**Range**
Reynolds Number, Re	$\frac{\rho N D^2}{\mu}$	Ratio of inertial force to viscous force	$(1-7)\cdot 10^6$
Froude Number, Fr	$\frac{DN^2}{g}$	Ratio of inertial force to gravitational force	$0.5-5$
Power Number, P_N	$\frac{P}{\rho N^3 D^5}$	Ratio of resistance force to inertial force	$0.5-5$
Aeration Number, N_A	$\frac{Q_a}{ND^3}$	Ratio of gas flow to pumping capacity	$0.01-0.2$
Weber Number, We	$\frac{\rho N^2 D^3}{\sigma}$	Ratio of inertial force to surface tension force	

Legend: ρ = fluid density, N = rotor's rotational speed, D = rotor diameter, μ = fluid viscosity, g = gravitational acceleration, P = power input, Q_a = airflow rate, and σ = surface tension

the use of sophisticated analytical tools, such as discreet element method (DEM) modeling and computational fluid dynamics (CFD) has become increasingly prevalent (Oravainen & Allenius, 2007; Weber & Tracyzk, 2007).

With much of the machine's influence being strongly tied to hydrodynamics and gas dispersion, several studies have attempted to standardize the measurement of various gas dispersion indices. The most widely utilized parameters include gas holdup (ε), superficial gas velocity (J_g), bubble size distribution (d_b), and bubble surface area flux (S_b). Since the mid-1990s and early 2000s, several analytical instruments have been developed to quantify these parameters. Schwarz and Alexander (2006) present the details of a gas dispersion database which includes measurements of these parameters collected over 10 years in over 800 industrial flotation cells of various sizes and in various mineral industries.

Gomez and Finch (2007) provide a comprehensive review of three instruments developed at McGill University over the previous ten years. The gas velocity sensor utilizes an inverted, closed cylinder which is immersed in the pulp. As gas builds in the cylinder, the pressure increased is measured and used to calculate the flow of gas entering the chamber. The air holdup sensor features two cylinders, which are immersed in the flotation cell. The first, open cylinder, allows to flow normally, while the second cylinder has a closed bottom and contains

Table 1.2: Select Hydrodynamic Parameters Used in Flotation Cell design, after (Weber & Tracyzk, 2007)

Name	**Expression**	**Description**
Specific airflow	Q_a/V	Airflow–cell volume
Circulation intensity	Q_r/V	Pulp circulation–cell volume
Liquid rise velocity	Q_r/A_{dt}	Pulp circulation–draft tube area
Power Intensity	P/V	Absorbed power–cell volume
Bubble Surface Area Flux	$6J_g/d_b$	Airflow rate–bubble size

Legend: Q_a = airflow rate, Q = cell volume, Q_r = liquid recirculation rate,A_{dt} = draft tube area P = power input, J_g = superficial gas velocity, d_b = mean bubble size

un-aerated pulp. By measuring the conductivity difference between the two cylinders, the amount of air in the open cylinder may be calculated. Finally, the bubble size measurement technique is based on ex-situ sampling, image capturing, and image processing. A bubble viewing chamber is positioned above the cell, and a capillary tube extends below the chamber into the flotation pulp. Bubbles in the flotation cell rise through the tube, into the chamber, where they contact an inclined plane. This plane disperses the bubbles into a single depth plane, and a video camera is used to capture images of the bubbles in the viewing chamber. These images are later analyzed to determine the full bubble size distribution (Gomez & Finch, 2007). This current method was shown to provide greater consistency and analytical ease than earlier iterations (Chen, Gomez, & Finch, 2001) and earlier direct measurement techniques developed at the University of Cape Town (Tucker, Deglon, Franzidis, Harris, & O'Connor, 1994).

Miskovic (2011) and Miskovic and Luttrell (2012) critically reviewed the ex-situ bubble sizing technique and proposed a new technique based on in-situ bubble size measurements and an alternate image processing approach. These tests included pilot-plant and industrial scale machines. Other authors have attempted to derive correlations which predict bubble size and S_b as a function of impeller speed (Girgin, Do, Gomez, & Finch, 2006), from gas

holdup information (Finch et al., 2000), from various operational parameters and fitting constants (Gorain, Franzidis, & Manlapig, 1999), from drift flux analysis (Banisi & Finch, 1994), and from artificial neural networking (Massinaei & Doostmohammadi, 2010).

In a conventional cell, the rotor is the predominant source of power for the entire flotation system. This power provides the necessary energy for a number of flotation subprocesses including: air dispersion, solid suspension, micro-turbulence generation, and bubble-particle collision. A series of comprehensive experimental studies analyzed and compared several industrial rotors with respect to various gas dispersion variables (Gorain et al., 1995a; Gorain, Franzidis, & Manlapig, 1995b, 1996; Gorain et al., 1997; Gorain, Napier-Munn, et al., 1998). Each of these papers individually studied the effects of specific various gas dispersion variables, including bubble size distribution, gas holdup, and superficial gas velocity. Comparisons between the various rotor types included in the study were made with respect to overall flotation performance. Most of the studies included tests of the Chile-X, Pipsa, Outokumpu, and Dorr-Oliver rotors over a wide range of impeller speeds and gas velocities.

Given the date of the rotor studies, the authors chose to implement the U.C.T bubble size analyzer which was the best available method at the time (Tucker et al., 1994). In the end, the authors concluded that individual gas dispersion variables do not universally correlate well to flotation performance; however, the derived bubble surface area flux (S_b) parameter showed a consistent linear relationship with the measured flotation rate constant at a given froth depth (Figure 1.4). The latter of these studies and later studies by the same authors showed that froth depth has a non-linear effect on flotation performance (Gorain, Napier-Munn, et al., 1998; Gorain, Harris, et al., 1998). With regard to rotor design, though, the authors showed that within practical reason all of the tested rotors were able of producing the same flotation rate at a given S_b value. Unfortunately, these studies and no other studies on flotation rotors directly measure the power requirements of the rotor.

Nevertheless, outside of the froth flotation research, other studies have addressed power consumption and gas dispersion in stirred vessels. Dohi, Takahashi, Minekawa, and Kawase (2004) compared the solid suspension capabilities of three different impeller designs in aerated vessels. Here, the state of off-bottom solid suspension and ultimately homogeneous solid suspension were measured for both gassed and ungassed conditions. The authors developed an empirical correlation which relates the power required for suspension to the percent solids, the liquid density, the superficial gas velocity, the terminal settling velocity of the particles, and a proportionality constant unique for each rotor. Another study investigated the effects of solid concentration and particle size on power consumption in simple stirred vessels (Angst & Kraume, 2006). The authors used an endoscope to examine the concentration of particles

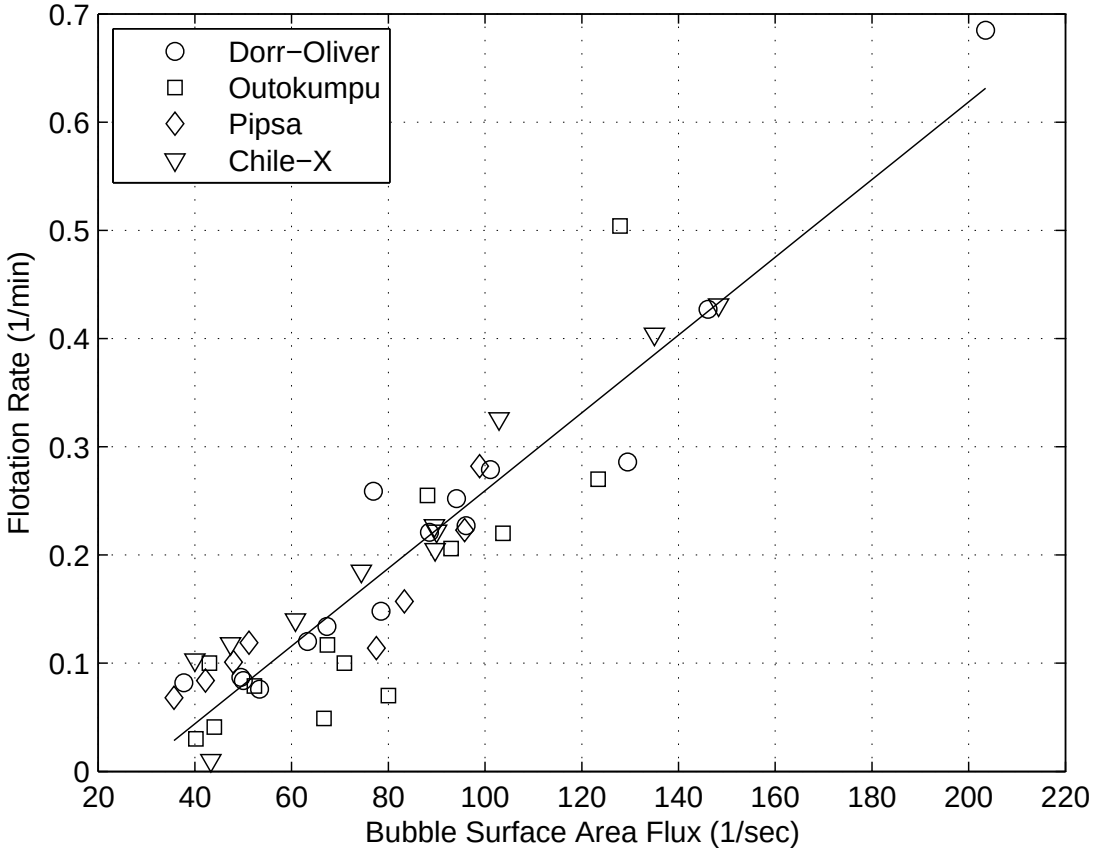

Figure 1.4: Flotation rate constant plotted against bubble surface area flux for various industrial rotors. Data after (Gorain et al., 1997).

at various locations in the tank, comparing the local solids concentration with the mean solids concentration of the vessel. This study was conducted for various tank sizes in the laboratory. The results show that the power required to suspend and homogenize the solids in the vessel can be strongly correlated to the particle volume fraction. In yet another study, the authors test several rotor designs and configurations in an attempt to maximize the gas holdup while minimizing power consumption (Arjunwadkar, Saravanan, Pandit, & Kulkarni, 1998). The authors tested several dual rotor combinations at various power inputs and gas velocities. The results show that different combinations are capable of drastically different results (maximum holdup values span from 3.0% to 7.5% at a given power input), with the most favorable rotor set-up being a disk-turbine - pitched blade turbine downward combination.

These results and other outside studies bring to light the lack of fundamental understanding and empirical investigations in power consumption relating to froth flotation rotor design. As other studies in other industries have shown, different rotor designs are capable of varying levels of energy-efficiency, depending upon the application. While solid suspension, solution homogeneity, and gas dispersion are significant in flotation, these factors do not necessarily directly correlate to metallurgical performance, as power input further affects a number of flotation subprocesses, such as attachment and detachment rates. A focused experimental study is needed to ascertain the role of power consumption on metallurgical performance and the variations solely dependent on rotor design.

1.3 Research Objectives and Overview

The singular goal of this research is to characterize and compare laboratory-scale flotation rotors in an attempt to provide future design criteria which can be used to develop energy-efficient rotors. This goal was approached in three stages: (1) methodology development and equipment design, (2) exploratory testing, and (3) detailed testing.

During the methodology development, equipment size limitations were imposed to restrict the breadth experimental options and appropriately scope the project within the laboratory-scale paradigms. As a result, the term, “laboratory-scale,” in this study refers to rotors measuring less than 3 inches in diameter and corresponding tank volumes up to 30 liters. Furthermore, the appropriate equipment and assessment criteria were established during this stage.

The exploratory experimental campaign prioritized the breadth of the analysis in terms

of rotors examined. During this phase, 14 rotors were assessed in a battery of tests. Due to the rapid and iterative development during this stage, not all prototype rotors were subjected to an identical test matrix. Some rotors were abandoned prior to prolonged tests, while others were developed after experimental procedures were refined. From the overall appraisal of this exploratory campaign, the field of prototype rotors was narrowed to the three designs possessing the best all-around performance.

These final three rotors were then subjected to the second, detailed testing campaign which alternatively prioritized analytical depth, data reproducibility, and error quantification. From the collaborative analysis of the two testing campaigns, future rotor design criteria was established.

In summary, the itemized objectives of this study were to:

- Design and construct equipment that can assess small-scale forced-air flotation rotors and prototypes;
- Develop a methodology to provide consistent and fair appraisal of different rotor designs at the laboratory scale;
- Assess the existence of variation in flotation performance as a function of the rotor design;
- Quantify the performance differences through detailed testing and analysis
- Provide empirically-based recommendations and criteria for flotation rotor design.

1.4 Document Organization

The body of this thesis is organized into five chapters, with the primary works presented individually as standalone papers describing a separate phase or objective of the work. The three main phases of the work (experimental development, exploratory testing, and detailed testing) constitute the three informative chapters, while an introductory and a concluding chapter complete the thesis. References are listed individually for each chapter.

Chapter 1 includes an overview of the flotation process, general background information, and a full description of the work completed as a part of this study.

Chapter 2 provides descriptions of the design, construction, and commissioning of the

laboratory-scale experimental equipment as well as descriptions of the experimental methodology developed during this research.

Chapter 3 describes the experimental results of the exploratory testing campaign. Both Chapters 3 and 4 are presented in parallel structure providing tabular and graphic results of investigations involving power consumption, gas dispersion, operational limits, and flotation performance. This study provides a cursory evaluation of 14 rotors, while highlighting the veracity of the experimental approach and the existence of unique distinctions between vastly different rotor designs.

Chapter 4 similarly provides results of the detailed testing campaign. This study seeks to quantify the actual performance differences between rotor designs by incorporating a more thorough experimental matrix and replicate testing. Consequently, only three rotors were selected from the original 14 for this study. The rotor selection was based on the best all-around performance measured in the original exploratory testing.

Chapter 5 includes a brief summary of all of the experimental studies, holistic conclusions derived from the studies, and recommendations for future or continued development.

1.5 Bibliography

Angst, R., & Kraume, M. (2006). Experimental investigations of stirred solid/liquid systems in three different scales: Particle distribution and power consumption. *Chemical Engineering Science*, *61*(9), 2864–2870.

Arjunwadkar, S., Saravanan, K., Pandit, A., & Kulkarni, P. (1998). Optimizing the impeller combination for maximum hold-up with minimum power consumption. *Biochemical engineering journal*, *1*(1), 25–30.

Banisi, S., & Finch, J. (1994). Technical note reconciliation of bubble size estimation methods using drift flux analysis. *Minerals Engineering*, *7*(12), 1555–1559.

Berg, J. (2009). *An introduction to interfaces & colloids: the bridge to nanoscience*. World Scientific Pub Co Inc.

Bessel, G. (1877). *Berlin patent 42.*

Bessel, G. (1886). *Berlin patent 39,369.*

Bloom, F., & Heindel, T. (1997). A theoretical model of flotation deinking efficiency. *Journal of colloid and interface science*, *190*(1), 182–197.

Bulatovic, S. (2007). *Handbook of flotation reagents: Chemistry, theory and practice: Flotation of sulfide ores* (Vol. 1). Elsevier Science.

Chen, F., Gomez, C., & Finch, J. (2001). Technical note bubble size measurement in flotation machines. *Minerals Engineering*, *14*(4), 427–432.

Do, H. (2010). *Development of a turbulent flotation model from first principles.* Unpublished doctoral dissertation.

Dobby, G., & Finch, J. (1988). Flotation column scale-up and modeling. *Can. Inst. Min. Metall. Bull.*, *79*(889), 89-96.

Dohi, N., Takahashi, T., Minekawa, K., & Kawase, Y. (2004). Power consumption and solid suspension performance of large-scale impellers in gas–liquid–solid three-phase stirred tank reactors. *Chemical Engineering Journal*, *97*(2), 103–114.

Dowling, E., Klimpel, R., & Aplan, F. (1985). Model discrimination in the flotation of a porphyry copper ore. *Minerals and Metallurgical Processing*, *2*(2), 87–101.

Fichera, M., & Chudacek, M. (1992). Batch cell flotation models–a review. *Minerals engineering*, *5*(1), 41–55.

Finch, J., Cilliers, J., & Yianatos, J. (2007). Column flotation. In M. Fuerstenau, J. G., & R. Yoon (Eds.), *Froth flotation a century of innovation* (pp. 681–737). SME.

Finch, J., & Dobby, G. (1990). *Column flotation* (Vol. 9). Pergamon Press Oxford.

Finch, J., Xiao, J., Hardie, C., & Gomez, C. (2000). Gas dispersion properties: bubble surface area flux and gas holdup. *Minerals Engineering*, *13*(4), 365–372.

Fuerstenau, D. (2007). A century of developments in the chemistry of flotation processing. In M. Fuerstenau, J. G., & R. Yoon (Eds.), *Froth flotation a century of innovation* (pp. 3–64). SME.

Fuerstenau, M. (1999). Froth flotation: The first ninety years. In B. Parekh & J. Miller (Eds.), *Advances in flotation technology.* SME.

Gaudin, A. (1957). *Flotation.* McGraw-Hill.

Gaudin, A., Schuhmann Jr, R., & Schlechten, A. (1942). Flotation kinetics. ii. the effect of size on the behavior of galena particles. *The Journal of Physical Chemistry*, *46*(8), 902–910.

Girgin, E., Do, S., Gomez, C., & Finch, J. (2006). Bubble size as a function of impeller speed in a self-aeration laboratory flotation cell. *Minerals Engineering*, *19*(2), 201–203.

Gomez, C., & Finch, J. (2007). Gas dispersion measurements in flotation cells. *International Journal of Mineral Processing*, *84*(1-4), 51–58.

Gomez, C., Watson, J., & Finch, J. (1995). Recycled-paper deinking using column flotation. In *The 3rd research forum on recycling* (pp. 41–44).

Gorain, B. (2007). Mechanical froth flotation cells, section i: Design, operating principles, and optimization of mechanical flotation cells. In M. Fuerstenau, J. G., & R. Yoon (Eds.), *Froth flotation a century of innovation* (pp. 637–656). SME.

Gorain, B., Franzidis, J., & Manlapig, E. (1995a). Studies on impeller type, impeller speed and air flow rate in an industrial scale flotation cell. part 1: Effect on bubble size distribution. *Minerals Engineering*, *8*(6), 615–635.

Gorain, B., Franzidis, J., & Manlapig, E. (1995b). Studies on impeller type, impeller speed and air flow rate in an industrial scale flotation cell. part 2: Effect on gas holdup. *Minerals Engineering*, *8*(12), 1557–1570.

Gorain, B., Franzidis, J., & Manlapig, E. (1996). Studies on impeller type, impeller speed and air flow rate in an industrial scale flotation cell. part 3: Effect on superficial gas velocity. *Minerals Engineering*, *9*(6), 639–654.

Gorain, B., Franzidis, J., & Manlapig, E. (1997). Studies on impeller type, impeller speed and air flow rate in an industrial scale flotation cell. part 4: Effect of bubble surface area flux on flotation performance. *Minerals Engineering*, *10*(4), 367–379.

Gorain, B., Franzidis, J., & Manlapig, E. (1999). The empirical prediction of bubble surface area flux in mechanical flotation cells from cell design and operating data. *Minerals Engineering*, *12*(3), 309–322.

Gorain, B., Franzidis, J., Manlapig, E., Ward, K., & Johnson, N. (2000). Modeling of the mount isa rougher-scavenger copper flotation circuit using size-by-liberation data. *Minerals and Metallurgical Processing(USA)*, *17*(3), 173–180.

Gorain, B., Harris, M., Franzidis, J., & Manlapig, E. (1998). The effect of froth residence time on the kinetics of flotation. *Minerals Engineering*, *11*(7), 627–638.

Gorain, B., Napier-Munn, T., Franzidis, J., & Manlapig, E. (1998). Studies on impeller type, impeller speed and air flow rate in an industrial scale flotation cell. part 5: Validation of k-sb relationship and effect of froth depth. *Minerals engineering*, *11*(7), 615–626.

Hanna, H., Somasundaran, P., & Fuerstenau, M. (1976). Flotation—am gaudin memorial volume. *Am. Miner. Inst., New York*.

Hernandez-Aguilar, J., Rao, S., & Finch, J. (2005). Testing the k-sb relationship at the microscale. *Minerals engineering*, *18*(6), 591–598.

Imaizumi, T., & Inoue, T. (1965). Kinetic consideration of froth flotation. *6th Int. Mineral Processing congr., Cannes, 1963*, 581–593.

Jameson, G., Nam, S., & Young, M. (1977). Physical factors affecting recovery rates in flotation. *Minerals Science and Engineering*, *9*(3), 103–18.

Jameson, G., Nguyen, A., & Ata, S. (2007). The flotation of fine and coarse particles. In M. Fuerstenau, J. G., & R. Yoon (Eds.), *Froth flotation a century of innovation* (pp. 339–372). SME.

Jowett, A. (1980). Formation and disruption of particle-bubble aggregates in flotation. *Fine Particles Processing*, *1*, 720–754.

Kelley, K., Noble, A., Luttrell, G., & Yoon, R. (2012). Development of a model-based flotation simulator. In C. Young & G. Luttrell (Eds.), *Separation technologies for minerals, coal, and earth resources* (pp. 699–708). SME.

Kemper, M. (1999). State-of-the-art and new technologies in flotation deinking. *International journal of mineral processing*, *56*(1), 317–333.

King, R. (2001). *Modeling and simulation of mineral processing systems*. Elsevier.

Klassen, V., & Mokrousov, V. (1963). *An introduction to the theory of flotation*. Butterworths.

Klimpel, R., Hansen, R., & Fee, B. (1986). The selection of flotation reagents for mineral flotation, chapter 26. *Design and Installation of Concentration and Dewatering Circuits, SME, Littleton, Colorado*, 388–404.

Kracht, W., Vallebuona, G., & Casali, A. (2005). Rate constant modelling for batch flotation, as a function of gas dispersion properties. *Minerals Engineering*, *18*(11), 1067–1076.

Levenspiel, O. (1998). Chemical reactions engineering. *Recherche*, *67*, 02.

Luttrell, G., & Yoon, R. (1991). A flotation column simulator based on hydrodynamic principles. *International journal of mineral processing*, *33*(1-4), 355–368.

Luttrell, G., & Yoon, R. (1992). A hydrodynamic model for bubble–particle attachment. *Journal of colloid and interface science*, *154*(1), 129–137.

Lynch, A., Johnson, N., Manlapig, E., & Thorne, C. (1981). *Mineral and coal flotation circuits*. Elsevier, Amsterdam.

Lynch, A., Watt, J., Finch, J., & Harbort, G. (2007). History of flotation technology. In M. Fuerstenau, J. G., & R. Yoon (Eds.), *Froth flotation a century of innovation* (pp. 65–92). SME.

Mao, L., & Yoon, R. (1997). Predicting flotation rates using a rate equation derived from first principles. *International journal of mineral processing*, *51*(1), 171–181.

Massinaei, M., & Doostmohammadi, R. (2010). Modeling of bubble surface area flux in an industrial rougher column using artificial neural network and statistical techniques. *Minerals Engineering*, *23*(2), 83–90.

Mathe, Z., Harris, M., O'Connor, C., & Franzidis, J. (1998). Review of froth modelling in steady state flotation systems. *Minerals engineering*, *11*(5), 397–421.

Meenan, G. (1999). Modern coal flotation practices. In B. Parekh & J. Miller (Eds.), *Advances in flotation technology* (pp. 309–319). SME.

Miskovic, S. (2011). *An investigation of the gas dispersion properties of mechanical flotation cells: An in-situ approach*. Unpublished doctoral dissertation, Virginia Polytechnic Institute and State University.

Miskovic, S., & Luttrell, G. (2012). Comparison of two bubble sizing methods for performance evaluation of mechanical flotation cells. In C. Young & G. Luttrell (Eds.), *Separation technologies for minerals, coal, and earth resources* (pp. 563–574). SME.

Napier-Munn, T. (1997). Invention and innovation in mineral processing. *Minerals Engineering*, *10*(8), 757–773.

Oravainen, H., & Allenius, H. (2007). Mechanical froth flotation cells, section ii: Development of outokumpu flotation machines. In M. Fuerstenau, J. G., & R. Yoon (Eds.), *Froth flotation a century of innovation* (pp. 656–666). SME.

Pan, L., Jung, S., & Yoon, R. (2011). Effect of hydrophobicity on the stability of the wetting films of water formed on gold surfaces. *Journal of colloid and interface science*, *361*(1), 321–330.

Peaker, R. (2007). Mechanical froth flotation cells, section iii: Metso minerals rcs flotation machine. In M. Fuerstenau, J. G., & R. Yoon (Eds.), *Froth flotation a century of innovation* (pp. 666–672). SME.

Phoochinda, W., White, D., & Briscoe, B. (2004). An algal removal using a combination of flocculation and flotation processes. *Environmental technology*, *25*(12), 1385–1395.

Schwarz, S., & Alexander, D. (2006). Gas dispersion measurements in industrial flotation cells. *Minerals Engineering*, *19*(6-8), 554–560.

Sherrell, I. (2004). *Development of a flotation rate equation from first principles under turbulent flow conditions*. Unpublished doctoral dissertation.

Sripriya, R., Rao, P., & Choudhury, B. (2003). Optimisation of operating variables of fine coal flotation using a combination of modified flotation parameters and statistical techniques. *International journal of mineral processing*, *68*(1), 109–127.

Sulman, H., Picard, H., & Ballot, J. (1905). *British patent 7,803.* (Duplicated as U.S. Patent 835,120)

Sutherland, K. (1948). Physical chemistry of flotation. xi. kinetics of the flotation process. *The Journal of Physical Chemistry*, *52*(2), 394–425.

Taggart, A., Behre, H., Breerwood, C., & Callow, J. (1945). *Handbook of mineral dressing, ores and industrial minerals*. Wiley.

Tatterson, G. (1991). *Fluid mixing and gas dispersion in agitated tanks*. McGraw-Hill New York.

Tatterson, G. (1994). *Scaleup and design of industrial mixing processes*. McGraw-Hill.

Tavera, F., Escudero, R., & Finch, J. (2001). Gas holdup in flotation columns: laboratory measurements. *International Journal of Mineral Processing*, *61*(1), 23–40.

Tomlinson, H., & Fleming, M. (1965). Flotation rate studies. In *International mineral processing congress* (Vol. 6, pp. 563–579).

Tucker, J., Deglon, D., Franzidis, J., Harris, M., & O'Connor, C. (1994). An evaluation of a direct method of bubble size distribution measurement in a laboratory batch flotation cell. *Minerals Engineering*, *7*(5), 667–680.

Vera, M., Mathe, Z., Franzidis, J., Harris, M., Manlapig, E., & O'Connor, C. (2002). The modelling of froth zone recovery in batch and continuously operated laboratory flotation cells. *International journal of mineral processing*, *64*(2), 135–151.

Vianna, S. (2011). *The effect of particle size, collector coverage and liberation on the floatability of galena particles in an ore*. Unpublished doctoral dissertation, The University of Queensland.

Wang, L., Fahey, E., & Wu, Z. (2005). Dissolved air flotation. *Physicochemical treatment processes*, 431–500.

Weber, A., & Tracyzk, F. (2007). Mechanical froth flotation cells, section iv: Dorr-oliver eimco flotation equipment. In M. Fuerstenau, J. G., & R. Yoon (Eds.), *Froth flotation a century of innovation* (pp. 672–680). SME.

Weber, A., Walker, C., Redden, L., Lelinski, D., & Ware, S. (1999). Scale-up and design of large-scale flotation equipment. In B. Parekh & J. Miller (Eds.), *Advances in flotation technology* (pp. 353–369). SME.

Wills, B., & Atkinson, K. (1991). The development of minerals engineering in the 20th century. *Minerals Engineering*, *4*(7-11), 643–652.

Wills, B., & Napier-Munn, T. (2006). *Wills' mineral processing technology: an introduction to the practical aspects of ore treatment and mineral recovery*. Butterworth-Heinemann.

Yoon, R., & Luttrell, G. (1989). The effect of bubble size on fine particle flotation. *Mineral Procesing and Extractive Metallurgy Review*, *5*(1-4), 101–122.

Yoon, R., & Mao, L. (1996). Application of extended dlvo theory, iv:: Derivation of flotation rate equation from first principles. *Journal of Colloid and Interface Science*, *181*(2), 613–626.

Yoon, R., & Wang, L. (2007). Hydrophobic forces in foam films. *Colloid Stability*, 161–186.

Young, D., Munson, B., Okiishi, T., & Huebsch, W. (2010). *A brief introduction to fluid mechanics*. Wiley.

Chapter 2

Development of an Experimental Methodology for Rotor Testing

(ABSTRACT)

In the past, laboratory-scale flotation testing has been reserved for ore characterization and reagent appraisals. This manuscript describes a consistent methodology for the normalized evaluation of small-scale flotation rotors. These evaluations focus on four performance factors which influence machine design and scale-up procedures: (1) power consumption, (2) air dispersion, (3) operational robustness, and (4) flotation performance. These criteria have shown marked influence on cost and metallurgical performance at the industrial scale, and their translation to the laboratory scale is supported via theoretical considerations. In this paper, restrictions on the size and nature of the equipment have been imposed so that the experimental methodology coincides with the accepted paradigms of laboratory flotation analysis. The required equipment includes items that may already be present in a working flotation laboratory or items that may be easily procured from laboratory equipment vendors. Additionally, the flotation rotors measure less than 3 inches in diameter, and the tank volumes fall between 9 and 30 liters. This paper presents the required equipment and measurement devices along with the experimental and analytical procedures.

2.1 Introduction and Scope

To date, few studies have thoroughly addressed flotation rotor design at the laboratory scale. Most researchers over the past 50 years have generally reserved laboratory-scale

testing to characterize the ore, evaluate reagent interactions, and determine grinding sizes, leaving the concerns of equipment design and plant operation to larger scale testing and experienced-based scaling factors (Gaudin, 1957; Wills & Napier-Munn, 2006; Crozier, 1992). With regard to the rotor design, a series of studies by Gorain and others assessed various gas dispersion variables, including air holdup, bubble size distribution, and superficial gas velocity, in several pilot-scale machines (Gorain, Franzidis, & Manlapig, 1995a, 1995b, 1996, 1997; Gorain, Napier-Munn, Franzidis, & Manlapig, 1998). While these studies incorporate different rotor configurations, the research goals did not include the direct comparison of different rotor designs. Rather, the researchers wanted to assess the extent of the gas dispersion variables, including the rotor and other operational factors as independent variables. The authors admittedly did not necessarily operate the machines under the recommended settings in an attempt to cover the widest range of operational conditions. Furthermore, these studies did not consider the influence of power consumption, as the parameter was not measured or reported. Such an omission negates any meaningful comparison between the rotor designs, as power consumption strongly influences flotation performance and operational cost.

While the Gorain studies and others emphasize the role of gas dispersion in flotation, other performance factors have been attributed to the rotor design, but lack comprehensive evaluation. One such factor is the state of solid suspension or mixing in the vessel. Zwietering (1958) performed one of the first experimental evaluations of solid suspension in stirred vessels primarily intended for the chemical mixing industry. The author defined the *just-suspended* parameter (or *critical impeller speed*) as the minimum impeller rotational speed required to suspend all of the solid particles from the vessel's floor. An analytical expression was empirically derived to predict the critical speed from various dimensionless equipment and operational parameters unique to the mixing system. Similar studies have been applied to flotation cells in order to develop similar empirical correlations which incorporate additional, industry-specific parameters such as cell shape and forced-air rate (Westhuizen & Deglon, 2007; Lima, Deglon, & Leal Filho, 2009). In each of the aforementioned studies, the critical speed expression includes a proportionality constant which accounts for the specific rotor design. Few studies include an exhaustive treatment of the power required to suspend particles.

In light of the lapses in flotation rotor design characterization and evaluation, the initial objective of this study is to develop a methodology for the fair comparison of different forced-air flotation machine designs at the laboratory scale. Unfortunately, given the large number of independent and interdependent variables which affect flotation performance, this task requires due consideration. Different machine designs perform optimally in different geometric

and operational conditions. Furthermore, the drastic difference in scale between the laboratory and the plant may magnify some changes in machine performance while suppressing others. As a result, this task first seeks to establish normalized testing procedures which may provide reliable and beneficial data on flotation equipment design at the laboratory-scale.

With consideration from theoretical principles and industrial experience, four principle factors which influence flotation machine design and scale-up were selected for the performance evaluations (1) power consumption, (2) gas dispersion, (3) operational robustness, and (4) flotation performance.

When applicable, the measured performance indicators were normalized on the basis of power input. Since factors such as rotational speed and superficial gas velocity have an interactive and interdependent effect on flotation performance, normalizing results by these inputs may prove deleterious and misleading. Instead, power consumption represents a common factor, and a significant flotation equipment cost that is easily measured at the laboratory scale. Consequently, prior to any other performance analysis, a detailed understanding of the rotors' power draw at various speeds and gas rates is necessary.

Throughout this introduction and the literature review (Section 1.2), the role of gas dispersion in flotation performance has been defended theoretically and validated experimentally by numerous authors. While the measurement methods may change at the laboratory-scale, the surrogacy of gas dispersion to flotation performance is well-formulated, experimentally vetted, and proven scalable.

In this thesis, operational robustness refers to the range of operational conditions (in terms of rotational speed and air velocity) that a rotor can stably operate without inducing solid sanding or gas flooding. Both particle suspension and flooding are functions of rotational speed and air velocity, and both represent a marked digression from standard equipment operation. The extent that a given rotor can operate without inducing either of these conditions marks the freedom the operator has in changing the operation to meet a secondary process goal (i.e. a process control response to a downstream indicator).

Finally, differences in flotation performance between the rotors should be directly measured to ensure that the surrogate measurements (i.e. gas dispersion, fluid mixing) are indeed valid indicators of a rotor's ultimate capability. The lack of correlation between surrogate variables may indicate that other unknown phenomena are not influencing flotation behavior and should prompt more extensive study to undermine additional effects.

This chapter first describes the experimental and analytical equipment that was procured, constructed, and commissioned in order to evaluate the desired performance criteria.

These components are described both as independent devices and as collective flotation testing systems. Next, the experimental and analytical procedures needed to determine each of the performance criteria are described. Finally, the conclusions provide the context of these procedures in the larger spectrum of complete equipment design and evaluation. These experimental and analytical procedures were continually revised throughout the experimental phases while balancing testing ease with data reliability. The desired results consistently revealed more information on the four principle performance criteria.

2.2 General Experimental Equipment

2.2.1 Rotors

The primary independent variable examined during this research was the flotation rotor design. Throughout the research project, 15 rotors were developed and tested. Each of these 15 rotors was subjected to at least one laboratory test; however, not all rotors were equally tested. Given the iterative and rapid development phase, some rotors were abandoned prior to experimental procedure revision, while others were developed after less refined procedures were abandoned. This author acknowledges this marked lack of consistency but still chooses to present all of the available data in order to provide the most exhaustive information.

Physically, all rotors are 2.75 inches (7 centimeters) in diameter and between 1.25 to 2.0 inches (3.2 and 5.0 centimeters) tall. The initial rotors were manufactured from various materials, primarily stainless steel and aluminum via cast molding, while the later rotors were procured from the rapid prototype manufacturer ZoomRP.com. These rotors were constructed by a 3D printer using PolyJet White production material (ZoomRP.com, 2011). While the casted rotors show greater durability, the rapid prototyping process allowed more innovative shapes and design components. All of the rapid prototyped rotors were able to withstand consistent operation at rotation speeds up to 1800 RPM and torque loads up to 60 N-cm, while passing solid concentrations of 40% and particle sizes up to 200 microns. Rotor components and webs less than 2 mm were most prone to damage, especially in routine daily handling and transport.

Table 2.1 summarizes the rotors, dimensions, providers, and short abbreviations. These abbreviations will be used to identify individual rotors throughout the remainder of this report. Table 2.2 describes the technical details used to categorize and identify the rotors. Figure 2.1 shows a typical rotor.

Table 2.1: Summary of technical information regarding flotation rotors included in laboratory testing.

Rotor ID	**Material**	**Height**	**No. of Blades**	**Develop Date**
SP - A1	Aluminum	1.75	6	Sept. 2009
SP - A2	Aluminum	1.75	6	Sept. 2009
SP - A3	Aluminum	1.75	6	Sept. 2009
SP - B1	Stainless Steel	1.50	8	Sept. 2009
SP - C1	Stainless Steel	1.75	6	Sept. 2009
SP - C2	Stainless Steel	1.25	6	Sept. 2009
VT - A4	PolyJet White	2.00	6	Sept. 2009
VT - A5	PolyJet White	2.00	6	Jan. 2010
VT - A6	PolyJet White	1.50	6	Oct. 2009
VT - B2	PolyJet White	1.75	8	Dec. 2009
VT - B3	PolyJet White	1.75	8	May 2011
VT - D1	PolyJet White	2.25	6	Sept. 2009
VT - D2	PolyJet White	2.25	6	Dec. 2009
VT - E1	PolyJet White	2.00	6	Sept. 2009
VT - E2	PolyJet White	1.75	6	Sept. 2009

Table 2.2: Rotor Classification Key

Rotor Class	Technical Details
A	6 blades; bottom-side suction; peripheral and internal air introduction
B	8 blades; bottom-side suction; internal air introduction
C	6 blades; bottom-side suction; peripheral air introduction
D	6 blades; mid-point suction; internal air introduction
E	6 blades; distributed suction; peripheral air introduction
SP	Aluminum and cast molding
VT	Rapid prototyped, PolyJet White material

Figure 2.1: Typical rotor used in laboratory testing [Photo by Aaron Noble:10/24/2009].

Figure 2.2: Generic stator used in laboratory testing [Photo by Aaron Noble:3/29/2010].

2.2.2 Stators

While synergies between the rotor and stator are postulated, the scope of this research is relegated only to the rotor design. As a result, generic stators were used in combination with the various rotor designs, rather than unique stators for each rotor. In the experimental phases, two stators were utilized. Initially, a top-ring mounted stator was used in combination with the rotors. Like many of the prototype rotors, a second stator was also developed via rapid prototyping (Figure 2.2). This stator is similar in size to the original; however, the blades are oriented vertically and are mounted to a ring on both the top and bottom. This extended lower opening provides compatibility for many of the larger rotors that do not fit within the slope of the original stator. Like the prototype rotors, this stator was procured from the rapid prototype manufacturer ZoomRP.com and constructed by a 3D printer using the PolyJet White production material.

2.2.3 Tanks

Several flotation tanks geometries were designed and fabricated for use in the experimental phase. The most frequently used tanks were cylindrical tank cells ranging in volume from 9 to 35.3 liters. The technical details of these tanks are summarized in Table 2.3. Each of the three primary tanks was designed and utilized for specific testing purposes. Silva et al. (2012) has suggested that the appropriate "scaled-down" size for the 2.75 inch rotor is the 35.3 liter, 14 inch diameter tank. Nevertheless, the smaller tank size adequately reflects an oversized-rotor design which is common in some industries. Furthermore, the fully transpar-

Table 2.3: Summary of technical information regarding flotation tanks included in laboratory testing.

Parameter	**Tank 1**	**Tank 2**	**Tank 3**
Nominal Size	9.75 in RT	10 inch RT	14 inch RT
Shape	Cylinder	Cylinder	Cylinder
Construction Material	1/4 in. PVC with Window	1/4 in. Trasparent Lexan	1/8 in. Trasparent Polycarbonate
Diameter (in.)	9.75	10	14
Fill Height (in.)	7.36	7.25	14
Volume (L)	9.00	9.33	35.3
Volume (gal)	2.38	2.46	9.32
Launder Style	Batch Weir	No Launder	Radial Launder
Lip Length (in.)	5.0	–	44
Flow Style	Batch	Batch	Continuous

ent tanks (10 inch RT and 14 inch RT) allow uninhibited visual inspection of the flotation region from any angle while in operation. This feature allows convenient investigation in solid suspension and air holdup determination. Alternatively, the viewing window in the 9.75 inch RT only provides limited visual information on the tank's water level.

The launder design also dictates which cells may be used in the flotation performance evaluations. The 9.75 inch RT has a batch-style overflow weir. The weir has a total lip length of 5 inch and is located 9.75 inches from the tank bottom. Alternatively, the 14 inch RT has an external radial launder which extends along the full periphery of the tank cell. The launder bottom slopes downward at 15° expelling the froth concentrate at a single port. The 10 inch RT has no launder.

Furthermore, the 14 inch RT has been outfitted with openings for feed and tailings. These inlets are approximately one inch from the cell bottom, and they allow the cell to be operated in a continuous flow state. The tailings port includes a gate valve which may be closed to operate the cell in a batch condition. The other tanks do not include inlets and must always be operated in batch conditions. Pictures of these three cells are shown in Figure 2.3.

(a) 9.75 in. RT (b) 10 in. RT (c) 14 inch RT

Figure 2.3: Pictures of flotation tanks used in laboratory testing [photos by Aaron Noble:10/24/2009; 5/24/12; 7/30/2010].

2.2.4 Mixing Devices and Power Measurements

Throughout the testing campaigns, modified overhead laboratory mixers were used to drive the flotation rotor. These mixers included variable speed control and an integrated torque meter. During the exploratory testing campaign, a Heidolph RZR 2102 Control electronic laboratory mixer (Figure 2.4a) was procured and utilized. This model allows speeds ranging from 40 to 2000 RPM and torque measurements from 0 to 47 N-cm. Typically, the torque limit was the limiting factor for this mixer. Few rotors could be operated at tip speeds in excess of 4.5 meters per second (1200 RPM) without overloading the mixer's capabilities

To accommodate the higher torque required at high tip speeds, a second mixer (1/5 horsepower Caframo brushless –Figure 2.4b) was procured for the detailed testing campaign. This mixer's maximum capacity is 70 N-cm at 1800 RPM; however, periodic torque overloads may be sustained for short periods of time. Of the available rotors, most were able to achieve a maximum tip speed of 6.5 meters per second (1776 RPM) while remaining within the torque limitations.

A custom one inch diameter shaft (Figure 2.5) was designed and mounted into the mixers via a 3/8 inch chuck. This shaft includes a hollow center and a low-friction bearing which allows compressed air to flow from the laboratory's compressed air source through the rotor. Additionally, the shaft features screw mounts at the mixing end which allow interchangeable rotors.

(a) RZR 2102 Mixer

(b) 1/5 Horsepower Caframo Mixer

Figure 2.4: Laboratory mixing units [photos by Aaron Noble 10/24/2009; 5/24/2012].

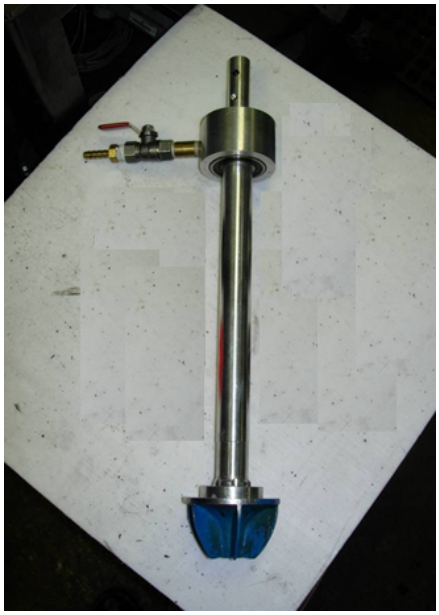

Figure 2.5: Custom Shaft with attached rotor [photo by Aaron Noble: 10/24/2009].

2.2.5 Bubble Size Analysis

Bubble size measurements were completed using a visual method similar to the one described by Hernandez-Aguilar, Gomez, and Finch (2002). This method uses a bubble sampling device, consisting of a capillary tube and a chamber with a slanted viewing window. Bubbles recovered from the flotation tank rise through the tube and form an approximate single layer on the slanted window, where they are captured by high speed photography. For most laboratory-scale testing, the sampling tube was positioned along the wall of the tank slightly above the stator. At least 2,500 individual bubbles were analyzed, depending on the operating conditions.

Image acquisition was achieved by a GP-21400 GEViCAM with a HR9HA-1B Fujinon 9 millimeter lens. Controlled by automated computer input, the camera can produce 5 megapixel images with a maximum acquisition rate of 30 frames per second. Initially, a 200 watt halogen lamp was used as an illumination source, to generate a nearly consistent background. This illumination source was later upgraded to an LED light board.

2.2.6 Air Flow Measurements

For the exploratory testing, air flow to the flotation tank was measured by a calibrated stainless steel variable-area flowmeter. The capacity of the flowmeter ranges from 2,182 to 90,454 milliliters per minute. For the given tank geometries, these flow rates correspond to superficial gas velocities ranging from 0.07 to 3.00 centimeters per second. For the detailed testing, a larger capacity, direct reading variable-area flowmeter was procured. The capacity of this flowmeter ranges from 1.0 to 4.0 standard cubic feet per minute or superficial velocities of 0.5 to 2.0 centimeters per second for the given tank geometries.

2.2.7 Batch Flotation System

The batch flotation system (Figure 2.6) was used exclusively throughout the exploratory testing campaign. The components of this system include the low-torque RZR mixer, the custom bubble size sampler, the low air meter, and either the 9.75 inch RT or the 10 inch RT depending on the specific test. Other than the standard ring stand for the mixing unit and the bubble size analyzer, no special mounting or equipment was needed to support the system. This basic setup allows rapid cleanup and straightforward modification in terms of rotor or material change. However, as pictured, this setup does not allow visual access to

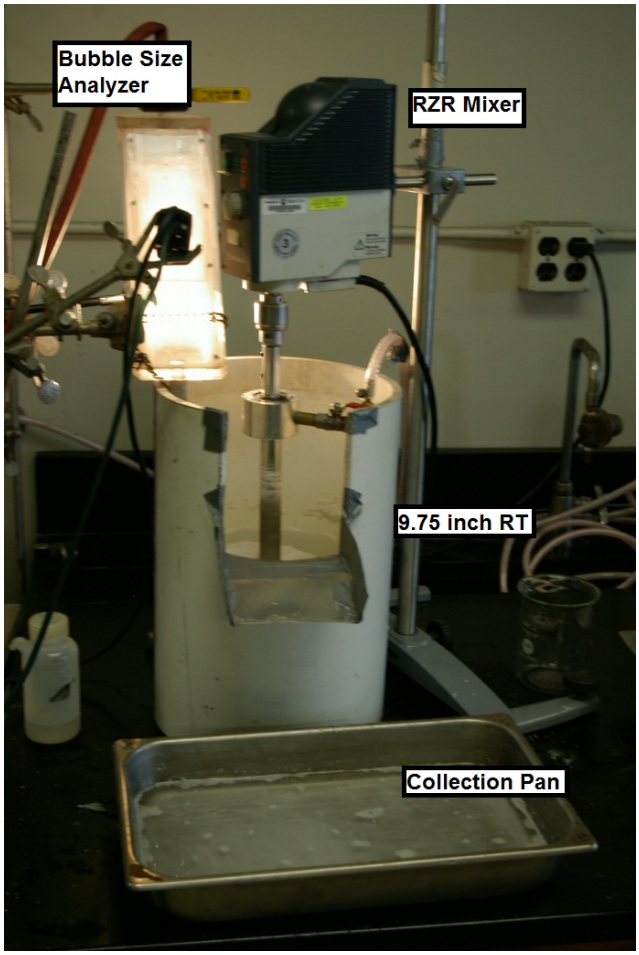

Figure 2.6: Batch flotation system [photo by Aaron Noble: 12/17/2009].

the tank bottom, thus limiting the appraisal of off-bottom solid suspension.

2.2.8 Continuous Flotation System

The continuous-flow flotation system (Figure 2.7) was used exclusively throughout the detailed testing campaign. This system is most easily described as three modular subsystems: the framework, the flotation tank, and the recycle sump and pump. The flotation cell, feed pump, and their auxiliary systems are housed on a welded steel frame (1.25 inch square steel tubing) with three shelves. A detachable side frame supports the sump and its auxiliary systems. The entire device measures approximately 4.5 by 2 by 6.5 feet in length, width, and height, respectively, and when empty, the system weighs approximately 150 pounds. Given the modest size and weight, the system may be considered reasonably portable.

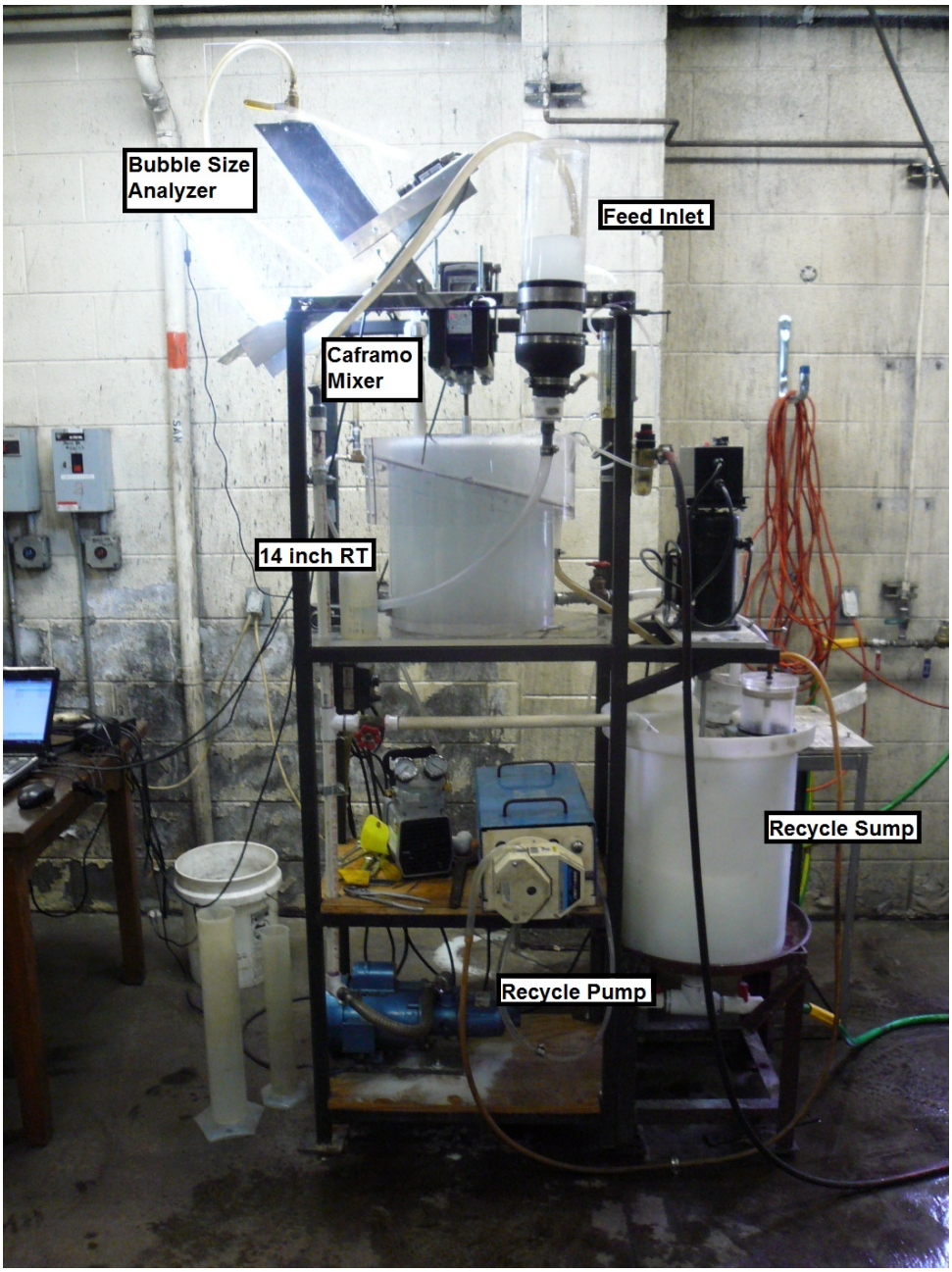

Figure 2.7: Continuous flotation system [photo by Aaron Noble: 9/30/2010].

The 14 inch RT was the primary flotation tank used with the continuous flotation system. As mentioned above, this tank includes inlets/outlets for the feed and tailings streams as well as a radial concentrate launder. Stator assemblies were mounted onto the tank floor with glue. In the continuous system, the flotation tank rests on a clear Plexiglas shelf. This setup extends visual access to the tank bottom, allowing simple assessment of off-bottom solid suspension. Furthermore, the Caframo mixer was exclusively utilized in the continuous flotation system due to the higher torque capacities.

Both the tailings and the concentrate streams are returned to a central sump prior to being recycled into the flotation tank. The sump is a standard 15 gallon, conical-bottom polyethylene tank. In order to ensure complete mixing of the product streams, agitation is supplied to the sump by a 0.5 horsepower DC powered variable speed mixer. Material from the sump is returned to the flotation tank by a 0.5 horsepower positive displacement feed pump. A bypass valve following the pump allows a fraction of the material to be returned to the sump, thereby controlling the apparent feed rate to the tank. All piping from the sump to the flotation tank is 0.5 inch PVC.

2.3 Experimental and Analytical Procedures

2.3.1 Power Measurements

Both mixing units used in these studies include integrated torque meters and digital speed controls. Both units display the current torque and the current speed via digital output on the faceplate. Power measurements were determined by first recording the rotational speed (N in RPM) and the torque (T in N-cm) directly from the mixing unit. The power (P) is then calculated by:

$$P[watts] = \frac{2\pi(N[RPM])(T[N-cm])}{6000}. \tag{2.1}$$

Per the procedures in the mixer's documentation, the device was calibrated daily for each rotor, prior to any measurements. To calibrate, the mixing unit was first turned on and run at full speed for 20 minutes in open air with the desired rotor attached. After the unit had properly warmed up, torque measurements were taken at the speeds desired for subsequent testing. These "open-air" torque measurements were later subtracted from the test readings in order to mitigate the latent torque from the rotor's weight and the friction in the mixing drive. In this report, the initial studies of power consumption in both testing

campaigns were used to determine the rotors' power curves and the power numbers (Sections 4.2 and 5.2). These tests were performed in a water-only solution, without solid particles, reagents, or forced air. Power measurements for other tests (air holdup, flotation, etc.) were measured independently during each specific test.

With respect to precision, both mixers were delivered with a calibration certificate which verifies the speed measurements within ±1% and the torque measurements within ±5%. Furthermore, preliminary testing was conducted to determine the repeatability of power measurements in specific test conditions (rotational speed and superficial gas rate). The effect of solid density and slurry temperature were not studied during these tests. Reagent dosage was studied but was found to have no significant effect on power measurements over the conditions under investigation.

During the repeatability testing, a specific test condition was set (air velocity and rotational speed), and the machine was given several moments to accelerate to the desired condition. Once at steady state, the speed and torque were recorded, and the power was calculated for that condition. Each condition was repeated three times, and an average was determined from the three measurements. The tip speeds and air velocities covered the full range of anticipated test conditions (3 to 6 m/s tip, 0 to 2 cm/s air), producing 385 independent measurements. To interpret this data, each individual measurement's deviation from the mean (or *relative residual*) was determined as a percentage of the mean value for the specific test condition:

$$Residual = 100\left(\frac{x - \overline{x}}{\overline{x}}\right)$$

where x is the measured value at a specific test condition and $\overline{x}$ is the average of three values at that test condition.

Residuals for each measurement were plotted against the measured power, and a frequency distribution of the residuals was generated (Figure 2.8). As shown in the frequency distribution, the residuals are normally distributed around zero with a standard deviation (shown by the red dashed line in both plots) of 7.58. As interpreted from Figure 2.8, a noticeable correlation exists between the residual and the magnitude of the power measurement. The degree of measurement variability is most severe in those readings with a relatively low power measurement. Most of the data outside of the one single standard deviation limit was recorded at power measurements below 60 Watts. Similar analyses show no noticeable correlation between tip speed or gas velocity and measurement variability (Figure 2.9).

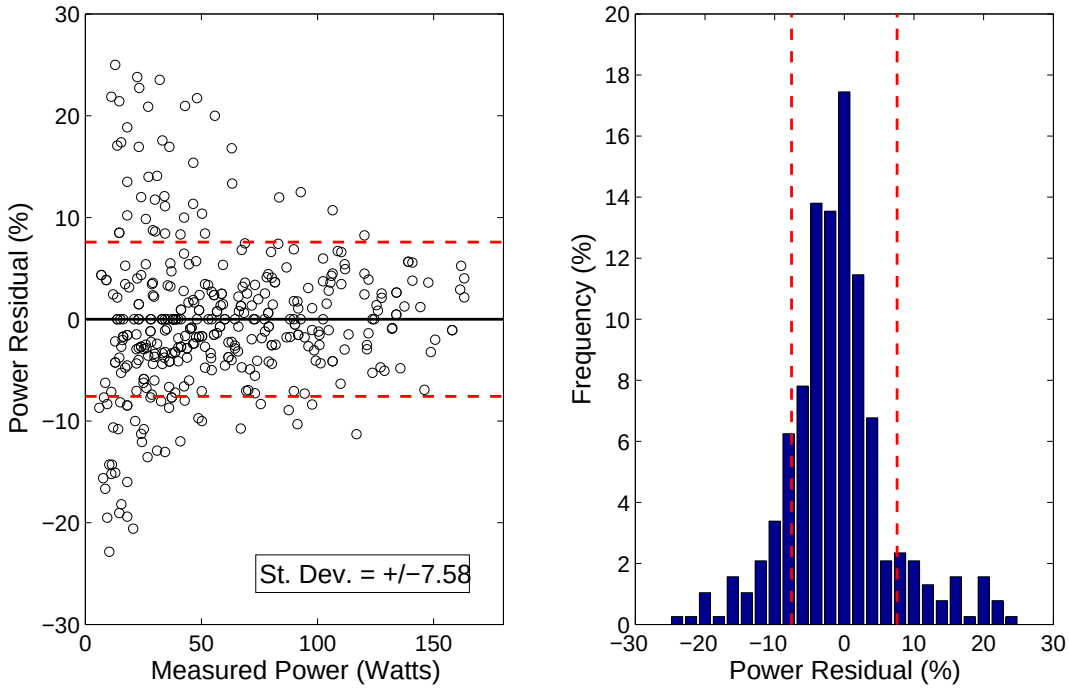

Figure 2.8: Power measurement repeatability as a function of measured power. Left: Abscissa value represents the measured power for a single test. Ordinate value represents the difference between individual power measurements and the average of three measurements at the same test condition. The red lines indicate the standard deviation calculated for all residuals. Different test conditions refer to specific rotational speeds and gas velocities. Right: Frequency diagram of the residuals. Red lines indicate one standard deviation of +/-7.58%.

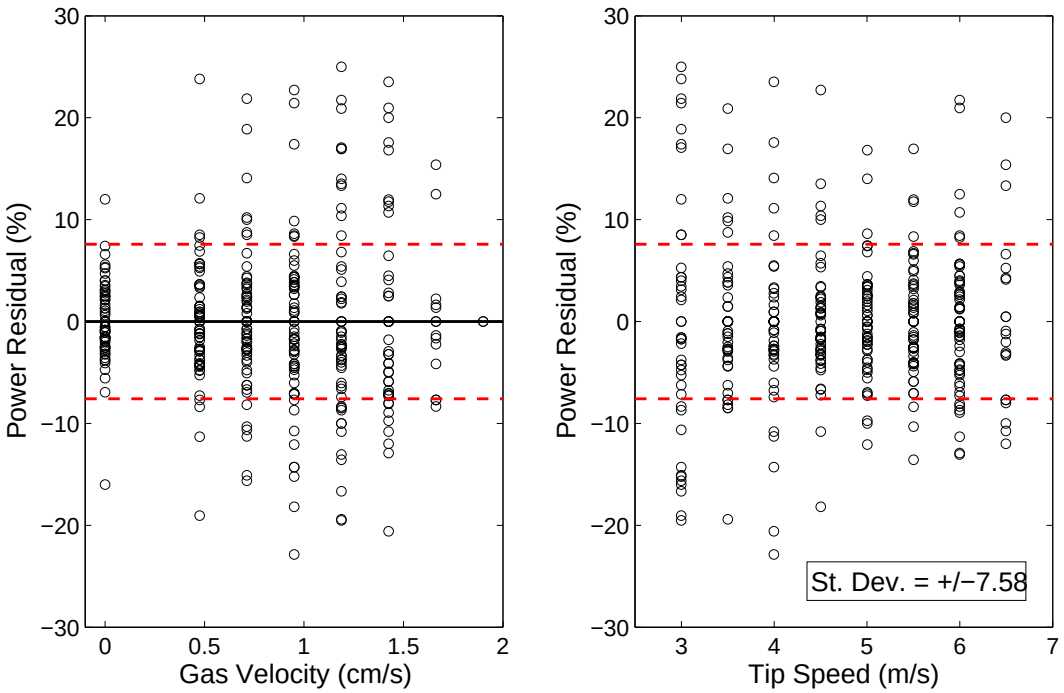

Figure 2.9: Power measurement repeatability as a function of gas velocity (left) and tip speed (right). Ordinate value represents the difference between individual power measurements and the average of three measurements at the same test condition. The red lines indicate the standard deviation calculated for all residuals. Different test conditions refer to specific rotational speeds, gas velocities, and rotors.

2.3.2 Holdup Measurements

As widely documented in the literature, gas dispersion is a key variable which influences flotation performance. One holistic measure of the gas dispersion and available gas surface area is the air holdup. While many researchers have devised methods of local air holdup (Grau & Heiskanen, 2003; Gomez & Finch, 2007; Schwarz & Alexander, 2006), the equipment is usually too obtrusive to conveniently provide data in the laboratory scale. Alternatively, the global air holdup provides easy-to-obtain, yet powerful comparative data for flotation machine design.

Global air holdup was determined by one of two methods. During the exploratory test campaign, the simple method was used. Air holdup was determined by first setting the desired rotational speed with the air flow turned off. The liquid level was noted, and the air flow was initialized. Once the system stabilized at a steady state in terms of power draw and new liquid level, the torque and rotational speed were recorded, and the increase in water level was measured manually (Figure 2.10). From the torque and speed measurements, the power draw was calculated according to Equation 2.1. The global air holdup (ε) was determined from the measured increase in water level (h_g) and the original water level (h_t) by:

$$\varepsilon = 100 \left(\frac{h_g}{h_t + h_g} \right).$$

During the detailed testing phase, global air holdup was determined by the displaced volume method. Since the detailed testing utilized the 14 inch RT tank which has a radial launder, water displaced from the cell may be collected and measured. During these tests, the tank was first filled to the point of overflow. The desired speed was set with the air disengaged, and any volume displaced by the rotational action of the impeller was noted. The air flow was then initiated to the desired level. All the displaced water was collected in the launder, and the volume was recorded along with the torque and rotational speed. The global air holdup was calculated from the tank volume (V_t) and the displaced volume (V_d) by:

$$\varepsilon = 100 \left(\frac{V_d}{V_t} \right).$$

All holdup tests were performed in the absence of frother.

(a) No Air (b) With Air

Figure 2.10: Simple method of air holdup determination [photos by Aaron Noble: 10/12/2009].

2.3.3 Operational Limits Determination

In this study, the "operational limits" or "operational robustness" refer to two conditions which prevent normal operation of a flotation cell: the sanded condition and the flooding condition. The sanded condition refers to a degree of incomplete solid suspension in the tank. Insufficient agitation from the rotor will cause solids in the tank to settle and accumulate on the tank bottom. The degree of agitation is enhanced by increasing the rotor tip speed but mitigated by increasing the gas velocity. Other operational factors, such as solid density, slurry viscosity, and particle size also have an effect on solid suspension (Zwietering, 1958; Lima et al., 2009).

The degree solid suspension can be characterized by many factors (apparent fluid density, visible bed depth at the tank wall, rotor power draw, etc.); however, prior studies have shown that the most indicative measurement is the minimum speed (or power) needed to initiate off-bottom suspension(Zwietering, 1958; Lima et al., 2009). Off-bottom suspension refers to the absence of persistent settling on the tank bottom. This condition is most easily assessed by visual access to the tank bottom; however, manual observation with a probe serves as a reasonable substitute when visual access is not available.

During the exploratory testing, the solid suspension tests were conducted in the 10 inch

RT which is made of transparent Lexan. While visual access was not available to the tank bottom, solid accumulation at the wall was noted, and a simple probe was used to assess the degree of solid settling on the tank bottom. During the detailed testing, visual access was available to the tank bottom, so solid suspension was affirmed by simple observation. During both testing campaigns, the minimum speed (and power) required for solid suspension was determined as a function of rotor selection and air speed. By this measurement technique, the degree of pumping loss as a result of rotor aeration may be ascertained.

Various materials of different densities and mean particle sizes were used throughout the solid suspension tests. Some of the more prevalent materials include: course grained silica beads and iron ore rougher feed. However, since this study prioritizes the comparative analysis of rotor design, the effect of material and operational parameters on solid suspension was not emphasized or fully investigated.

The second operational limit, the flooding condition, is defined as the maximum gas volume that a rotor can disperse at a given rotational speed. Once this limit is exceeded, very large pockets of air begin to escape the rotor region and are expelled at the surface near the shaft. Colloquially, this condition is commonly referred to by a number of terms: boiling, geysering, surface turbulence, etc. In this thesis, the term "boiling" may be used to indicate rotor flooding; however, use of this term is purely semantic and not indicative of an actual phase change occurring in the liquid.

For a given air velocity, the flooding condition may be averted by increasing the rotational speed. For a given rotation speed, the air velocity must be reduced until the flooding is halted. For both testing campaigns, the flooding limit of each rotor was determined as a function of rotational speed. During the tests, a speed was designated, and the air velocity was increased until the flooding condition was first observed. Both the speed and air velocity were noted prior to setting a different test condition.

Because this test attempts to quantify descriptive information, the data are prone to subjective influence. Nevertheless, the comparative analysis of data from a single experimenter will provide a reliable basis for evaluation of different flotation rotors.

2.3.4 Batch Flotation Testing

During the exploratory testing campaign, single-species batch flotation testing was used to determine the relative performance of each rotor, in terms of flotation recovery. In addition to the first-order rate constant, the mean bubble size and the power draw were recorded

for each rotor in order to standardize the results on the basis of energy efficiency and bubble surface area efficiency. During this phase, each rotor was tested at multiple rotational speeds, while the air velocity and the chemical conditions were held constant. By varying the rotational speeds, each test produced a different power draw and a different bubble size. The resulting data produced two comparative plots for each rotor: flotation rate constant as a function of power draw and flotation rate constant as a function of bubble surface area flux.

The procedure for standard batch flotation kinetics tests has been described thoroughly in the literature (Crozier, 1992; Fichera & Chudacek, 1992; Wills & Napier-Munn, 2006). In general, a batch kinetics test requires timed samples to be taken as floated material is removed from the cell. By weighing these samples as well as the tailings material, cumulative recovery can be determined as a function of time. In the exploratory testing, flotation tests were conducted up to a maximum time of 4 minutes, with the first sample being taken at 10 seconds and progressive samples at longer time intervals (10, 20, 30, 60, 120, and 240 seconds). After completing each test, the samples were dewatered by a vacuum filter and dried in a 100 °C oven overnight.

The material used in the exploratory flotation tests was A-Series Technical Quality glass spheres (nominal size 35 microns) procured from Potters Industries (Potters Industries, Incorporated, 2001). These samples were hydrophobized in a $4 \cdot 10^{-6}$ molar solution of dodecylamine (DDA) collector. Prior to any test work, a large amount of collector solution was made by completely dissolving the lot DDA in pure ethanol. The collector for each test was appropriated from this same solution to ensure similarity between the tests. In addition to the DDA collector solution, MIBC was added as frother. Both of the reagents along with the glass spheres were added to the flotation cell and agitated for two minutes without air. This conditioning time immediately preceded the flotation tests.

From the collected cumulative recovery data, flotation rate constants (k) were determined for each test. Considering first order reaction kinetics, the rate of change of material in the cell (dN/dt) is directly proportional to the amount of material in the cell (N). The proportionality constant (k) is defined as the flotation rate constant:

$$\frac{dN}{dt} = kN.$$

By solving the differential equation for the batch boundary condition ($N(0) = 1$ or $R(0) = 0$) and recognizing that $R = 1 - N$, the expression simplifies to (Levenspiel, 1998):

$$\ln(1 - R) = kt.$$

Thus, by plotting $\ln(1-R)$ against t, the rate constant can be determined by the slope of the resulting straight line. Typically, flotation material exhibits a distribution of rate constants which is conveniently discretized into fast-, slow-, and non-flotation components as indicated by separate linear portions of the $\ln(1-R)$ vs. t plot. For ease of comparison, only the fast kinetics were evaluated during this portion of the investigation. Consequently, the bubble size and power measurements were also taken during the time period corresponding to fast kinetics (less than 30 seconds into the test).

2.3.5 Continuous Flotation Testing

To supplement the batch testing, continuous flotation tests were conducted during the detailed campaign. Since most laboratory tests are conducted in a semi-batch fashion, flow characteristics and process dynamics inherently contrast the continuous processes seen in full-scale plants. Also, since batch tests are, by definition, never at a steady-state, variables such as reagent concentration and pulp density are constantly and uncontrollably changing. These fluctuations result in continual variances in other dependent variables, such as bubble size and power draw. While results from batch tests do carry comparative meaning, more consistent and applicable data can be derived from continuous testing.

A well-defined continuous flotation testing and sampling routine was developed to promote consistency between the individual rotor tests. Similar equipment and procedures have been described in the literature (Welsby, Vianna, & Franzidis, 2010). The order of reagent preparation, sample preparation, operation, and sampling was strictly established to provide the most non-invasive measurement strategy, while minimizing disturbances to the flotation cell and maximizing data reproducibility.

During the tests, the rotor mixer was first initiated and given 20 minutes to warm up prior to calibration (See Section 2.3.1). While the mixer was warming up, reagents and flotation samples were prepared. The sump was then filled with municipally supplied water, the flotation sample, and the reagents solution. The feed pump was turned on and diverted sampling bucket/cylinder. After taking a preliminary residence time measurement, the feed rate was adjusted and resampled until at the desired level. Once the residence time was fixed, the feed pump was diverted to the flotation tank. With the air disengaged and the rotor set at the desired tip speed, the flotation tank was filled, and the tailings valve was adjusted until a desired liquid level (or froth depth) was attained. Next, the air regulator was released and adjusted until the desired air flow was achieved. After making any other final adjustments, the tank was allowed to operate freely, recycling product material back

to the sump, for at least three residence times, until a steady-state was attained. Once at steady state, timed samples were taken from each of the product streams and the feed stream. Both product streams were sampled simultaneously. The wet sample weight and the sampling time were recorded. After dewatering and thoroughly drying the sample, the dry weight was also recorded, in order to calculate the dry mass rate, water rate, and percent solids of each stream. Finally, the torque was measured and recorded.

After taking samples for a single test condition, the air rate and rotation speed were reset to a new condition, and a three residence time delay was permitted to allow the system to return to a new steady state prior to any further sampling. During the detailed testing, a two factor central composite experimental design was used to provide variations in tip speed and air velocity encompassing the operational range of a typical laboratory cell (tip speed: 4.2 to 6.31 m/s; air velocity: 0.9 to 1.6 cm/s). These procedures were repeated for various rotors and mean particle sizes.

After acquiring the experimental data, the measured mass and liquid rates were first subjected to a mass balancing routine to reconcile the redundant measurements. The procedure for the mass balance was to minimize the weighted sum of the squared errors between the experimental and the adjusted values, while enforcing a strict zero-sum balance. From the reconciled data, simple mass and solids recovery were determined. A more accurate residence time (τ) value was determined by considering the mass balanced tailing flow rate (Q_t), the cell volume (V) less the air holdup (ε):

$$\tau = \frac{V(1-\varepsilon)}{Q_t}.$$

The kinetic coefficient for the continuous tests was determined by assuming a perfectly mixed reactor model for the laboratory cell. Under the perfectly mixed condition, the flotation recovery (R) is given in terms of the residence time and rate constant (k) by (Levenspiel, 1998):

$$R = \frac{k\tau}{1+k\tau}.$$

By simply algebraic manipulation, the rate constant can be determined by:

$$k = \frac{R}{\tau - R\tau}.$$

Using these analytical procedures, the numerous data produced from the central composite experimental design were used to populate the $k-S_b$ plot. Additionally, measurements taken at similar air velocities were compared to populate the rate constant-power plot. These

data interpretation strategies allow consistent comparisons between the batch and continuous data. Variations in the holistic results should prompt further study in the contrasts of process dynamics and scalability between batch and continuous flow mechanisms.

2.4 Summary and Conclusions

In summary, this manuscript has presented descriptions of the following experimental and analytical equipment:

- The 15 rotors which were considered in the study;
- The 2 stators which match with the various rotors;
- The 3 flotation tanks offering different testing abilities;
- The 2 laboratory mixers with integrated torque meters used to propel the rotors;
- The method of bubble size analysis used throughout the testing;
- The compilation of equipment required for the batch system testing; and
- The compilation of equipment required for the continuous system testing.

In addition, this manuscript has provided descriptions of various experimental and analytical procedures used throughout the exploratory and detailed testing, including:

- Power measurements along with repeatability testing;
- Two methods of air holdup determination;
- Methods of determining operational robustness via the sanding condition and the flooding condition;
- Flotation performance by batch testing; and
- Flotation performance by continuous testing.

In conclusion, the experimental equipment and procedures along with the analytical methods for comparative rotor testing have been presented in spirit of the laboratory testing paradigm. By understanding the limitations and benefits of the laboratory scale, the tests

have sought to exploit comparative, rather than, deterministic data. Additionally, the procedures prioritize rapid execution and analysis, in order to allow more testing combinations and modifications. While no single laboratory test is the ultimate predictor of full-scale success, the holistic analysis of the full data-set should support reliable conclusions that can be used to direct larger scale studies.

2.5 Bibliography

Crozier, R. (1992). Flotation. theory, reagents and ore testing. *Pergamon Press plc(UK), 1992,*, 356.

Fichera, M., & Chudacek, M. (1992). Batch cell flotation models–a review. *Minerals engineering*, *5*(1), 41–55.

Gaudin, A. (1957). *Flotation*. McGraw-Hill.

Gomez, C., & Finch, J. (2007). Gas dispersion measurements in flotation cells. *International Journal of Mineral Processing*, *84*(1-4), 51–58.

Gorain, B., Franzidis, J., & Manlapig, E. (1995a). Studies on impeller type, impeller speed and air flow rate in an industrial scale flotation cell. part 1: Effect on bubble size distribution. *Minerals Engineering*, *8*(6), 615–635.

Gorain, B., Franzidis, J., & Manlapig, E. (1995b). Studies on impeller type, impeller speed and air flow rate in an industrial scale flotation cell. part 2: Effect on gas holdup. *Minerals Engineering*, *8*(12), 1557–1570.

Gorain, B., Franzidis, J., & Manlapig, E. (1996). Studies on impeller type, impeller speed and air flow rate in an industrial scale flotation cell. part 3: Effect on superficial gas velocity. *Minerals Engineering*, *9*(6), 639–654.

Gorain, B., Franzidis, J., & Manlapig, E. (1997). Studies on impeller type, impeller speed and air flow rate in an industrial scale flotation cell. part 4: Effect of bubble surface area flux on flotation performance. *Minerals Engineering*, *10*(4), 367–379.

Gorain, B., Napier-Munn, T., Franzidis, J., & Manlapig, E. (1998). Studies on impeller type, impeller speed and air flow rate in an industrial scale flotation cell. part 5: Validation of k-sb relationship and effect of froth depth. *Minerals engineering*, *11*(7), 615–626.

Grau, R., & Heiskanen, K. (2003). Gas dispersion measurements in a flotation cell. *Minerals engineering*, *16*(11), 1081–1089.

Hernandez-Aguilar, J., Gomez, C., & Finch, J. (2002). A technique for the direct measurement of bubble size distributions in industrial flotation cells. In *Proceedings of the 34th annual meeting of the canadian mineral processors* (pp. 389–402).

Levenspiel, O. (1998). Chemical reactions engineering. *Recherche*, *67*, 02.

Lima, O., Deglon, D., & Leal Filho, L. (2009). A comparison of the critical impeller speed for solids suspension in a bench-scale and a pilot-scale mechanical flotation cell. *Minerals Engineering*, *22*(13), 1147–1153.

Potters Industries, Incorporated. (2001). *Speriglass solid glass spheres: A glass.* (`http://www.pottersbeads.com/markets/PolySpheriglassASpecs.asp`)

Schwarz, S., & Alexander, D. (2006). Gas dispersion measurements in industrial flotation cells. *Minerals Engineering*, *19*(6-8), 554–560.

Silva, R., Echeverri, L., Olson, T., Foreman, D., Yang, Y., & Caldwell, K. (2012). The effect of laboratory cell design on flotation machine hydrodynamics, solid suspension and particle recovery. In *2012 sme annual meeting and exhibit preprints* (pp. 452–457). SME.

Welsby, S., Vianna, S., & Franzidis, J. (2010). A continuous pilot-scale flotation rig for the systematic study of flotation variables. *Minerals Engineering*, *23*(10), 826–829.

Westhuizen, A. der, & Deglon, D. (2007). Evaluation of solids suspension in a pilot-scale mechanical flotation cell: The critical impeller speed. *Minerals engineering*, *20*(3), 233–240.

Wills, B., & Napier-Munn, T. (2006). *Wills' mineral processing technology: an introduction to the practical aspects of ore treatment and mineral recovery.* Butterworth-Heinemann.

ZoomRP.com. (2011). *Polyjet printer options.* (`http://www.zoomrp.com/polyjet-printer.aspx`)

Zwietering, T. (1958). Suspending of solid particles in liquid by agitators. *Chemical Engineering Science*, *8*(3-4), 244–253.

Chapter 3

Exploratory Testing of Flotation Rotor Design

(ABSTRACT)

A two-part experimental analysis identifying the influence of rotor design on power consumption and metallurgical performance in forced-air flotation equipment was conducted at the laboratory scale. This manuscript describes the results for the first experimental campaign. This phase of the research focused on the breadth of analysis in terms of number of rotors analyzed. In this study, replicate testing and exhaustive experimental conditions were overlooked in order to prioritize the wide variety of possible rotor designs. The goal of this approach is threefold: (1) validate the experimental methods, (2) verify that performance difference exist and can be measured between the rotors, and (3) reduce the viable field of rotor candidates for further testing and analysis. In this campaign 14 rotors were exposed to a battery of testing intended to analyze power consumption, gas dispersion, operational robustness, and batch flotation performance. The results show that while the experimental methodology may be subject to further refinement, the rotors do indeed exhibit varying levels of performance and energy efficiency. In conclusion, three of the best all-around rotors (with varying strengths and weaknesses) were selected for detailed testing.

3.1 Introduction and Scope

Prior research in froth flotation equipment has shown that slight performance differences exist between different rotor designs. Much of this work has been relegated to the pilot

scale (Gorain, Franzidis, & Manlapig, 1995a, 1995b, 1996, 1997; Gorain, Napier-Munn, Franzidis, & Manlapig, 1998) and the industrial scale (Yianatos et al., 2012). While some texts have noted differences in laboratory-scaled machines (Crozier, 1992), few provided a detailed or quantified analysis of performance capacities of particular design parameters. This manuscript provides an initial investigation into the detailed comparison of rotor design at the laboratory-scale. In addition to comparative analysis between the rotors, various dimensionless analysis has been incorporated in order to allow scaled comparison of prior and future studies.

During this research project, the laboratory evaluation of flotation rotors was conducted in two campaigns, exploratory testing and detailed testing. This manuscript describes the results and conclusions derived from the so-called exploratory testing. The primary goal of this work was to test a wide variety of rotor designs in order to establish benchmarks and ensure the veracity of the experimental and analytical methodology. Furthermore, this exploratory testing was used to identify the existence and extent of performance differences between the rotor designs, while providing evidence for the discontinued testing of fatally-flawed designs. Rather than establishing a deterministic conclusion on the single most successful rotor, this section seeks to provide a reliable means of comparison while noting the positive and negative factors which should influence the final design criteria.

In this manuscript, the results are presented individually for each of the four established performance criteria: (1) power consumption, (2) gas dispersion, (3) operational robustness, and (4) flotation performance. After establishing and summarizing these results, synthesized conclusions and observations will be noted. Chapter 4 provides a similar presentation of the data acquired from the detailed testing campaign.

3.2 Experimental Methods

An exhaustive description of the equipment, material samples, methodology, and analytical procedures has been provided in Chapter 2. To summarize, this exploratory testing campaign utilized 14 small-scale rotors, measuring 2.75 inches in diameter. These rotors were exposed to six distinct laboratory tests intended to define the four aforementioned performance criteria. Unfortunately, due to the rapid development and refinement during this phase, not all 14 rotors were evaluated by each test. Table 3.1 summarizes the test matrix used to evaluate each rotor.

Other equipment utilized in this testing phase include the generic stator model, the 9.75

Table 3.1: Exploratory Campaign Rotor Text Matrix

Rotor	**Power**	**Holdup**	**Flooding**	**Sanding (Iron Ore)**	**Sanding (Silica)**	**Batch Flotation**
SP - A1	X	X	X	X	X	X
SP - A2	X	X	X	X		
SP - A3	X	X	X	X		
SP - B1	X	X	X	X		
SP - C1	X	X	X	X		
SP - C2	X	X		X	X	X
VT - A4	X	X	X	X	X	X
VT - D1	X	X	X		X	X
VT - D2					X	X
VT - E1	X	X	X		X	X
VT - E2	X	X	X	X		
VT - A5	X				X	X
VT - B2	X				X	X
VT - A6					X	X

Table 3.2: Exploratory Testing: Power Measurement Parameters

Parameter Type	Parameter	Value
Equipment	Rotor Diameter	2.75 in.
	Tank Diameter	10 in.
	Tank Volume	9.33 L
Material	Solids Material	None
Chemical	Frother Type	None
	Collector type	None
Operational	Superficial Gas Velocity	None
	Tip Speed	1.46 to 5.0 m/s
	Reynolds Number	3.2 to 11 x 10^4

inch and 10 inch round tank configurations, the Heidolph RZR 2102 low-torque mixing unit, a bubble sampler, the low-friction shaft, and a stainless-steel variable-area air flowmeter.

3.3 Results and Discussion

3.3.1 Power Consumption

Given the role of power consumption in normalizing performance results and as a means of comparison, each rotor was first subjected to an extensive power analysis. During these tests, power consumption was determined as a function of rotor speed in the absence of forced air, solid particles, and reagents. Specific experimental details are listed in Table 3.2.

Two dimensionless numbers were used in describing data from the power studies, the Reynolds number (Re) and the power number (P_N). The Reynolds number may be calculated from the fluid density (ρ), the rotational speed (N), the rotor diameter (D), and the fluid viscosity (μ):

$$Re = \frac{\rho N D^2}{\mu}. \tag{3.1}$$

Additionally, the power number may be calculated from the power draw (P), the fluid

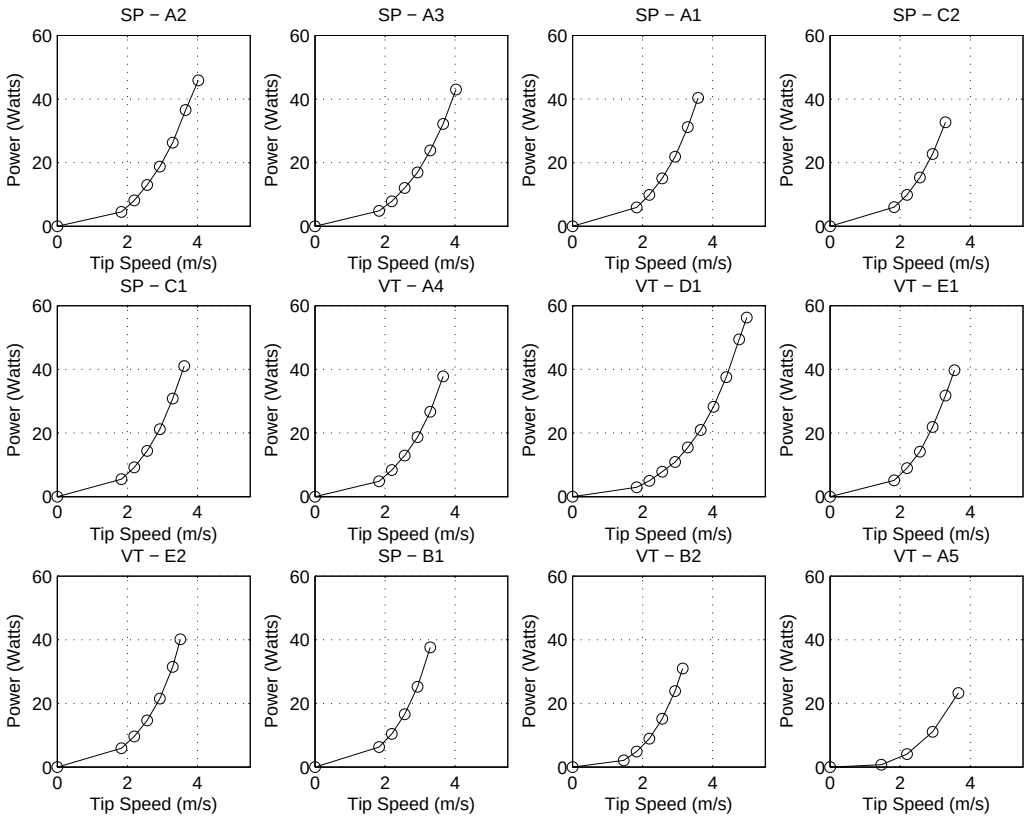

Figure 3.1: Measured power draw plotted against tip speed for each rotor included in exploratory testing. Tests were conducted in a 9.33 liter tank in the absence of air, solids, and reagents. All rotors were 2.75 inches in diameter.

density, the rotational speed, and the rotor diameter:

$$P_n = \frac{P}{\rho N^3 D^5}. \tag{3.2}$$

Figure 3.1 shows the power versus tip speed data plotted individually for each rotor. Figure 3.2 shows the same data plotted dimensionlessly as power number vs. Reynolds Number. The average power number shown on the graph was determined by finding the simple arithmetic mean of the power numbers over the full speed range.

Results from the exploratory testing indicate that all rotors generally retain a cubic relation between speed and power, confirming the $P \propto N^3$ relationship (Tatterson, 1991, 1994). Furthermore, all rotors are roughly within a comparable range of power numbers:

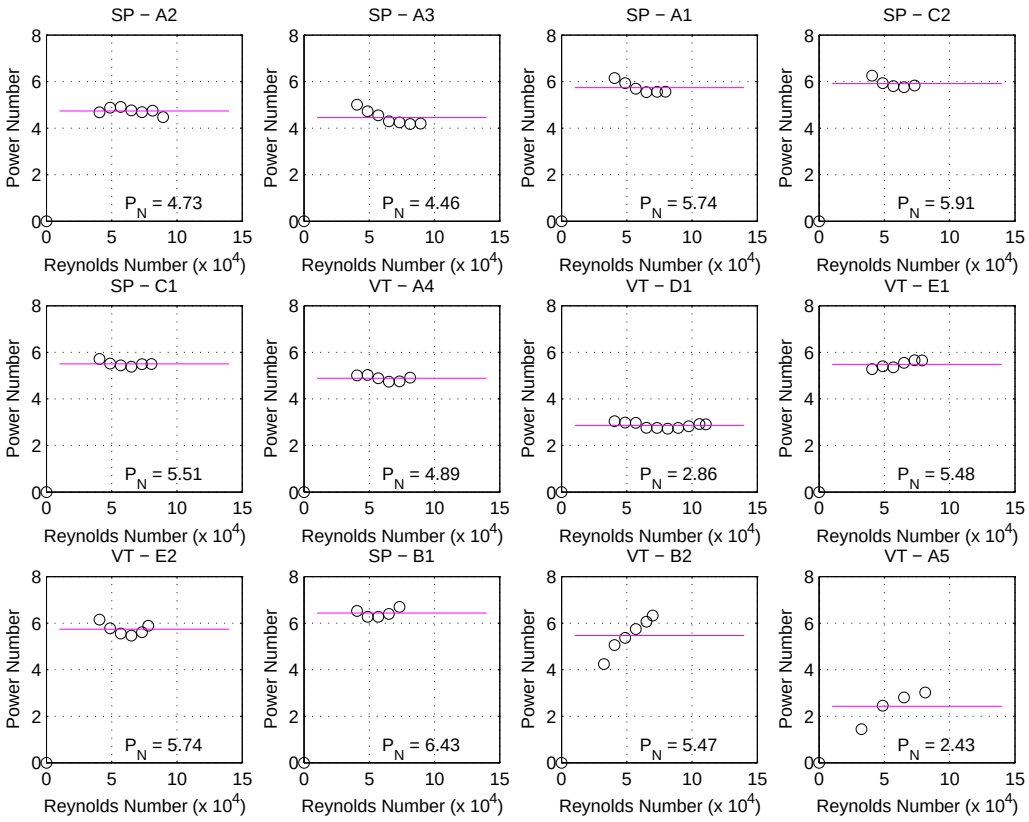

Figure 3.2: Dimensionless power plotted against Reynolds number for each rotor included in exploratory testing. The pink line and the printed value show the average power number for the range of Reynolds numbers shown. Tests were conducted in a 9.33 liter tank in the absence of air, solids, and reagents. All rotors were 2.75 inches in diameter.

Table 3.3: Summary of Power Numbers Collected in Exploratory Testing

Rotor	**Average Power Number**	**Standard Deviation (%)**	**Number of Measurements**
SP - B1	6.43	2.82	5
SP - C2	5.91	3.4	5
SP - A1	5.74	4.32	6
VT - E2	5.74	4.43	6
SP - C1	5.51	2.06	6
VT - E1	5.48	2.92	6
VT - B2	5.47	13.79	6
VT - A4	4.89	2.51	6
SP - A2	4.73	3.06	7
SP - A3	4.46	7.11	7
VT - D1	2.86	4.02	10
VT - A5	2.43	28.79	4

the average power number for 9 of the 12 rotors fell between 4.00 and 6.00. The three exceptions were the VT - D1 ($P_N = 2.86$), the VT - A5 ($P_N = 2.43$), and the SP - B1 ($P_N = 6.43$). Of these exceptions, the SP - B1 result is expected since the SP - B1 rotor has two additional blades when compared to most of the others (eight versus six blades).

Most of the rotors generally retain a constant power number over the tested speed range. The most prevalent exceptions to this behavior are seen in the VT - B2 and the VT - A5 rotor. Both of these rotors show a moderate correlation between increasing Reynolds number and increasing power number. Theoretically, the power number should remain constant over this speed range (Tatterson, 1994). As a result, the perceived correlation is likely coincidental, and the average power number was still found by the simple arithmetic mean of the values over the full speed range.

Table 3.3 summarizes these results by listing the rotors in order of average power number.

Table 3.4: Exploratory Testing: Gas Dispersion Measurement Parameters

Parameter Type	Parameter	Value
Equipment	Rotor Diameter	2.75 in.
	Tank Diameter	10 in.
	Tank Volume	9.33 L
Material	Solids Material	None
Chemical	Frother Type	None
	Collector type	None
Operational	Superficial Gas Velocity	0.23 to 2.38 cm/s
	Tip Speed	1.83 to 6.58 m/s

3.3.2 Air Water Mixtures and Gas Dispersion

Each rotor's ability to effectively disperse air was determined by measuring global air hold up as a function of tip speed and air velocity. Specific experimental details are listed in Table 3.4. Air holdup was measured as a function of tip speed for two air velocities: namely 1.0 and 2.0 cm/s. Additionally, the ungassed to gassed power ratio was determined as a function of air velocity for a fixed rotor speed (700 RPM or 2.56 m/s). These data are presented by two methods in Figure 3.3 (holdup versus power draw) and Figure 3.4 (gassed power ratio versus air velocity). Missing data for the VT - E2 rotor indicates that this rotor could not overcome flooding at the given test conditions.

Figure 3.3 indicates that significant variations in gas dispersion efficiency exist between the different rotors. Generally, the air hold-up increases sharply as power is initially added to the system. This increase subsides at higher power inputs, with each rotor approaching a distinct maximum hold up value for a given air velocity. Although this general trend remains constant, some rotors were able to attain significantly higher air holdup values at similar power inputs. For the low gas velocity (1.0 cm/s), the greatest air holdup values were experienced by the SP - A3, the VT - A4, the VT - E2, and the VT - E1. At the higher gas velocity (2.0 cm/s), the SP - A1, VT - A4, and VT - D1 generally outperformed their counterparts, in terms of the maximum holdup value attained in the given range power inputs. While the VT - E2 performed well at low gas velocities, this rotor was prone to flooding at gas velocities greater than 1.0 cm/s.

Another way of interpreting the data is to interpolate (via "reverse interpolation") the

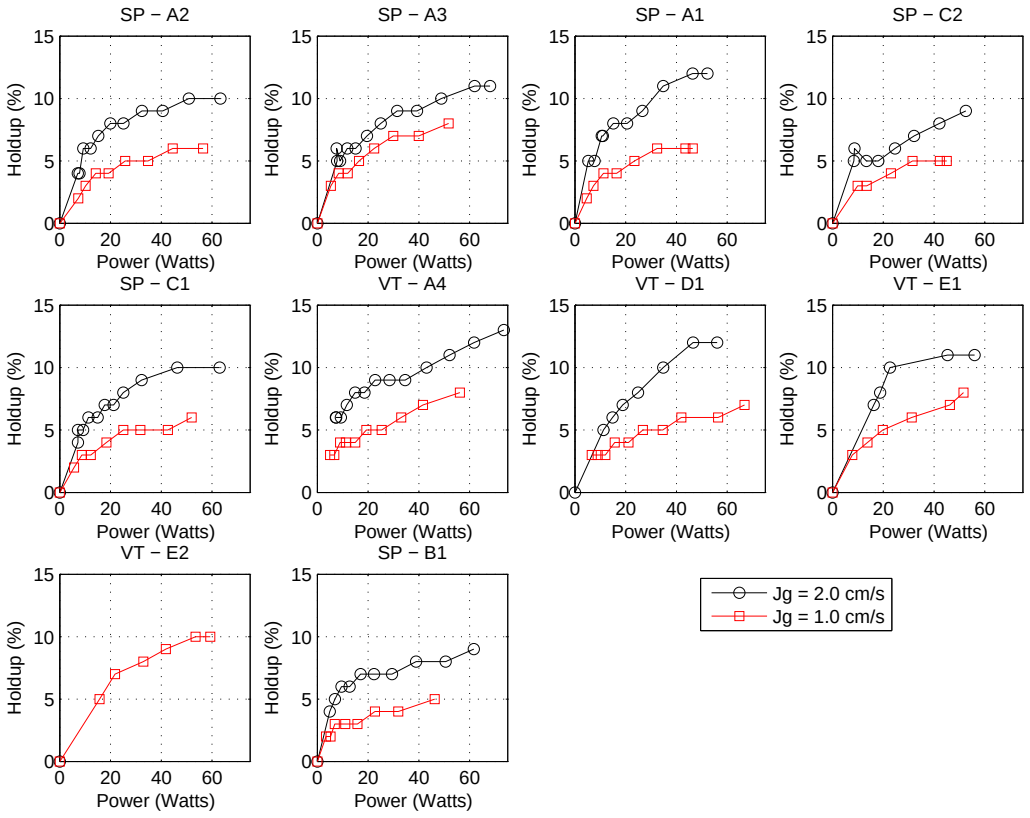

Figure 3.3: Air holdup plotted against power for each rotor included in the exploratory testing. Data is presented for both gas velocities of 1.0 and 2.0 cm/s. Tests were conducted in a 9.33 liter tank in the absence of solids and reagents. All rotors were 2.75 inches in diameter. Missing data series indicate that the select rotor could not consistently disperse air at the designated gas rate.

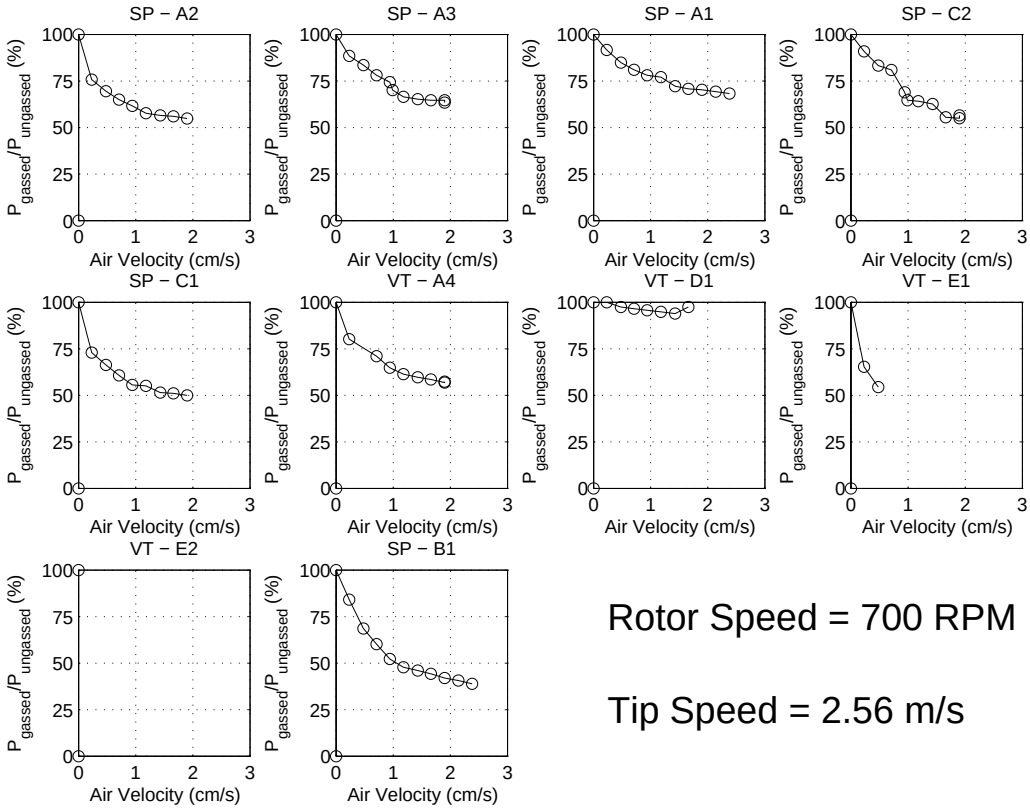

Figure 3.4: Power reduction ratio ($P_{gassed}/P_{ungassed}$) plotted as a function of air velocity. Tests were performed at a rotor speed of 700 RPM (tip speed of 2.56 m/s). Tests were conducted in a 9.33 liter tank in the absence of solids and reagents. All rotors were 2.75 inches in diameter. Missing data series indicate that the select rotor could not consistently disperse air at the designated tip speed.

Table 3.5: Summary of Air Holdup Data Collected in Exploratory Testing.

Rotor	**Power (W) to achieve 5% Air Holdup** [$J_g = 1.0$ **cm/s**]	**Power (W) to achieve 9% Air Holdup** [$J_g = 2.0$ **cm/s**]
VT - E2	15.7	–
SP - A3	16.4	31.6
VT - A4	19.4	22.8
VT - E1	19.8	20.8
SP - A1	23.5	26.7
SP - C1	25.1	32.4
SP - A2	25.9	32.5
VT - D1	26.8	30.2
SP - C2	31.6	52.5
SP - B1	46.2	61.7

power needed to attain a common air holdup between the rotors. Table 3.5 summarizes the results in this fashion by interpolating the power needed to attain 5% air holdup at a gas velocity of 1.0 cm/s and 9% air holdup at 2.0 cm/s. The decision to interpolate to these points is somewhat arbitrary, but they do represent holdup values that most rotors were able to achieve during the tests. Consequently, this listing provides a single-value summary useful for pairwise comparison. These data have been listed in the order of ascending power values for the 1.0 cm/s scenario.

Figure 3.4 shows the reduction in power draw experienced as air is added to the cell. This reduction is represented as a ratio of the power draw at the gassed condition to the power draw at the ungassed condition. This data shows similar behavior for all rotors with the exceptions of the VT - D1, the VT - E1, and the SP - B1. The VT - D1 experienced almost no reduction in power draw, while the VT - E1 experienced a much sharper drop off. The behavior of the SP - B1 rotor appears similar, but the magnitude of the power reduction is substantially greater. Once again, data was not presented for the VT - E2 since this rotor could not effectively disperse air at the given rotor speed. Furthermore, while the magnitude of the power loss is similar, the behavior of the SP - C2 appears more linear when compared to the diminishing losses of other rotors.

Table 3.6: Exploratory Testing: Flooding Condition Measurement Parameters

Parameter Type	Parameter	Value
Equipment	Rotor Diameter	2.75 in.
	Tank Diameter	10 in.
	Tank Volume	9.33 L
Material	Solids Material	None
Chemical	Frother Type	None
	Collector type	None
Operational	Superficial Gas Velocity	2.0 cm/s
	Tip Speed	1.83 to 6.58 m/s

3.3.3 Operational Limits

During the exploratory testing, the operational limits were tested to identify the relative robustness each rotor has to changing working conditions. As forced air is added or the tip speed is reduced, the flotation rotor will lose the ability to fully disperse the air and the ability to suspend solids. Either of these limits signifies a condition in which the flotation cell cannot operate normally. Depending on the specific design, each rotor inherits a distinct range of tip speeds and air velocities marked by stable operation. Ultimately, this evaluation seeks to define this two-dimensional "area-of-operation." The area-of-operation graph lends itself to quick interpretation, since a simple comparison of the area extent will yield the more proficient rotor. Simply, a larger area signifies a better rotor design, capable of operating in a wider range of conditions. Here, the two primary operational limits, the flooding condition and the sanded condition, were independently evaluated.

During this testing campaign, the flooding condition was only studied at a single gas velocity. Specific experimental details of the flooding test are listed in Table 3.6.

Data for the flooding tests are included in Figure 3.5. This data presents a one dimensional area-of-operation for each rotor at a gas velocity of 2.0 cm/s. The left side of this range identifies the onset of the flooding condition (or the critical air dispersion speed). When operated at speeds lower than this limit, the rotor cannot sufficiently break the volume of forced air. The indication of this condition is the appearance of extremely large air pockets erupting on the water surface near the shaft region (commonly called boiling, geysering, or flooding). Depending on geometry and sparger design, some rotors are more

efficient at breaking air pockets and thus have a lower critical air dispersion speed.

The right side of the range indicates the maximum speed prior to the torque limit imposed by the flotation mixer used in laboratory testing. This limit is related to the individual rotor's power draw. The RZR 2102 Mixer has a maximum torque limit of approximately 47 N-cm. The precise torque limit is somewhat dependent on the speed; this data is provided in the mixer's calibration documentation. Speeds greater than the right limit shown in Figure 3.5 exceed this torque limit. Overall, rotors that can effectively disperse air and draw less power have a wider range and greater robustness.

As shown in Figure 3.5, most rotors are able to disperse air in a comparable speed range. In exception, the SP - A1 and SP - B1 disperse air at lower speeds, potentially due to better sparging mechanisms. Additionally, the VT - A4 and the SP - A3 have the widest overall range, exhibiting the greatest combined robustness in terms of air dispersion and power consumption. The VT - E2 and the VT - E1 have the narrowest range, due to poor sparger design and high power consumption.

The second operational limit, the sanding condition, was assessed in two tests. The first test used an iron ore sample as the solid constituent. This rougher feed material is 95% passing 106 microns and has a specific gravity of 4.0. The second sanding test used 35 micron monosized silica beads. Both materials were tested over several gas velocities. Specific experimental details of both sanding tests are listed in Table 3.7.

Data from the sanding test is interpreted by two means. For the iron ore test these data are presented in Figure 3.6 and Figure 3.7. Figure 3.6 shows bar graphs for each rotor. The value of these bar graphs indicates the speed (and power) needed to completely suspend all solids from the tank floor (or critical solid suspension speed). Depending on the flow condition induced by each rotor, some are capable of suspending solids at lower speeds and powers. The data is also presented for varying air velocities. Since pumping power is reduced as air is introduced, these additional data points indicate each rotor's resilience to added air. Omission of data for individual rotors indicates the lack of a stable operating condition at the designated air velocity. Some rotors were unable to overcome the flooding condition at high gas velocities (VT - E2, VT - A4), while others exceeded the torque capacity of the mixing unit at low gas velocities (SP - B1).

The second means of interpreting sanding data is an area plot, depicted for each rotor (Figure 3.7). In this plot, tip speed is plotted on the abscissa, while air velocity is plotted on the ordinate. The boundary of the shaded area indicates the critical tip speed required for solid suspension for the designated air velocity. Consequently, the blue area represents

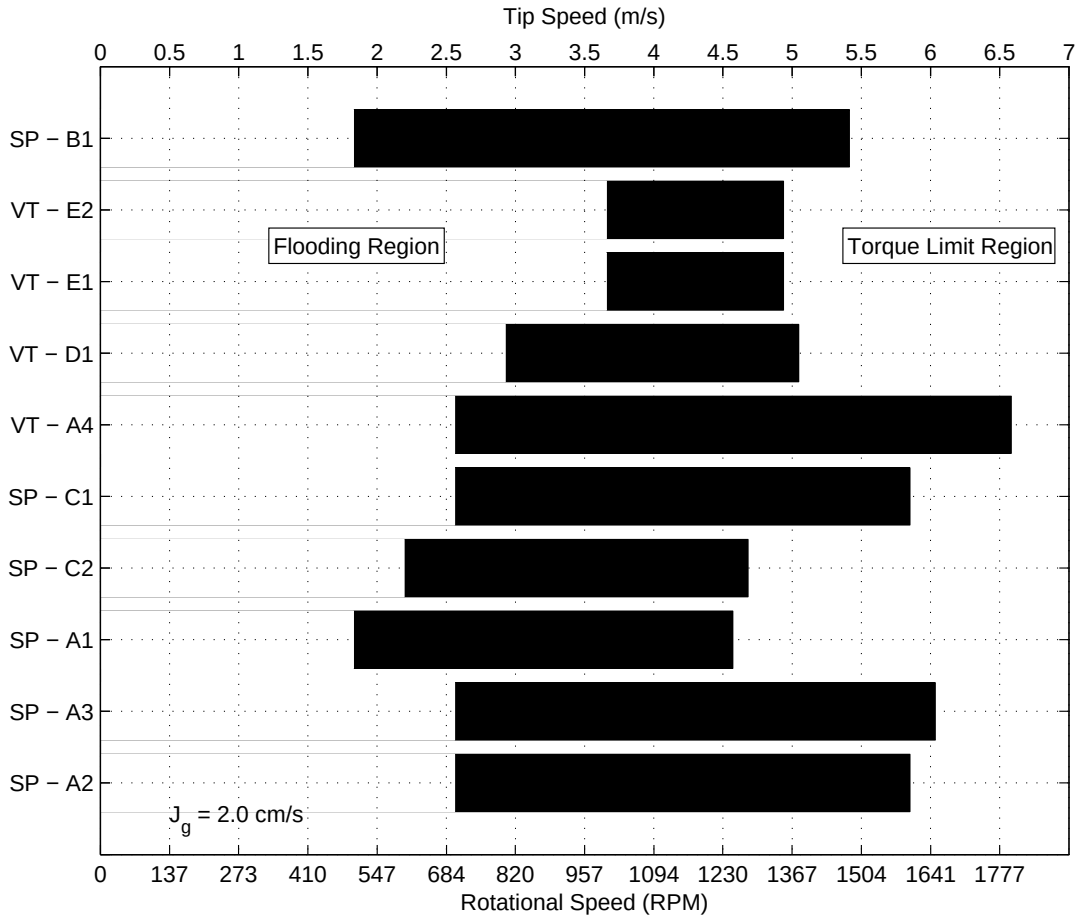

Figure 3.5: Operational limits determination for exploratory testing: onset of the flooding condition and torque limitation at a gas velocity of 2.0 cm/s. The stable area-of-operation is presented for each rotor in terms of rotational speed and tip speed. The left side of the limit signifies the critical air dispersion speed. Speeds lower than these values induce the flooding condition. The right side of the limit signifies the speed/torque limit of the mixing device. Speeds greater than this are not attainable with the RZR 2102 mixer. A wider bar signifies more robustness. All rotors were 2.75 inches in diameter. Tests were performed in the absence of reagents and solids.

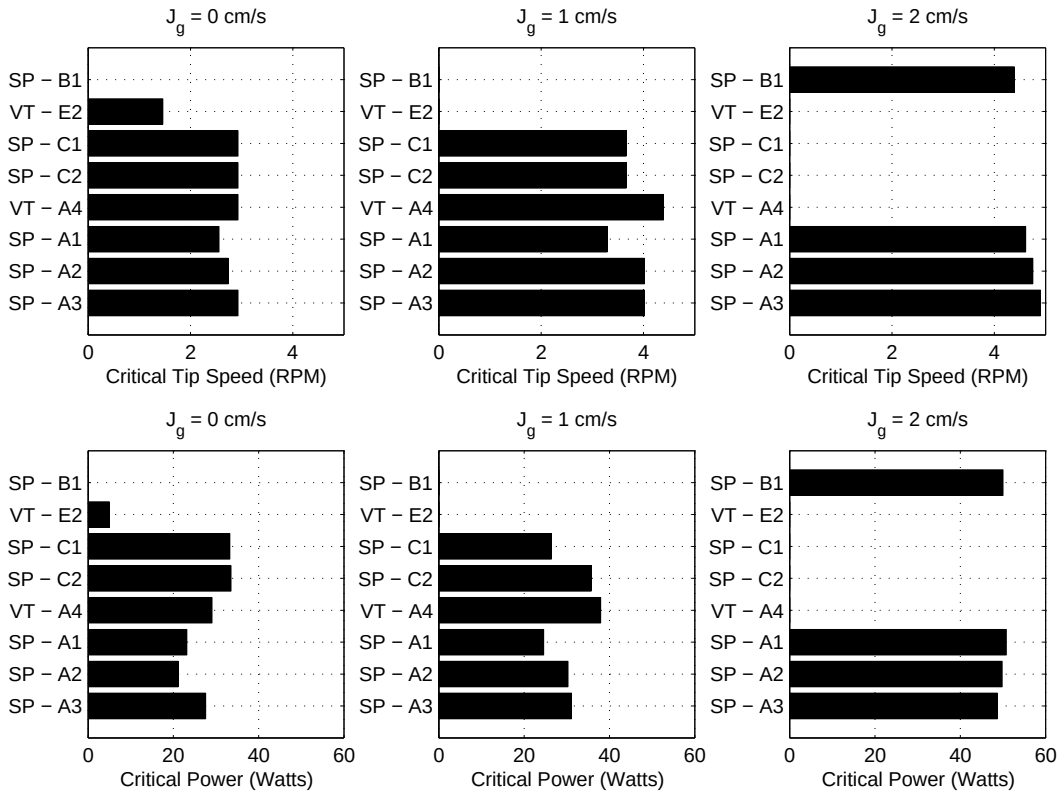

Figure 3.6: Operational limits determination for exploratory testing: iron ore sanding test bar graphs. The bar graphs indicate the critical solid suspension speed and power at the designated gas rates. Missing data series indicate that the off-bottom suspension condition was not attainable at the test conditions, due to the torque limitations of the mixer or the air dispersion limits of the rotor. All rotors were 2.75 inches in diameter.

Table 3.7: Exploratory Testing: Sanding Condition Measurement Parameters

Parameter Type	**Parameter**	**Value (Iron Ore Test)**	**Value (Silica Test)**
Equipment	Rotor Diameter	2.75 in.	2.75 in.
	Tank Diameter	10 in.	10 in.
	Tank Volume	9.0 L	9.0 L
Material	Solids Material	Iron Ore	Silica Beads
	% Solids	40%	30%
	Particle Size	95% -106 microns	35 micron
	Material SG	4.0	2.5
Chemical	Frother Type	None	None
	Collector type	None	None
Operational	Superficial Gas Velocity	0 to 2.0 cm/s	0, to 2.0 cm/s
	Tip Speed	1.46 to 4.90 m/s	1.97 to 5.27 m/s

the two dimensional area-of-operation. Area outside of the blue region is marked by some form of interoperability, either the sanded condition at low air velocities or the flooding and sanded condition at higher air velocities. At the highest air velocity tested (2.0 cm/s), the graph is extended horizontally in lieu of additional data points at greater air velocities. Comparisons between the different rotors can be made by simply assessing the relative area of each shaded region. Larger areas signify greater robustness in terms of suspending solids. Table 3.8 summarizes these results by ranking each rotor in order of operable area.

As indicated in Figure 3.6, the class A rotors performed substantially better than the other rotors tested in terms of solid suspension normalized by power consumption. The SP - A1, SP - A2, and SP - A3 rotors were able to suspend solids at a relatively low power input and maintain this solid suspension at higher gas rates. Additionally, the marked outlier of the data set, the VT - E2, was able to suspend particles at a drastically lower speed and power than its counterparts at no air flow. Unfortunately, this rotor was unable to overcome the flooding condition at higher gas rates.

In addition to the power-normalized comparisons, the family of SP - A rotors exhibited a larger area-of-operation (Figure 3.7). The SP - A1 conclusively outperforms the other rotors in terms of robustness as it relates to solid suspension.

Data for the silica sanding tests are shown in Figure 3.8 and Figure 3.9. Here the data

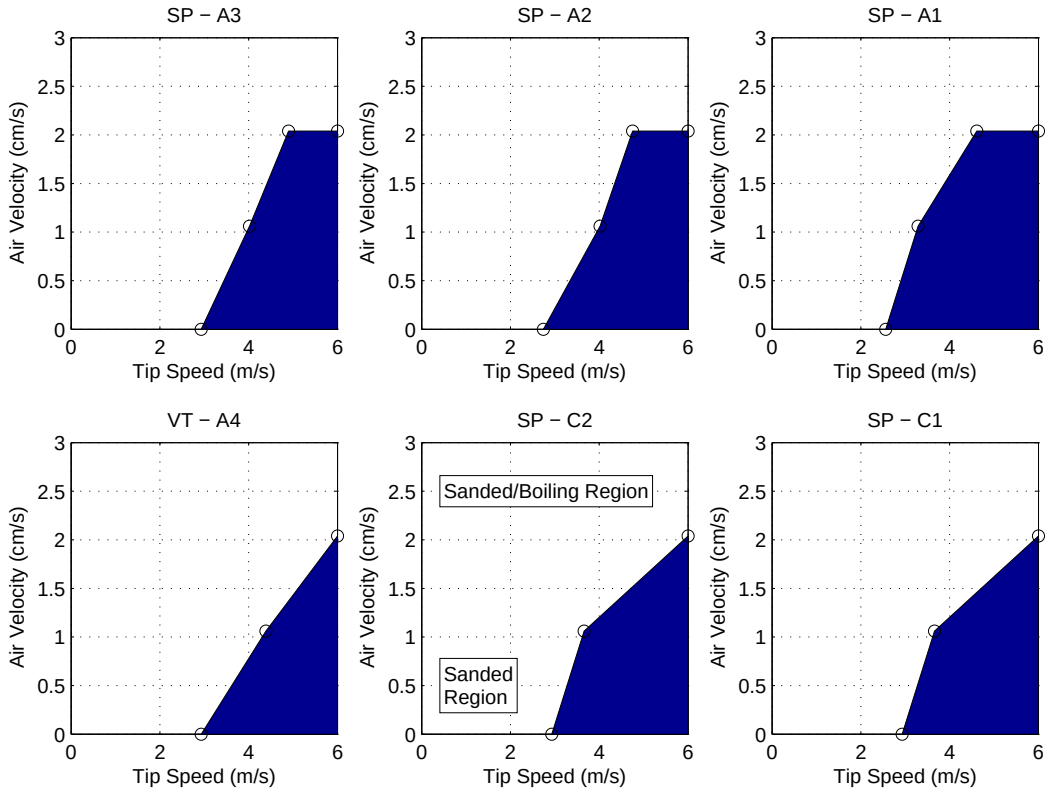

Figure 3.7: Operational limits determination for exploratory testing: iron ore sanding test area plots. The blue region indicates the combination of tip speed and air velocities required for stable operation. Areas outside of the blue region indicate the sanded region or the sanded and flooding region. All rotors were 2.75 inches in diameter.

Table 3.8: Summary of Area-of-Operation Area for Iron Ore Sanding Test.

Rotor	**Nominal Area of Stable Operation**
SP - A1	5.27
SP - A2	4.36
SP - A3	4.19
SP - C2	4.01
SP - C1	4.01
VT - A4	3.27

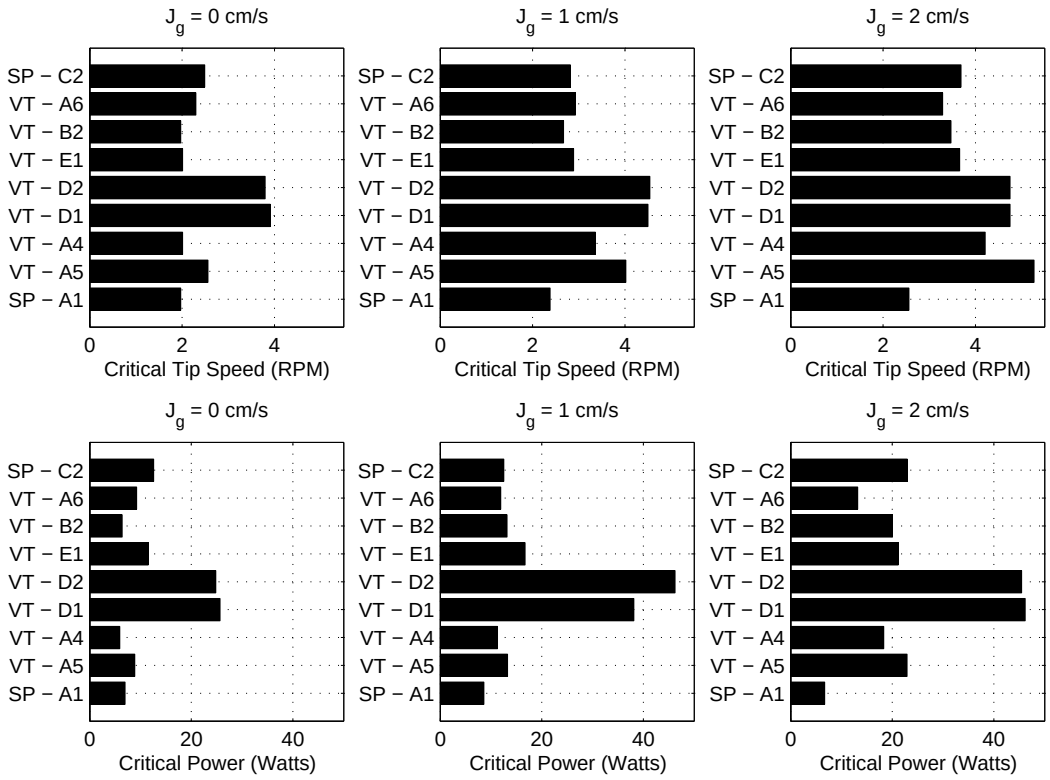

Figure 3.8: Operational limits determination for exploratory testing: silica sanding test bar graphs. The bar graphs indicate the critical solid suspension speed and power at the designated gas rates. All rotors were 2.75 inches in diameter.

is presented in similar fashion as the iron ore tests; however, more rotors were tested with this material. Since the material size and density significantly affect the solid suspension characteristics, the analysis should remain comparative between the rotors, rather than between the two tests. The data from the area plot is summarized in Table 3.9 in order of descending nominal area.

Upon examination of the silica sanding data (Figure 3.8), the VT - D1 and VT - D2 required significantly greater power and speed to suspend particles when compared to their counterparts. This trend is intensified as the air rate is increased. At high air flow rates, VT - A5 and VT - A4 also require significantly higher speeds to suspend particles; however, the power draw for these two rotors is still comparable to other designs (a result of the relatively low power number of these rotors – Section 3.3.1). Coinciding with the results of iron ore testing, the SP - A1 remains one of the leaders with regard to particle suspension, especially at high air velocities. This result is also reflected by the enlarged relative area exhibited in

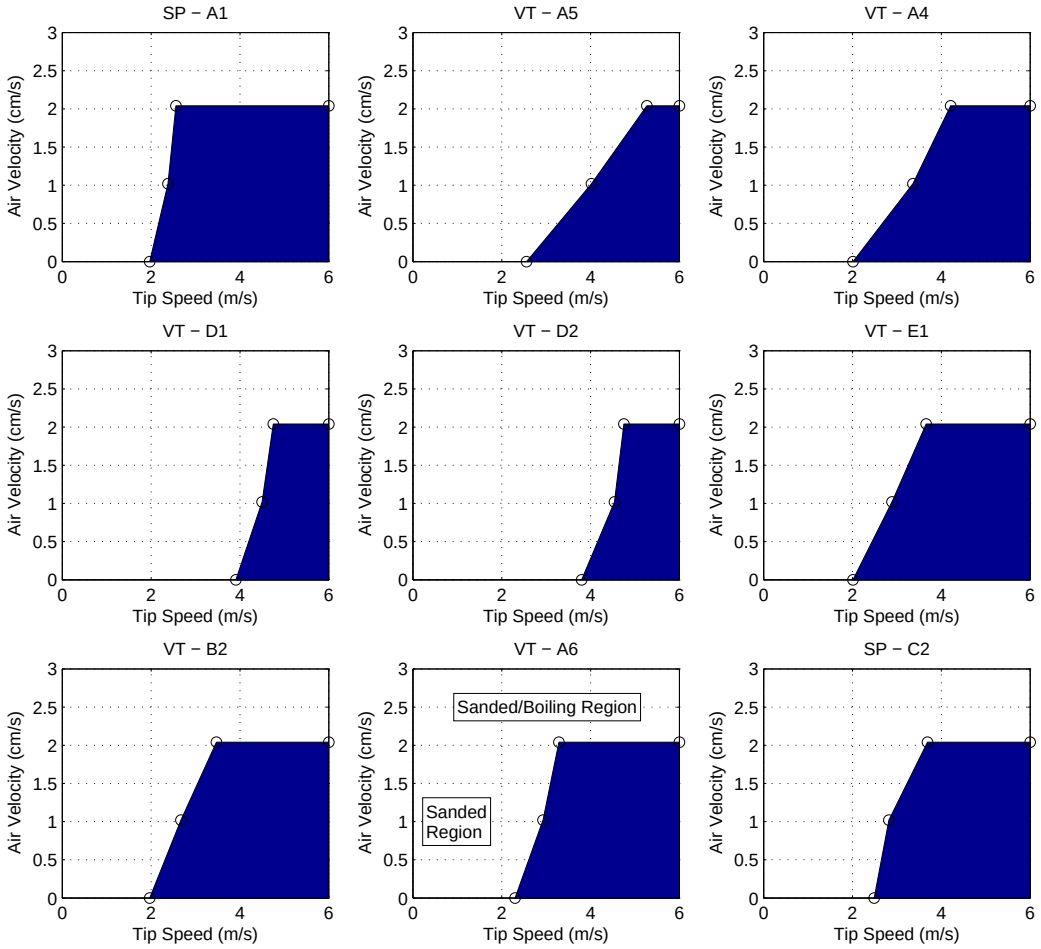

Figure 3.9: Operational limits determination for exploratory testing: silica sanding test area plots. The blue region indicates the combination of tip speed and air velocities required for stable operation. Areas outside of the blue region indicate the sanded region or the sanded and flooding region. All rotors were 2.75 inches in diameter.

Table 3.9: Summary of Area-of-Operation Area for Silica Sanding Test.

Rotor	**Nominal Area of Stable Operation**
SP - A1	7.50
VT - B2	6.74
VT - E1	6.40
VT - A6	6.40
SP - C2	6.21
VT - A4	5.64
VT - A5	4.15
VT - D2	3.25
VT - D1	3.23

the window-of-operation data (Figure 3.9 and Table 3.9).

3.3.4 Batch Flotation Performance

During the exploratory campaign, flotation performance for each rotor was determined by a series of standard batch kinetics tests. In the kinetics tests, the experimental conditions were rigidly controlled in order to form a reliable comparison between the various rotors. Each rotor was tested in identical chemical conditions and at a consistent air velocity. With these conditions fixed, each individual rotor was tested at no less than three discrete tip speeds unique to each rotor. The specific tip speeds were selected to produce flotation rate versus power curves within a similar range of abscissa values.

The material used throughout the batch tests was 35 micron silica beads hydrophobized by dodecylamine at neutral pH. Due to their purely spherical shape and small size range, this material minimizes the effects of inconsistent collector absorption. Furthermore, since the pure flotation rate is the desired response, the tests were conducted with only a single, floatable species. The absence of a hydrophilic species eliminated the need to assay the test results, hastening the data collection phase.

For the rotor comparisons, true flotation, rather than effects from the froth, was desired. Consequently, the weight percent solids was kept intentionally low (<5%) to reduce the risk

Table 3.10: Batch Flotation Test Parameters

Parameter Type	Parameter	Value
Equipment	Rotor Diameter	2.75 in.
	Tank Diameter	9.75 in.
	Tank Volume	9.0 L
	Launder Lip Length	5.0 in.
Material	Solids Material	Silica Beads
	Solids Mass	460 grams
	% Solids	4.9%
	Mean Particle Size	35 micron
Chemical	Frother Type	MIBC
	Frother Dosage	8.1 ppm
	Collector Type	Dodecylamine
	Collector Dosage	14.8 g/tonne (4.1×10^{-6} M)
Operational	Froth Depth	1.5 in.
	Superficial Gas Velocity	2.0 cm/s
	Tip Speed	2.2 to 5.9 m/s
	Flotation Time	10 to 240 sec

of froth overloading. Specific experimental details are listed in Table 3.10.

Raw data from the flotation tests are shown in Figure 3.10. Here the data is presented as cumulative recovery plotted against time for each incremental product collected during the test (10, 20, 30, 60, 120, and 240 seconds). Individual curves on each plot indicate independent tests at varying tip speeds.

Data collected up to 30 seconds consistently demonstrated first order kinetics. Consequently, these three points and the zero recovery at zero time point were used to determine the fast floating kinetic coefficient. Figure 3.11 shows $\ln(1 - R)$ plotted against time for each experiment. The kinetic coefficient was determined by finding the slope of the straight line which fits these data points.

After determining the kinetic coefficient, the data was interpreted by plotting the rate constant against the power draw for each independent test (Figure 4.3.4). Since all tests were performed under the same chemical conditions and gas velocity, the variations in kinetics can

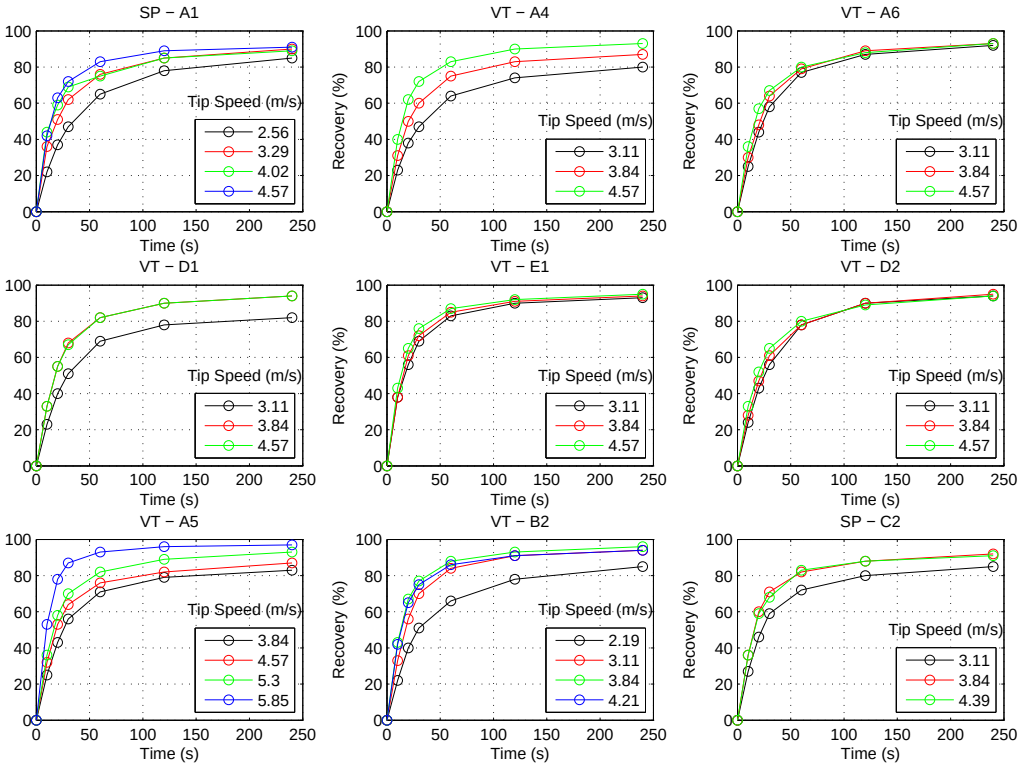

Figure 3.10: Flotation recovery plotted against time for batch flotation test. Different data series identify different tip speeds. Air Velocity = 2.0 cm/s. Solids = 35 micron monosized silica.

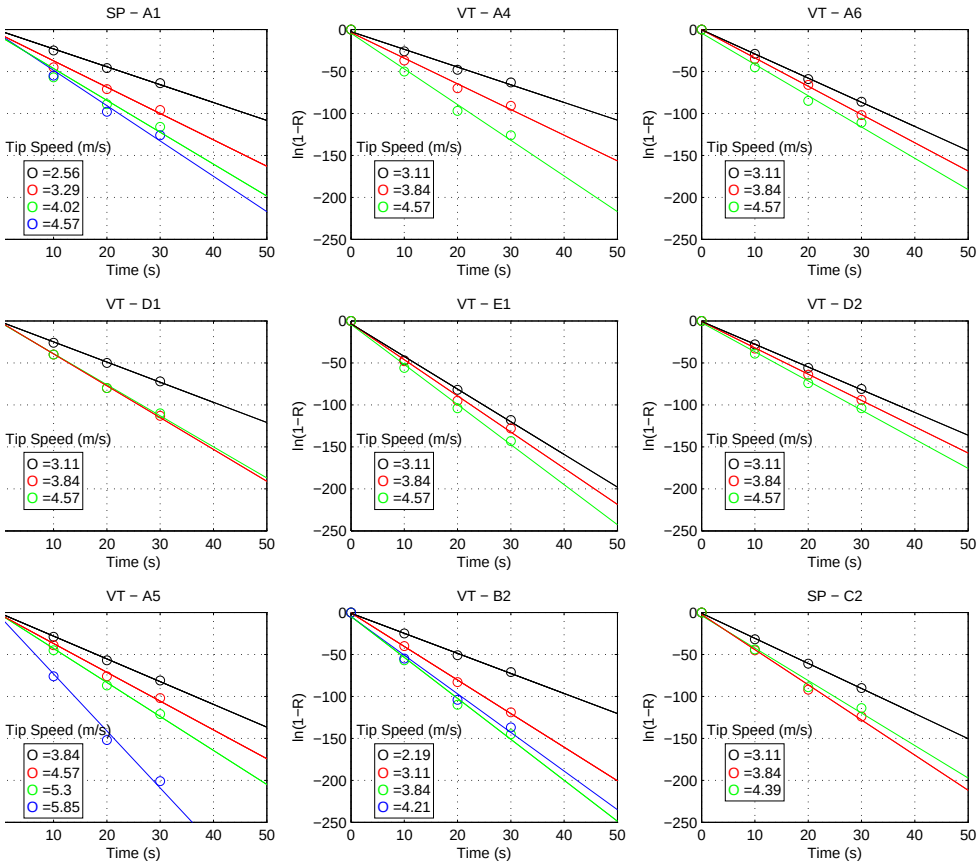

Figure 3.11: Kinetic coefficient determination for batch flotation tests. Different data series identify different tip speeds. Data is only shown for the fast kinetics range (up to 30 seconds). The kinetic coefficient is the slope of the fitted line. Air Velocity = 2.0 cm/s. Solids = 35 micron monosized silica.

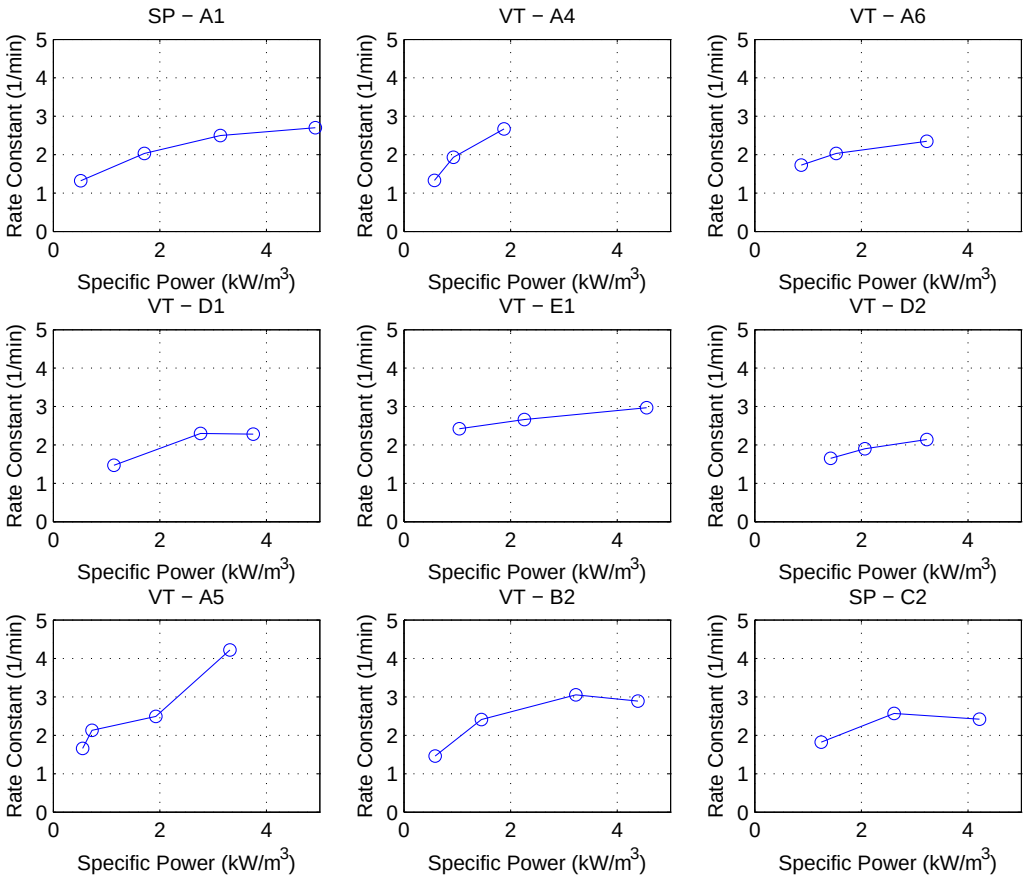

Figure 3.12: Flotation rate constant plotted against specific power for batch flotation test. Air Velocity = 2.0 cm/s. Solids = 35 micron monosized silica.

solely be attributed to changing hydrodynamic conditions. Consequently, this plot may be used to ascertain the energy efficiency of each rotor. The abscissa (power input) represents a cost. Higher power draw implies poor rotor design. The ordinate (the flotation rate constant) represents a benefit. Higher rate constants imply faster flotation and less residence time requirements. While the rate constant generally trends upward with the power input, rotors closer to the northwest corner produce higher rate constants at lower power demands.

Figure 3.13 and Figure 3.14 show the kinetics rate constant plotted against bubble surface area flux (S_b) for each rotor and all rotors, respectively. S_b is a derived term, which summarizes the air dispersion conditions in the cell (calculated as $S_b = 6J_g/d_b$, where Jg is the superficial gas velocity and db is the average bubble size). Many researchers have

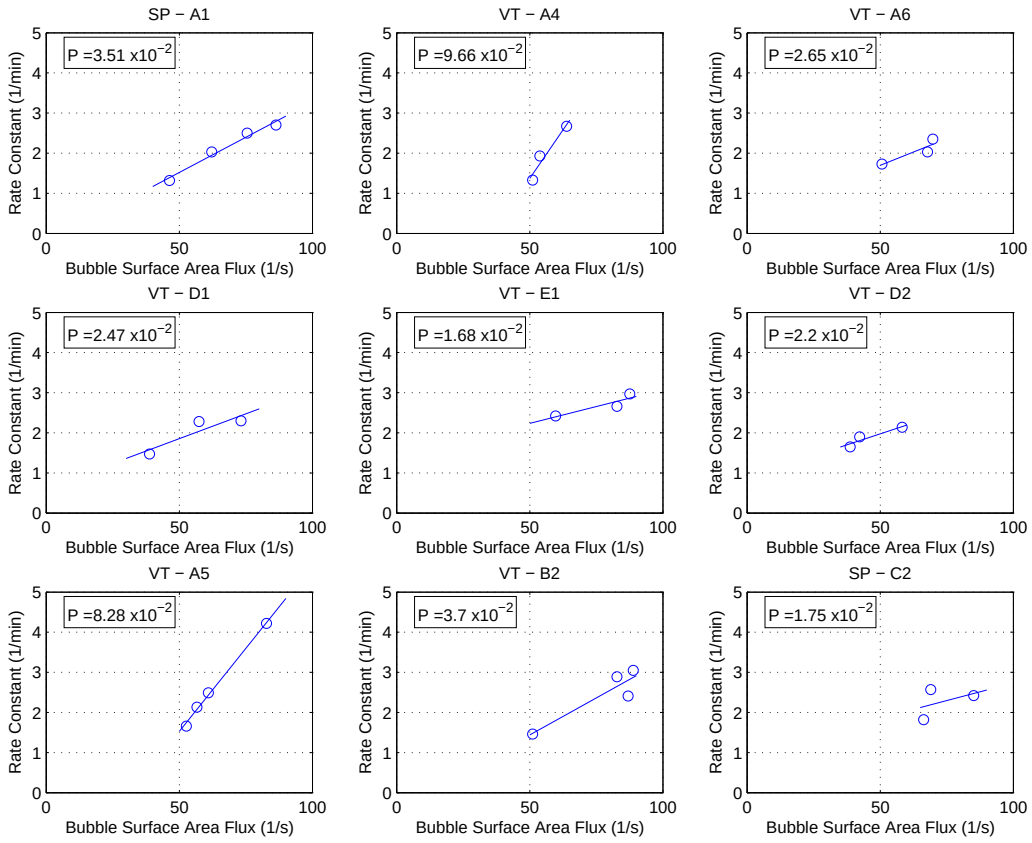

Figure 3.13: Flotation rate constant plotted against bubble surface area flux for batch flotation test (individually for each rotor). Air Velocity = 2.0 cm/s. Solids = 35 micron monosized silica.

proposed a linear relationship between k and S_b, with the slope of the line being equal to P, a term related to particle floatability (Gorain et al., 1997, 1998; Hernandez-Aguilar, Rao, & Finch, 2005; Kracht, Vallebuona, & Casali, 2005; Massinaei et al., 2009; Wills & Napier-Munn, 2006). None of the current research suggests different probabilities between different rotors.

While Figure 4.3.4 (rate constant versus power draw) assesses the energy efficiency of various rotors, Figure 3.13 assesses the hydrodynamic efficiency of the rotors. Once again, the abscissa represents a cost while the ordinate reflects a benefit. Lines exhibiting a greater slope (or P value) indicate that the rotor is capable of causing a higher frequency of fruitful bubble-particle collisions while using the same amount of bubble surface area.

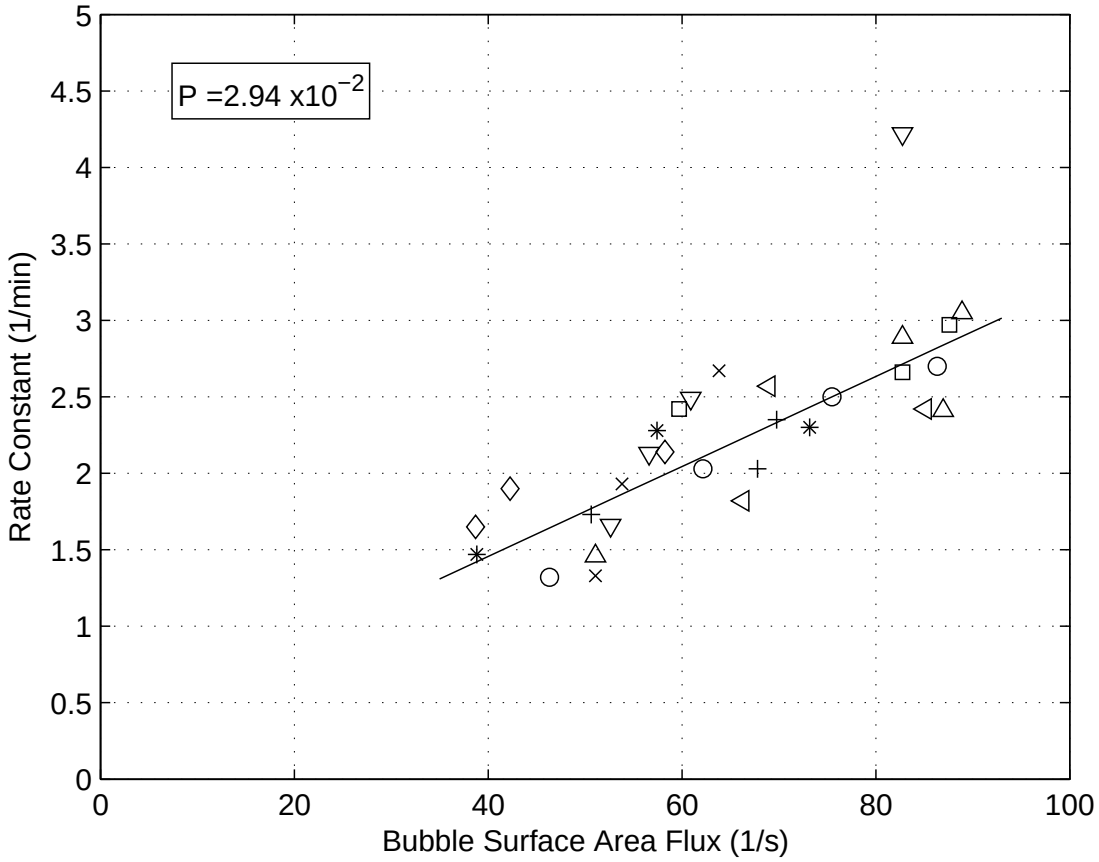

Figure 3.14: Flotation rate constant plotted against bubble surface area flux for batch flotation test (all rotors). Air Velocity = 2.0 cm/s. Solids = 35 micron monosized silica.

Table 3.11: Summary of P values determined in Exploratory Flotation Testing

Rotor	**Average P (x 10^{-2})**
VT - A4	9.66
VT - A5	8.28
VT - B2	3.70
SP - A1	3.51
VT - A6	2.65
VT - D1	2.47
VT - D2	2.20
SP - C2	1.75
VT - E1	1.68

As shown in Figure 4.3.4, the flotation rate constant generally increases with increasing power input. As the power input increases, the incremental gain in rate constant diminishes. The shape of these plots generally reflects the trends found in the air holdup versus power plots (Figure 3.3). Using the SP - A1 as a benchmark, many of the new prototypes provide significantly greater power efficiency, including VT - E1, VT - A4, and VT - A5. Other rotors, namely the VT - D1, VT - D2, and SP - C2, showed trends inconsistent with the other rotors. The VT-SB rotors only experienced marginal gains with increasing power, while the SP - C2 actually experienced a decreased rate constant at the highest power value.

Most of the hydrodynamic efficiency data coincides with the expectations presented in the literature. The slope of most $k - S_b$ plots were very similar and within an anticipated range. As shown in Figure 3.14, all of the data points, excluding the single outlier lie within a reasonable band. Nevertheless, Figure 3.13 does indicate that the VT - A5 and the VT - A4 rotors have slightly elevated P values when compared to their counterparts. This result may suggest that these rotors are capable of producing hydrodynamic conditions (i.e. fluid velocities, turbulent kinetic energies) more conducive for bubble-particle collisions and flotation. To summarize this data Table 3.11 ranks the rotors in order of the calculated P value.

3.4 Summary and Conclusions

Small-scale laboratory flotation tests were performed to assess the operational capabilities of various rotors in four performance areas: power consumption, air holdup, operational robustness, and flotation performance. In total, 14 rotors were exposed to numerous laboratory experiments. In forming a more concise and collective evaluation, both quantitative and qualitative evaluation matrices were generated (Table 3.12 and Table 3.13) from the data presented in this chapter. These tables summarize the data by integrating at least one indicative measurement from the evaluation of each of the four performance criteria. These comparisons include: average power number, single-point interpolation from the holdup versus power graph, the critical air dispersion speed, the critical solid suspension power from the iron ore sanding test, the critical solid suspension power from the silica sanding test, the average P value, and single-point interpolation from the rate constant versus power graph. While seemingly arbitrary and eclectic, the presented measurements were selected for this summary since they efficiently convey the most useful data, retain the conclusions found in the full data set, and generally preserve the paradigm of power-normalization as a basis for a fair comparison.

In this context, "single-point interpolation" provides a means of comparing an entire curve at a single point. For example, Section 3.3.2 provides curves describing air holdup as a function of power input. Since all rotors were not tested at an identical power input value, no abscissa value can be easily selected for a single point comparison. Rather, by fitting the curves with a cubic spline, the estimated power required to achieve a desired holdup can be interpolated. For the data presented in Table 3.12, the value of 9% holdup was selected, and the estimated power value was calculated. As a result, the various curves of air holdup and power are summarized at a single ordinate point, namely 9%.

Table 3.13 provides another level of simplification by categorizing the measurements into above, below, and average designations. The average designation represents the numerical values within one standard deviation of the average of all rotors for the given measurement. The above and below average designations represent those variances greater than one standard deviation from the mean.

Table 3.12: Summary of Selected Exploratory Testing Results - Raw Data

Test:	Power	Holdup	Boililng	Sanding	Sanding	Flotation	Flotation
Parameter (J_g =):	0 cm/s	2.0 cm/s	2.0 cm/s	0 cm/s	2.0 cm/s	2.0 cm/s	2.0 cm/s
Desired Result:	–	Holdup = 9.0%	Dipserse Air	Suspend Iron Ore	Suspend Silica	k = 2.0 (min^{-1})	–
Measurement:	Power Number	Power (W)	Tip Speed (m/s)	Power (W)	Power (W)	Power (kW/m^3)	Average P (x 10^{-2})
SP - A1	5.75	26.7	1.83	23.2	6.67	1.63	3.51
SP - A2	4.73	32.5	2.56	21.1	–	–	–
SP - A3	4.46	31.6	2.56	27.6	–	–	–
SP - B1	6.43	61.7	1.83	–	–	–	–
SP - C1	5.51	32.4	2.56	33.3	–	–	–
SP - C2	5.91	52.5	2.19	33.5	22.95	1.65	1.75
VT - A4	4.89	22.8	2.56	29.1	18.31	0.99	9.66
VT - D1	2.86	30.2	2.93	–	46.15	2.09	2.47
VT - D2	–	–	–	–	45.47	2.47	2.2
VT - E1	5.48	20.8	3.66	–	21.15	<1.00	1.68
VT - E2	5.74	–	3.66	4.98	–	–	–
VT - A5	2.43	–	–	–	22.92	0.68	8.28
VT - B2	5.47	–	–	–	20	1.11	3.7
VT - A6	–	–	–	–	13.19	1.45	2.65

Table 3.13: Summary of Selected Exploratory Testing Results - Comparative Analysis

Test:	Power	Holdup	Boililng	Sanding	Sanding	Flotation	Flotation
Parameter (J_g =):	0 cm/s	2.0 cm/s	2.0 cm/s	0 cm/s	2.0 cm/s	2.0 cm/s	2.0 cm/s
Desired Result:	–	Holdup = 9.0%	Dipserse Air	Suspend Iron Ore	Suspend Silica	k = 2.0 (min^{-1})	–
Measurement:	Power Number	Power (W)	Tip Speed (m/s)	Power (W)	Power (W)	Power (kW/m^3)	Average P (x 10^{-2})
SP - A1	◐	◐	●	◐	●	◐	◐
SP - A2	◐	◐	◐	◐	–	–	–
SP - A3	◐	◐	◐	◐	–	–	–
SP - B1	○	○	●	–	–	–	–
SP - C1	◐	◐	◐	○	–	–	–
SP - C2	◐	○	◐	○	◐	◐	◐
VT - A4	◐	◐	◐	◐	◐	◐	●
VT - D1	●	◐	◐	–	○	○	◐
VT - D2	–	–	–	–	○	○	◐
VT - E1	◐	●	○	–	◐	●	◐
VT - E2	◐	–	○	●	–	–	–
VT - A5	●	–	–	–	◐	●	●
VT - B2	◐	–	–	–	◐	◐	◐
VT - A6	–	–	–	–	◐	◐	◐

●= Above Average; ◐= Average; ○= Below Average

From the summary evaluations presented in Table 3.12 and Table 3.13 along with the full data set collected during the exploratory testing campaign, eight key conclusions are ascertained:

1. The experimental methodology and analytical techniques provided useful comparative data amongst the various rotor designs. The tests produced results which coincide with theoretical expectations while highlighting subtle performance efficiencies between the rotor designs.

2. Across all performance criteria, the Class A rotors performed at or above average when compared to their counterparts. Of these A rotors, the SP - A1 and the SP - A4 showed the best overall performance, with the SP - A1 excelling in the areas of air dispersion and solid suspension at high gas velocities (2.0 cm/s). As a result, the SP - A1 was chosen as an initial benchmark to compare the other rotors.

3. The high power numbers (due to the additional blades) from the Class B rotors did not necessarily correspond to proportionally enhanced performance in all areas. While both rotors were more resistant to sanding and flooding, the SP - B1's normalized performance was especially hindered by its high power consumption.

4. The Class C rotors showed similar or somewhat reduced performance compared to the class A rotors. These rotors did not excel substantially in any particular area.

5. The inconsistent and wavering results from the Class D rotors are likely due to a mechanical design and mounting flaw. Of the available models, the D class rotors are the only two that lack bottom-side suction. In theory, if centered in the tank, these rotors will intake fluid from the vertical midpoint and eject fluid from the top and bottom edges. In the laboratory setting, the rotor cannot be perfectly centered in the tank. This slight misalignment causes the rotor to intake fluid from one half of the tank while ejecting the fluid on the other side. Measurements involving visual appraisal (air holdup, sanding) or a non-radial launder (batch flotation) are subject to inconsistency, depending if the measurement is tank from the suction or the outlet side of the tank. Furthermore, the degree of radial asymmetry (and variations in flow patterns) may also significantly influence measurements not involving visual appraisal, such as power.

6. Despite enhanced performance in a limited range of conditions, the class E rotors were unable to consistently overcome the flooding condition at even moderate gas rates. As a result, these rotors were abandoned at early stages in the experimental process.

Nevertheless, the VT - E2's noted ability to suspend solids at low power inputs should prompt future design criteria with distributed suction.

7. Several rotors, including the VT - A4, VT - A5, VT - E1, and VT - B2, showed enhanced flotation performance normalized by power efficiency when compared to the benchmark SP - A1. While the full data set in the $k - S_b$ plot follows expectations consistent with the literature, individual points suggests that the VT - A4 and the VT - A5 may exhibit increased P values as a result of favorable hydrodynamic efficiency. This result should prompt further investigation.

8. Of the prototype rotors, the VT - A4 and VT - B2 are most suitable for further testing. Across all performance criteria, these rotors consistently exhibit average or above average performance. Additionally, these rotors meet practical limitations (such as fabrication and wear resistance) and exhibit a wide area-of-operation. While the VT - A5 rotor also exhibited enhanced performance in various criteria, it is not recommended for further testing due to qualitative considerations. This rotor contains thin and delicate components which may not withstand the rigors of industrial flotation (extensive wear, passing grinding media, etc.).

3.5 Bibliography

Crozier, R. (1992). Flotation. theory, reagents and ore testing. *Pergamon Press plc(UK), 1992,*, 356.

Gorain, B., Franzidis, J., & Manlapig, E. (1995a). Studies on impeller type, impeller speed and air flow rate in an industrial scale flotation cell. part 1: Effect on bubble size distribution. *Minerals Engineering*, *8*(6), 615–635.

Gorain, B., Franzidis, J., & Manlapig, E. (1995b). Studies on impeller type, impeller speed and air flow rate in an industrial scale flotation cell. part 2: Effect on gas holdup. *Minerals Engineering*, *8*(12), 1557–1570.

Gorain, B., Franzidis, J., & Manlapig, E. (1996). Studies on impeller type, impeller speed and air flow rate in an industrial scale flotation cell. part 3: Effect on superficial gas velocity. *Minerals Engineering*, *9*(6), 639–654.

Gorain, B., Franzidis, J., & Manlapig, E. (1997). Studies on impeller type, impeller speed and air flow rate in an industrial scale flotation cell. part 4: Effect of bubble surface area flux on flotation performance. *Minerals Engineering*, *10*(4), 367–379.

Gorain, B., Napier-Munn, T., Franzidis, J., & Manlapig, E. (1998). Studies on impeller type, impeller speed and air flow rate in an industrial scale flotation cell. part 5: Validation of k-sb relationship and effect of froth depth. *Minerals engineering*, *11*(7), 615–626.

Hernandez-Aguilar, J., Rao, S., & Finch, J. (2005). Testing the k-sb relationship at the microscale. *Minerals engineering*, *18*(6), 591–598.

Kracht, W., Vallebuona, G., & Casali, A. (2005). Rate constant modelling for batch flotation, as a function of gas dispersion properties. *Minerals Engineering*, *18*(11), 1067–1076.

Massinaei, M., Kolahdoozan, M., Noaparast, M., Oliazadeh, M., Yianatos, J., Shamsadini, R., et al. (2009). Hydrodynamic and kinetic characterization of industrial columns in rougher circuit. *Minerals Engineering*, *22*(4), 357–365.

Tatterson, G. (1991). *Fluid mixing and gas dispersion in agitated tanks*. McGraw-Hill New York.

Tatterson, G. (1994). *Scaleup and design of industrial mixing processes*. McGraw-Hill.

Wills, B., & Napier-Munn, T. (2006). *Wills' mineral processing technology: an introduction to the practical aspects of ore treatment and mineral recovery*. Butterworth-Heinemann.

Yianatos, J., Bergh, L., Pino, C., Vinnett, L., Muñoz, C., & Yañez, A. (2012). Industrial evaluation of a new flotation mechanism for large flotation cells. *Minerals Engineering*(0), -. Available from `http://www.sciencedirect.com/science/article/pii/S0892687512001926`

Chapter 4

Detailed Testing of Flotation Rotor Design

(ABSTRACT)

A two-part experimental analysis identifying the influence of rotor design on power consumption and metallurgical performance in forced-air flotation equipment was conducted at the laboratory scale. This manuscript describes the results for the latter experimental campaign. While the initial study emphasized numerous rotor designs, this investigation only examines three designs. These selections were chosen from the original pool of 14 rotors during the exploratory testing phase. In lieu of the various rotors, this detailed study emphasized replicate testing, broad ranges of operational conditions, and more thorough analysis. The goals of this approach are to: (1) quantify the uncertainty in the measurements, (2) determine if the measured performance variations between the rotors exceed the uncertainty, (3) develop insight on the causes of these differences, and (4) provide dimensionless relationships to guide larger scale studies. The successful completion of these goals provides design criteria and standards for future rotor prototypes. The results of this work show that each of the three rotors exhibits varying strengths and weaknesses in the performance evaluation categories; therefore, each rotor may be more or less suitable, depending on the application.

4.1 Introduction and Scope

After the exploratory test campaign, the VT - A4, VT - B2 and SP - A1 rotors were selected for further detailed evaluation. During detailed testing, analytical depth and repeata-

bility were prioritized in lieu of the numerous rotor designs tested in the prior campaign. Similar performance criteria were evaluated (power consumption, air dispersion, operational robustness, and flotation performance), but given the breadth of operational conditions examined in this phase, a more comprehensive analysis has been conducted.

The unique aspects of this study when compared with the exploratory campaign are the properly-scaled tank dimension and the use of continuous testing. In this campaign, a 14 inch diameter tank was selected for all performance measurements. While this tank size retains proper geometric similitude for the given small rotor size (Silva et al., 2012), the resulting volume (35 liters) significantly deviates from standard laboratory size expectations. Furthermore, the use of a continuous flow, two-product recycle system represented a unique challenge in materials handling and experimental setup. Nevertheless, both of these features were selected and utilized in order to more closely reflect the industrial setting, since the ultimate goal of this testing phase is to provide recommendation for industrial rotor design and commercialization.

This chapter parallels the presentation and analysis of data presented in Chapter 3, including results independently describing, (1) power consumption, (2) air dispersion, (3) operational robustness, and (4) flotation performance. Holistic conclusions and observations are presented after the individual test data.

4.2 Experimental Methods

An exhaustive description of the equipment, material samples, methodology, and analytical procedures has been provided in Chapter 2. To summarize, this detailed testing campaign utilized 3 rotors small-scale rotors, measuring 2.75 inches in diameter. These rotors were exposed to five distinct laboratory tests intended to define the four aforementioned performance criteria. All rotors were subjected to the same test matrix and many experiments included multiple replicates. Table 4.1 summarizes the test matrix used to evaluate each rotor.

The continuous flotation system constitutes all of the other equipment utilized in this testing phase. Specific components include the generic stator model, the 14 inch round tank configuration, the Caframo brushless high-torque mixing unit, a bubble sampler, the low-friction shaft, and a stainless-steel variable-area air flowmeter.

Table 4.1: Detailed Campaign Rotor Text Matrix

Rotor	**Power**	**Holdup**	**Flooding**	**Sanding (Silica)**	**Continuous Flotation**
SP - A1	X	X	X	X	X
VT - A4	X	X	X	X	X
VT - B2	X	X	X	X	X

Table 4.2: Detailed Testing: Power Measurement Parameters

Parameter Type	**Parameter**	**Value**
Equipment	Rotor Diameter	2.75 in.
	Tank Diameter	14 in.
	Tank Volume	35.3 L
Material	Solids Material	None
Chemical	Frother Type	None
	Collector type	None
Operational	Superficial Gas Velocity	None
	Tip Speed	1.46 to 6.5 m/s
	Reynolds Number	6.7 to 14 x 10^4

4.3 Results and Discussion

4.3.1 Power Consumption

Each rotor's power consumption was determined as a function of rotor speed in the absence of forced air, solid particles, and reagents. Specific experimental details are listed in Table 4.2.

During this power study, individual measurements were repeated three times, in order to evaluate the repeatability and experimental uncertainty. Figure 4.1 depicts this experimental repeatability for each rotor. In this analysis, the residual is defined as the difference between an individual measurement and the average value for identical test conditions (See Chapter 2.3.1) . This difference is expressed as a percentage of the original measurement. The values

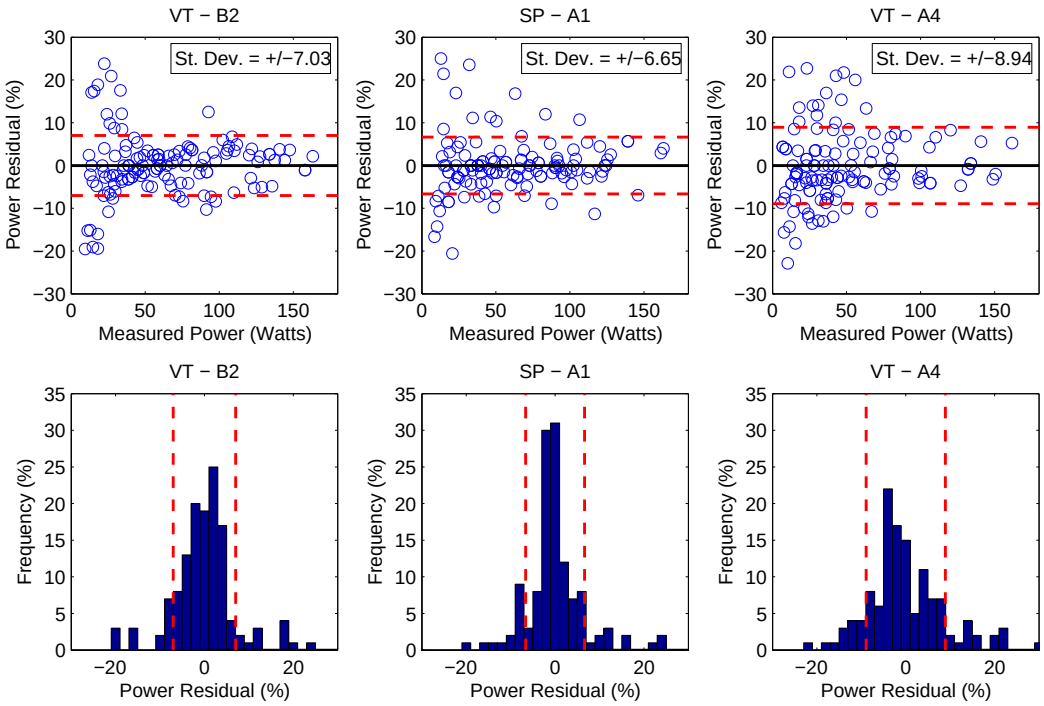

Figure 4.1: Power measurement repeatability as a function of measured power. Top: Abscissa values represent the difference between individual power measurements and the average of three measurements at the same test condition. The red lines indicate the standard deviation calculated for all residuals for the specified rotor. Different test conditions refer to specific rotational speeds and gas velocities. Bottom: Frequency diagram of the residuals. Red lines indicate one standard deviation.

in Figure 4.1 include measurements from various tip speeds and forced air velocities. The upper plots in Figure 4.1 present the residual as a function of the original measurement value. The lower plots show the frequency distribution of all residuals for each rotor. The red lines indicate the standard deviation of the population of residuals.

Figure 4.1 may be used to identify the relative repeatability of each rotor as a function of measured power. The relative repeatability of each rotor tends to increase as the measured power value increases. For all rotors, the largest residual values are found at measured power values less than 60 watts. Furthermore, the frequency distributions and the standard deviation values show that the SP - A1 provides more consistency in power measurements when compared to its counterparts. Nevertheless, most measurements show reasonable reliability. The relative residuals are normally distrusted around the mean, and since the residuals are

presented as a percentage of the original measurement, the perceived inconsistency at low power measurements actually corresponds to a relatively low absolute magnitude. Noting the results of this repeatability analysis, all power measurements throughout this testing campaign represent the average of three repeats.

The results of the power study are presented in Figure 4.2 and Figure 4.3. Figure 4.2 shows the power versus speed data plotted for each rotor. Figure 4.3 shows the same data plotted dimensionlessly as power number versus Reynolds number. The average power number shown on the graph was determined by finding the simple arithmetic mean of the power numbers over the full speed range. This power number was used to calculate the fitting line in Figure 4.2.

The results of the detailed power study generally confirm those found in the exploratory testing. The SP - A1 and the VT - B2 have similar power requirements over the tested speed range. Alternatively, the VT - A4 consistently requires less power at the same rotational speed. This result is manifested by the lower power curve (Figure 4.2) and the reduced power number (Figure 4.3). Furthermore, as shown in Figure 4.2, the power difference between the VT - A4 and the SP - A1 increases as the speed is increased.

4.3.2 Air Water Mixtures and Gas Dispersion

Each rotor's ability to effectively disperse air was determined by measuring global air hold up over a full range of tip speeds and air velocity. A full factorial experimental design was used incorporating tip speeds of 3.0, 3.5, 4.0, 4.5, 5.0, 5.5, 6.0, and 6.5 m/s and air velocities of 0, 0.48, 0.71, 0.95, 1.19, 1.43, 1.66, and 1.90, up to the operational limit of each rotor at each tip speed. Specific experimental details are listed in Table 4.3.

During detailed testing, air holdup was determined by the volume displacement method. In these experiments, individual measurements were repeated three times, in order to evaluate the repeatability and experimental uncertainty. Figure 4.4 depicts this experimental repeatability for each rotor. In this analysis, the residual is defined as the difference between an individual measurement and the average value for identical test conditions. This difference is expressed as a percentage of the original measurement. The upper plots in Figure 4.4 present the residual as a function of the measured power value. The lower plots show the frequency distribution of all residuals for each rotor. The red lines indicate the standard deviation of the population of residuals.

Figure 4.4 shows that in general, the air displacement method of determining air holdup

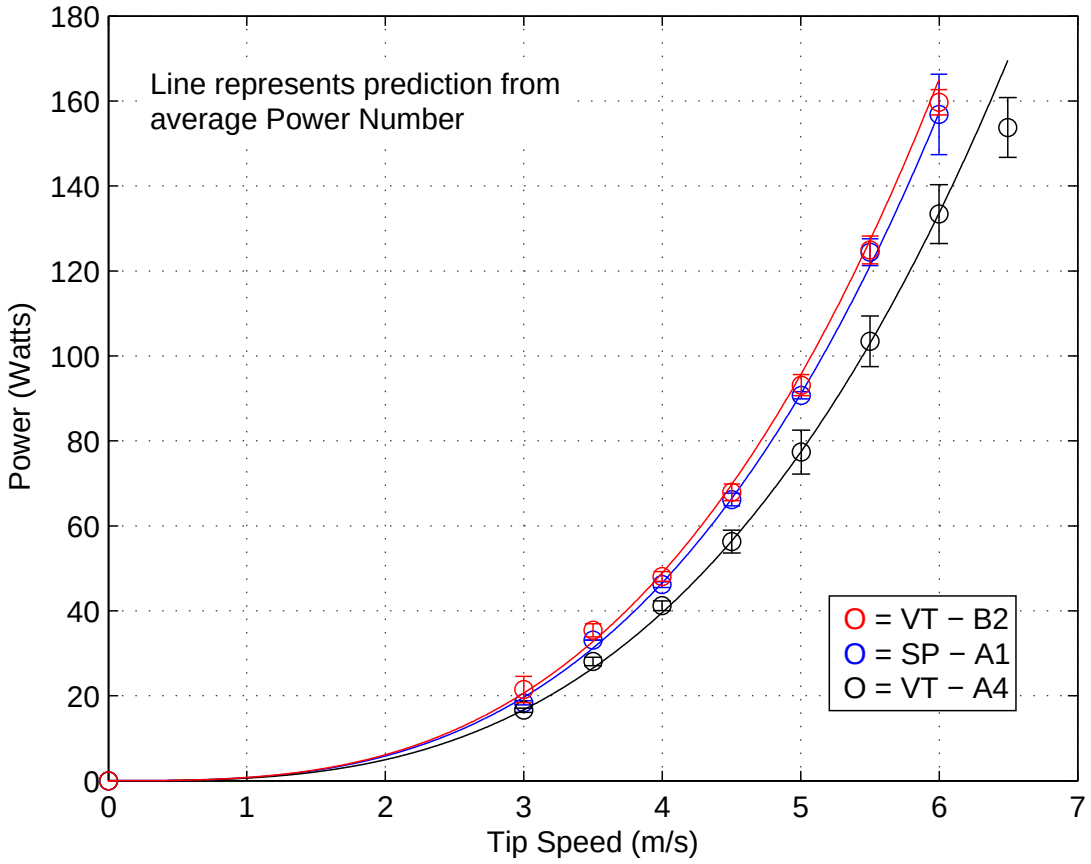

Figure 4.2: Measured power draw plotted against tip speed for each rotor included in detailed testing. Fitted lines show the prediction from the average power number. Error bars represent one standard deviation of three repeat measurements. Tests were conducted in a 35.3 liter tank in the absence of air, solids, and reagents. All rotors were 2.75 inches in diameter.

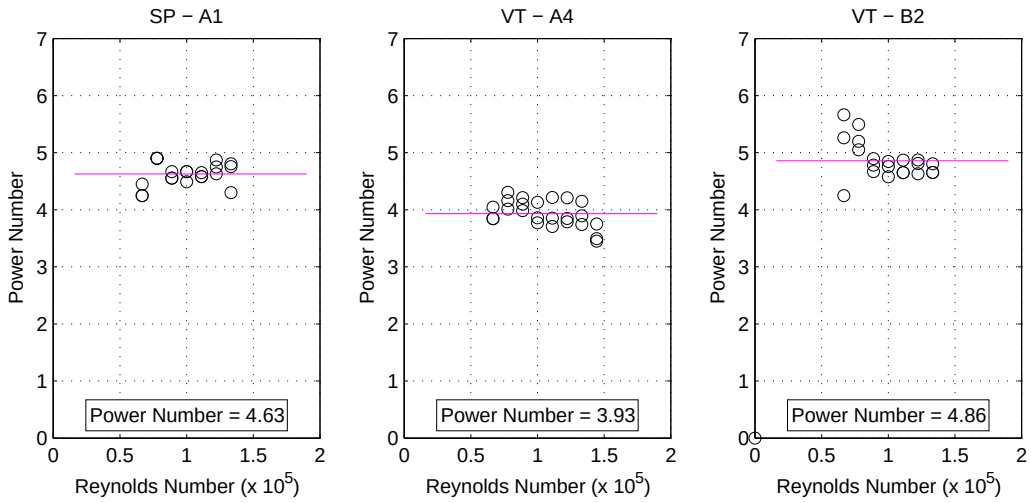

Figure 4.3: Dimensionless power plotted against Reynolds number for each rotor included in detailed testing. The pink line and the printed value show the average power number for the range of Reynolds numbers shown. Tests were conducted in a 35.3 liter tank in the absence of air, solids, and reagents. All rotors were 2.75 inches in diameter.

Table 4.3: Detailed Testing: Gas Dispersion Measurement Parameters

Parameter Type	**Parameter**	**Value**
Equipment	Rotor Diameter	2.75 in.
	Tank Diameter	14 in.
	Tank Volume	35.3 L
Material	Solids Material	None
Chemical	Frother Type	None
	Collector type	None
Operational	Superficial Gas Velocity	0.48 to 1.90 cm/s
	Tip Speed	3.0 to 6.5 m/s

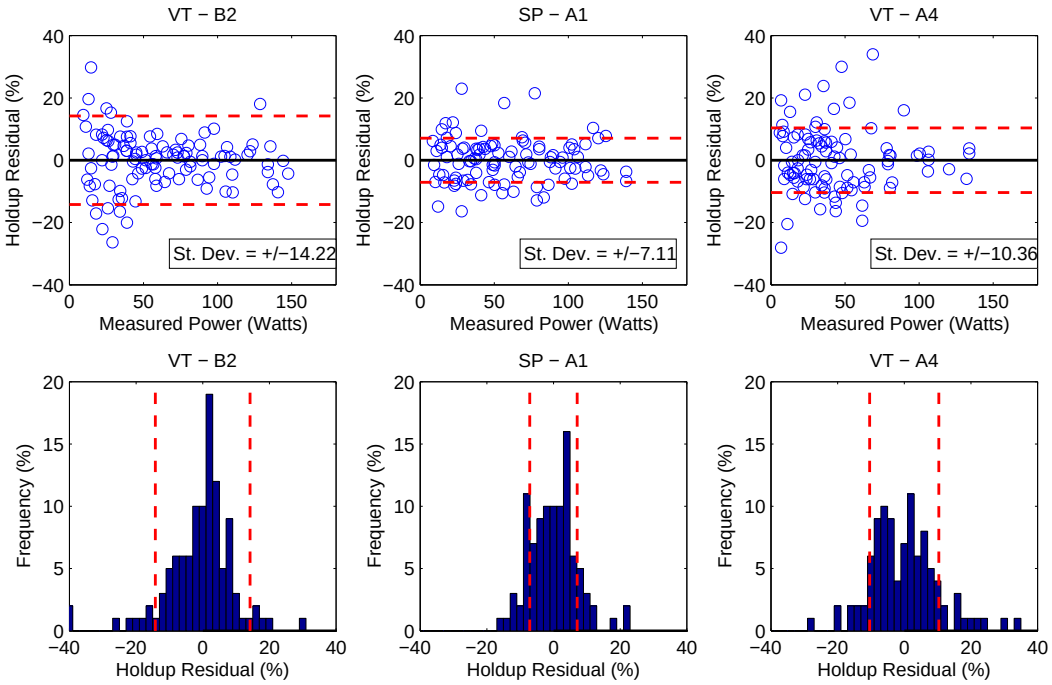

Figure 4.4: Holdup measurement repeatability as a function of measured power. Top: Abscissa values represent the difference between individual power measurements and the average of three measurements at the same test condition. The red lines indicate the standard deviation calculated for all residuals for the specified rotor. Different test conditions refer to specific rotational speeds and gas velocities. Bottom: Frequency diagram of the residuals. Red lines indicate one standard deviation.

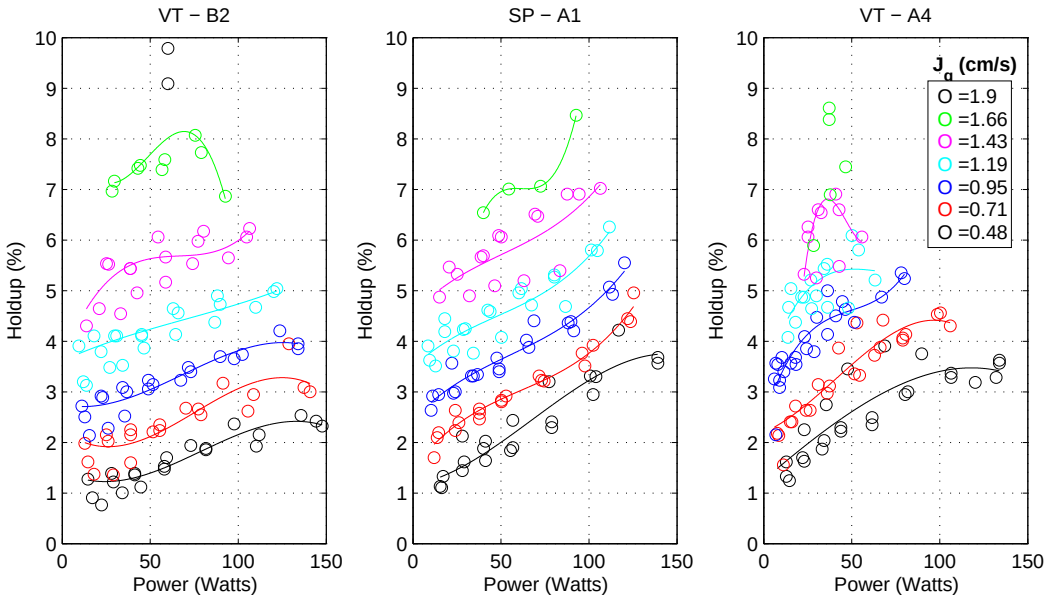

Figure 4.5: Air holdup plotted against power for each rotor included in the detailed testing. Data is presented for gas velocities ranging from 0.48 to 1.9 cm/s. Tests were conducted in a 35.3 liter tank in the absence of solids and reagents. All rotors were 2.75 inches in diameter.

is moderately reliable. The residuals are normally distributed about the mean, and of the 130 points for each rotor, only one or two lie outside the 20% residual range. The SP - A1 shows the most consistent behavior across all power ranges, while the VT - B2 and VT - A4 generally show higher residuals at lower measured power values. Furthermore, the VT - A4 has highest frequency of outliers greater than 20% residual.

Figure 4.4 plots holdup residual as a function of power. This choice of power as the independent variable depicts the most useful correlation. Similar plots, showing residual as a function of measured holdup or air velocity are more randomly dispersed and less meaningful.

Several means were used to interpret the air holdup and gas dispersion data. The most meaningful comparisons are made by analyzing data at similar rates and power draws. Figure 4.5 shows air holdup plotted against power draw. Each plot contains the data for a single rotor, and different data series show values at different air rates. This plot contains all the repeat measurements, and each data series has been fit to a cubic polynomial over the power range. Data series lacking a fit line have three or few points.

In general, the data in Figure 4.5 confirms the results of the exploratory testing. Air holdup increases with increasing power addition, and the largest incremental gains are made at relatively low power values. For many data series, diminishing returns are experienced

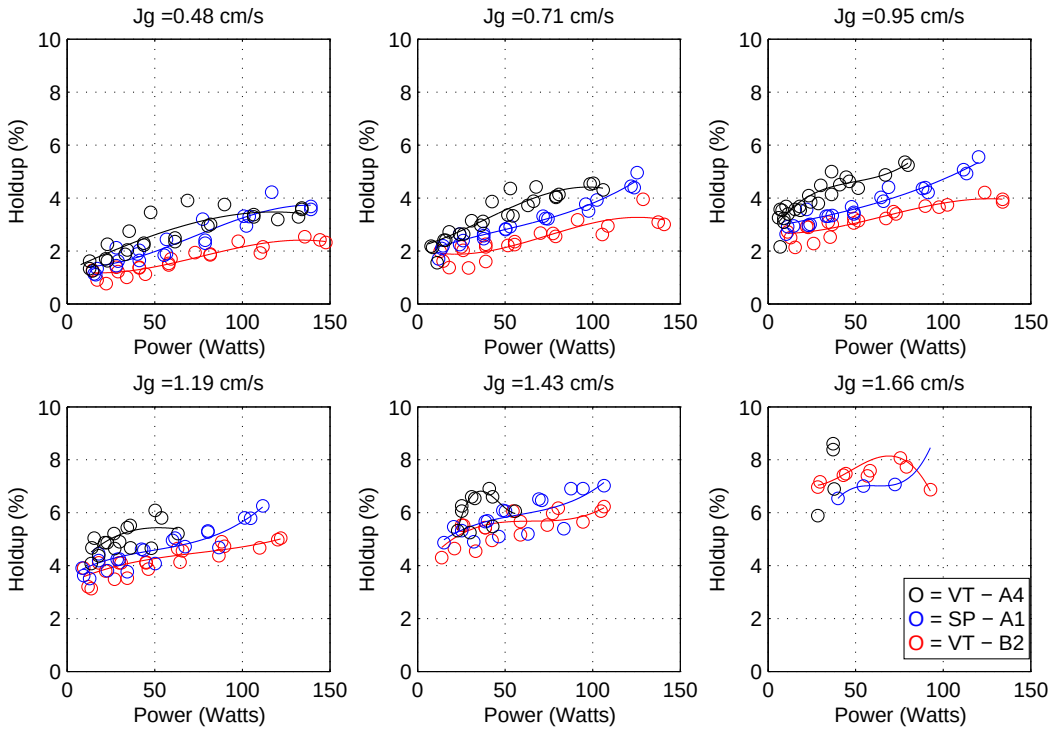

Figure 4.6: Air holdup plotted against power at various air velocities ranging from 0.48 to 1.66 cm/s for the three rotors included in detailed testing. Tests were conducted in a 35.3 liter tank in the absence of solids and reagents. All rotors were 2.75 inches in diameter.

at larger power inputs, as many of the curves begin to level (especially prominent at power gas velocities less than 1 cm/s). The incremental improvement of increasing air velocity at a constant power input can be determined by examining the length between the individual data series. Generally, larger incremental improvements in holdup are made at higher gas velocities. Finally, the general scatter in the data can be ascertained by comparing values of the same data series in Figure 4.5.

For comparative analysis, the data in Figure 4.5 was reconfigured to show data from different rotors on the same axes (Figure 4.6). Here the different data series show the different rotors, and the separate plots depict that comparison at different air velocities. Once again all repeat data has been presented, and a cubic polynomial has been fit to each data set.

Figure 4.6 consistently shows that over the collected data range, the VT - A4 rotor slightly outperforms the SP - A1, on the basis of air holdup as a function of power draw. While the SP - A1 reaches or exceeds the maximum air holdup of the VT - A4 (at a fixed

air velocity), the SP - A1 generally requires a substantially greater power requirement to do so. In example, at $J_g = 1.19$ cm/s, the VT - A4 reaches a maximum holdup of 6.09% at a power of 50.2 Watts. At the same air velocity, the SP - A1 reaches a maximum holdup of 6.26%, yet the power requirement is 111.6 Watts.

Furthermore, on the same basis of comparison, the SP - A1 consistently outperforms the VT - B2, with the exception of the highest air velocity, 1.66 cm/s. However, this air velocity only shows limited data compared to the other plots, since this condition nearly exceeded the operational limits of the machine (see Section 4.3.3).

A contour plot can also be used to visual the air holdup data and serve as a type of calibration or prediction curve for different conditions. Figure 4.7 shows air holdup plotted as a function of gas velocity and tip speed. Darker colors represent regions of low holdup, while lighter regions represent regions of higher holdup. The white region indicates the conditions in which the machine could not operate (i.e. the flooding condition). This plot may be used to identify the relative sensitivity air holdup has to changing operational conditions for each rotor. Wider contour regions indicate a lower gradient and lower sensitivity. Smaller contour regions indicate a steeper gradient and higher sensitivity. By visual comparison, the VT - B2 shows a shallower gradient at low tip speeds and gas velocities, while the VT - A4 shows a lower gradient at higher tip speeds and gas velocities. The SP - A1 maintains a roughly consistent and steep gradient across the range of tip speeds and gas velocities.

Besides air holdup, the power reduction ratio was determined during the investigations of air/water mixtures. This reduction ratio ($P_{gassed}/P_{ungassed}$) is simply defined as the power draw at an air-induced condition divided by the ungassed power draw at the same speed. Figure 4.8 and Figure 4.9 show this ratio as a function of air velocity and aeration number, respectively. The data in these plots includes tests at various tip speeds. Each data set has been fit to a cubic polynomial over the range of abscissa values. The points in the plots include repeat measurements. The ungassed condition used as the denominator in the calculations was the average of all repeats at the desired tip speed (thus, not all 0 cm/s air velocity points fall at 100%).

The apparent data scatter in Figure 4.8 shows that superficial gas velocity may not correlate fully to the power reduction ratio. Nevertheless, Figure 4.8 does show the general trend and the relative gradient of each rotor's power to induced air volume. However, since the data was collected at various tip speeds, a more appropriate correlation must also include this experimental variable. The aeration number (Q/ND^3) is a dimensionless value which accounts for volumetric air flow (Q), rotational speed (N), and rotor diameter (D). Figure 4.9 shows the power reduction ratio as a function of aeration number. Since this plot is

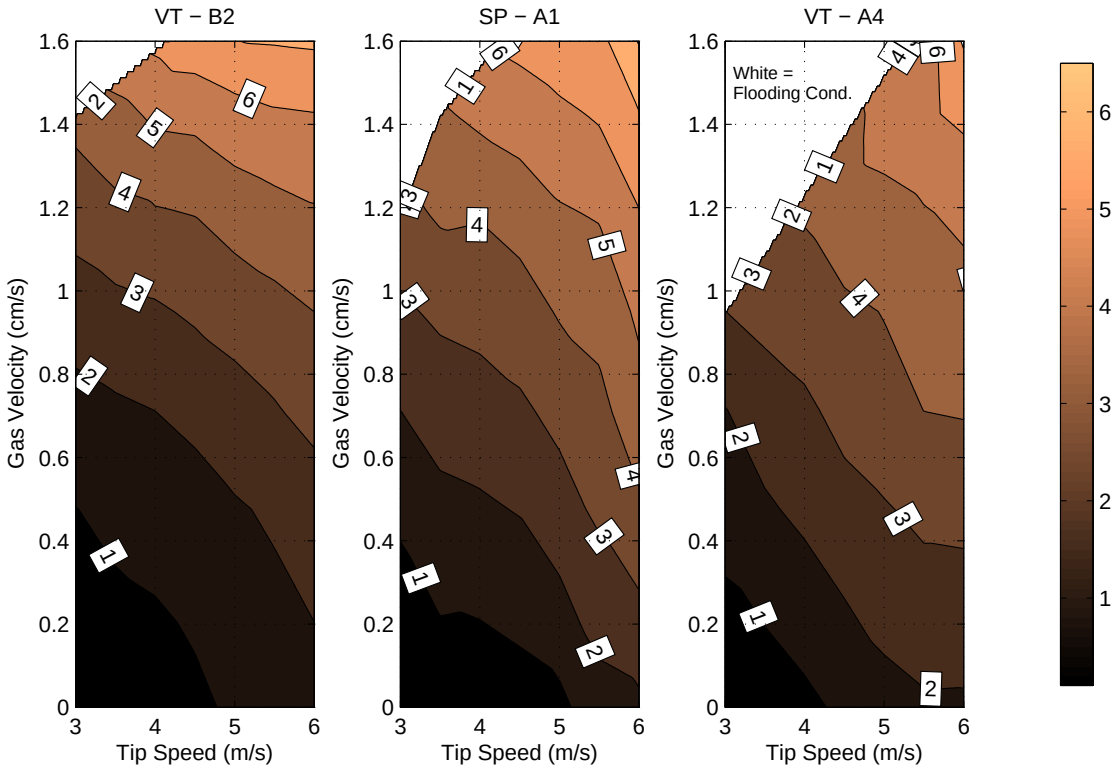

Figure 4.7: Contour plot showing air holdup as a function of both tip speed and gas velocity. The color pattern designates lighter colors as regions of high air holdup and darker colors as regions of low air holdup. Regions outside the colored portion signify the flooding condition.

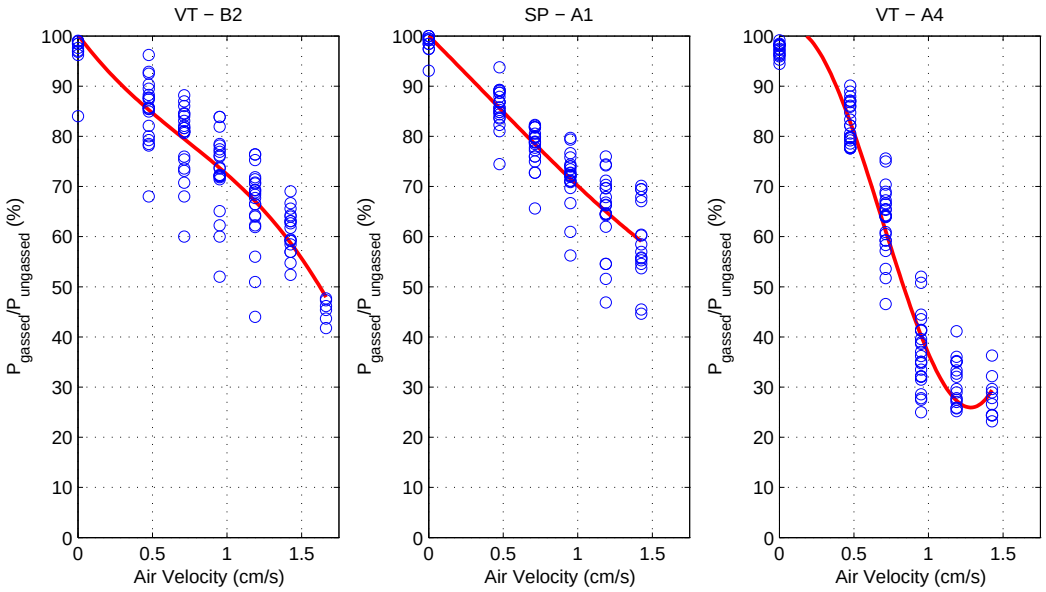

Figure 4.8: Power reduction ratio ($P_{gassed}/P_{ungassed}$) plotted as a function of air velocity for rotors included in detailed testing. Tests were performed at a various tips speeds ranging from 1.45 to 6.5 m/s. Tests were conducted in a 35.3 liter tank in the absence of solids and reagents. All rotors were 2.75 inches in diameter.

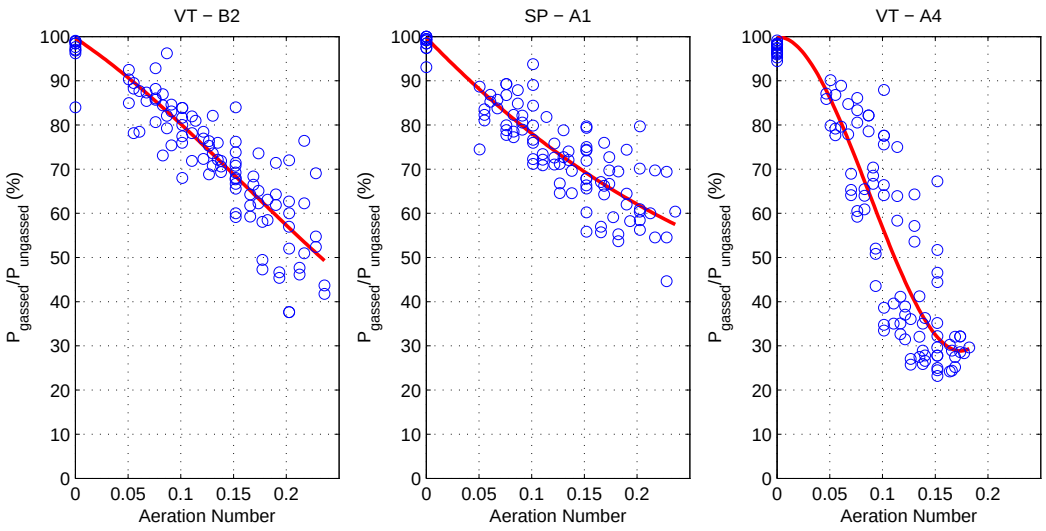

Figure 4.9: Power reduction ratio ($P_{gassed}/P_{ungassed}$) plotted as a function of aeration number for rotors included in detailed testing. Tests were performed at a various tips speeds ranging from 1.45 to 6.5 m/s. Tests were conducted in a 35.3 liter tank in the absence of solids and reagents. All rotors were 2.75 inches in diameter.

dimensionless along both axes, it should be applicable regardless of scale.

The correlation shown in Figure 4.9 depicts power reduction as a strong function of aeration number. The similarities in the slope of power reduction and the nature of the fitted function indicate that the VT - B2 and the SP - A1 are experiencing similar phenomena as air is introduced to the rotor. Over the experimental range, the power reduction of these rotors is nearly linear. Conversely, the behavior of the VT - A4 is drastically different. The slope is much steeper, the curve is obviously cubic, and the curve includes an apparent inflection point at Aeration Number = 0.088. Consequently, further investigation may show that the VT - A4 rotor may be fundamentally dispersing air differently than its counterparts. By physical comparison, the VT - A4 has wider blades, and larger air holes than the SP - A1. However from a practical standpoint, the behavior of these plots definitively indicates that the VT - A4 rotor will lose power more rapidly as air is introduced.

Another way to visualize the power reduction data is by contour plots. Similar to Figure 4.7, Figure 4.10 shows power draw as a function of tip speed and air velocity. Lighter colors in the plot indicate higher power draws while darker colors indicate lower power draws. White regions indicate the conditions in which the machines cannot operate (i.e. the flooding condition). This plot may be used to identify the relative sensitivity of power draw to changing operational conditions for each rotor. Wider contour regions indicate a

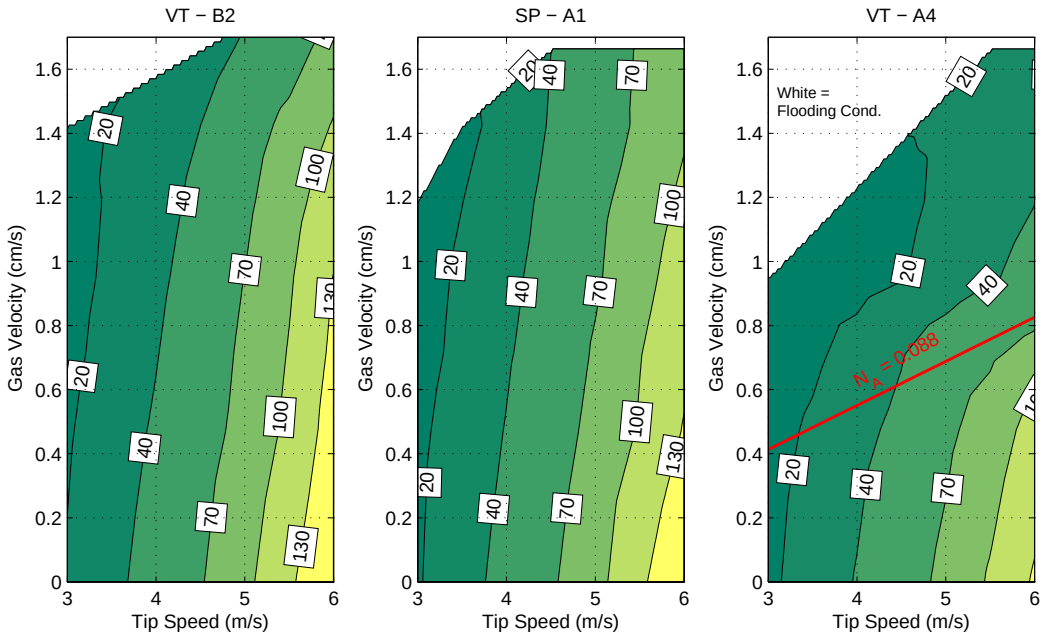

Figure 4.10: Contour Plot showing power draw as a function of both tip speed and gas velocity. The color scale signifies light color as regions of high power draw and dark colors as regions of low power draw. Regions outside the colored portion signify the flooding condition. The red line on VT - A4 indicates an aeration number of 0.088 – the coordinate of the inflection point in Figure 4.9. Power values are given in units of Watts.

lower gradient and lower sensitivity. Smaller contour regions indicate a steeper gradient and higher sensitivity. By visual comparison, the VT - B2 and the SP - A1 show extremely similar behavior over the experimental range. The VT - A4 shows similar, linear behavior up until the aeration number of 0.088 (the value of the inflection point from Figure 4.9, indicated by a red line in Figure 4.10). Above this value, the contour regions of the VT - A4 rotor show highly nonlinear behavior, indicative of the enhanced power reduction as air is added.

4.3.3 Operational Limits

During the detailed testing, the operational limits were tested to identify the relative robustness each rotor has to changing working conditions. As forced air is added or the tip speed is reduced, the flotation rotor will lose the ability fully disperse the air and the ability to suspend solids. Either of these limits signifies a condition in which the flotation

Table 4.4: Detailed Testing: Flooding Condition Measurement Parameters

Parameter Type	Parameter	Value
Equipment	Rotor Diameter	2.75 in.
	Tank Diameter	14 in.
	Tank Volume	31.5 L
Material	Solids Material	None
Chemical	Frother Type	None
	Collector type	None
Operational	Superficial Gas Velocity	1.12 to 2.42 cm/s
	Tip Speed	3.0 to 6.5 m/s

cell cannot operate normally. Depending on the specific design, each rotor inherits a distinct range of tip speeds and air velocities marked by stable operation. Ultimately, this evaluation seeks to define this area-of-operation or area of operation in the case of two dimensions (tip speed and air velocity). A larger area signifies a better rotor design, capable of operating in a wider range of conditions. Here, the two primary operational limits, the flooding condition and the sanded condition, were independently evaluated.

During this campaign, the flooding condition was studied at a range of tip speeds varying from 3.0 to 6.5 m/s at increments of 0.5 m/s. During the tests, a tip speed was set, and air was then added to the cell until the flooding condition was first witnessed. This procedure was then repeated for a new tip speed. Other specific experimental details are listed in Table 4.4.

The results of the flooding test are presented in Figure 4.11. This data presents an area of stable operation (blue region) for each rotor over the tested range of tip speeds. Conditions outside of the blue region are marked by large pockets of undispersed air erupting at the water surface near the shaft (the flooding condition). By comparing the relative magnitude of the blue areas, each rotor can be evaluated by its overall ability to overcome flooding. By this evaluation, the VT - B2 and the SP - A1 provide similar results, with the VT - B2 slightly outperforming its counterpart (nominal areas of 7.26 and 6.83 for the VT - B2 and SP - A1, respectively. Conversely, the VT - A4 shows a much greater susceptibility to flooding across the full range of air velocities (nominal area of 5.44).

As an alternate means of interpreting the data in Figure 4.11, the onset of the flooding condition can be identified as a critical aeration number, since the aeration number incor-

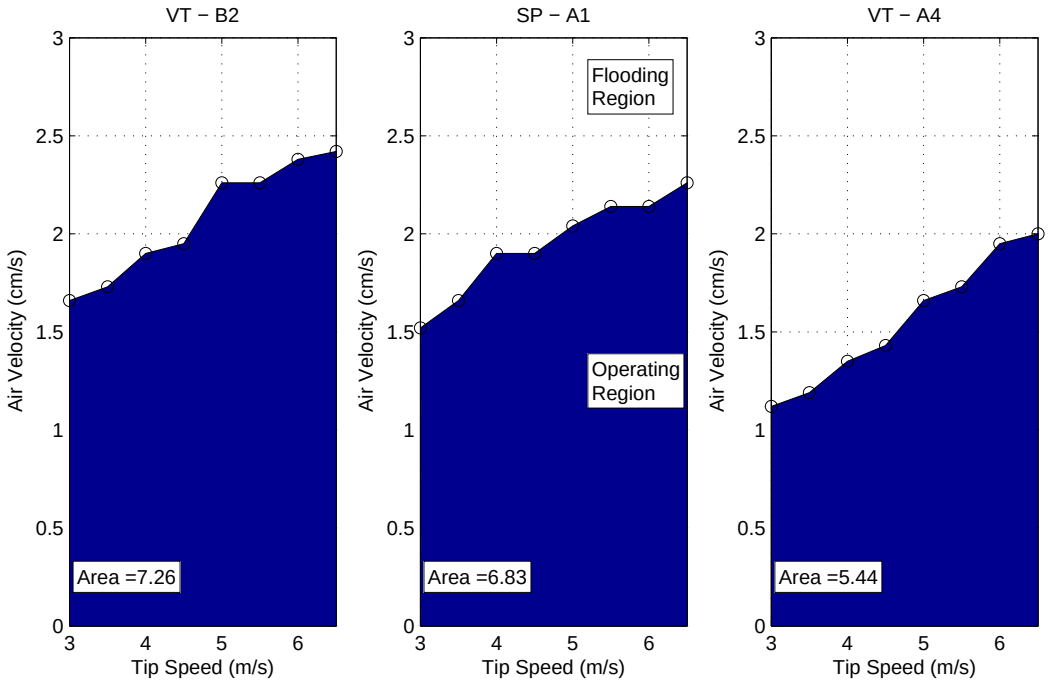

Figure 4.11: Operational limits determination for detailed testing: onset of flooding condition area plot. The blue region indicates the combination of tip speed and air velocities required for stable operation. Conditions outside of the blue region induce the flooding condition. Nominal areas of the blue regions are presented on the graphs. All rotors were 2.75 inches in diameter. Tests were conducted in the absence of reagents and solids.

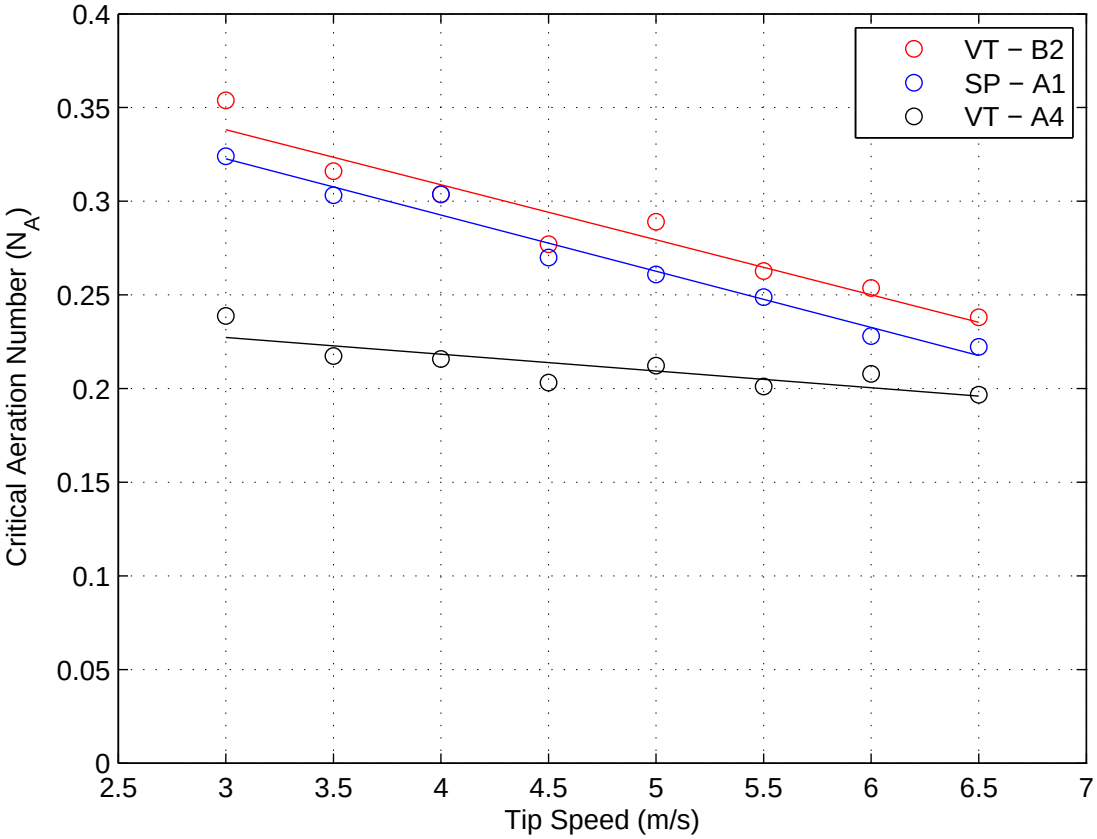

Figure 4.12: Operational limits determination for detailed testing: minimum aeration number to overcome flooding. All rotors were 2.75 inches in diameter. Tests were conducted in the absence of reagents and solids.

porates rotation speed and air flow rate. Values less than the critical aeration number are marked by stable operation, while values greater than the critical aeration number induce flooding. Figure 4.12 shows the critical aeration number as a function of tip speed.

Figure 4.12 shows that the critical aeration numbers of the VT - B2 and the SP - A1 have a stronger dependency on tip speed. Considering the calculation of the aeration number (Q/ND^3), this result indicates that for these rotors, the speed required to overcome flooding is increasing faster than the added air at flooding. While the VT - A4 shows some tip speed dependency, the slope of the fit line is much lower. As a result, the critical aeration number is relatively constant over the experimental range.

As a final strategy to normalize the flooding data, the maximum dispersible air flow

(prior to the onset of flooding) was plotted as a function of power draw (Figure 4.13). Since the power draw cannot be accurately measured at the flooding condition, Figure 4.9 was used to estimate the power draw at 80% of the critical aeration number. After the power reduction ratio was determined from Figure 4.9, the Power Number (Figure 4.3) was used to calculate the ungassed power draw at the experimental tip speed. From the ungassed power, and the power reduction ratio, the power at 80% of the critical aeration number was calculated. This procure was also repeated for the data gathered during the exploratory testing.

As shown in Figure 4.13, the maximum air flow normalizes very well to the supplied power, regardless of the rotor design. In order to disperse a given flow of air, a specific and consistent amount of power must be supplied from the rotor. Pumping affinity laws state that for a fixed pump efficiency and rotor diameter, the power is proportional to the cube of the volumetric flow. If the flooding condition is related to the volumetric flow of liquid leaving the rotor, Figure 4.13 should fit $Q = kP^{1/3}$. Since Figure 4.13 fits $Q = kP^{1/4}$, other factors may be controlling the flooding condition, the pump affinity laws do not necessarily apply to rotors, or the rotor efficiency is changing with the operating conditions.

The second operational limit, the sanding condition, was assessed using a 5.1% solids suspension of 203 micron monosized silica beads. During this testing campaign, the sanding condition was studied at a range of air velocities varying from 0 to 1.9 cm/s at increments of approximately 0.2 cm/s. During the tests, an air velocity was set, and the rotation speed was then added until no solids were persistently settling on the tank bottom. The test was then repeated at a new air velocity. Other specific experimental details are listed in Table 4.5.

Data from the sanding test is presented by two means. First, Figure 4.14 shows the minimum power required to suspend solids as a function of air velocity for each rotor. Figure 4.15 presents the suspension data as an area of stable operation, in terms of air velocity and tip speed.

Figure 4.14 indicates that the suspension capability of each rotor diminishes as air is added to the cell. As a result, more power is needed at higher air velocities to suspend the same amount of material. This result is expected since pumping capacity and energy dissipation to the fluid is reduced as air is added to the cell (Figure 4.8 and Figure 4.9). The data set here indicates that the suspension capability for each rotor is lineally diminished as air is added (with the exception of the last points in the VT - B2 and SP - A1 plots). From a comparative analysis, the VT - A4 outperforms its counterparts at low air velocities (and no air), while the VT - B2 performs better at high air velocities. The SP - A1 consistently

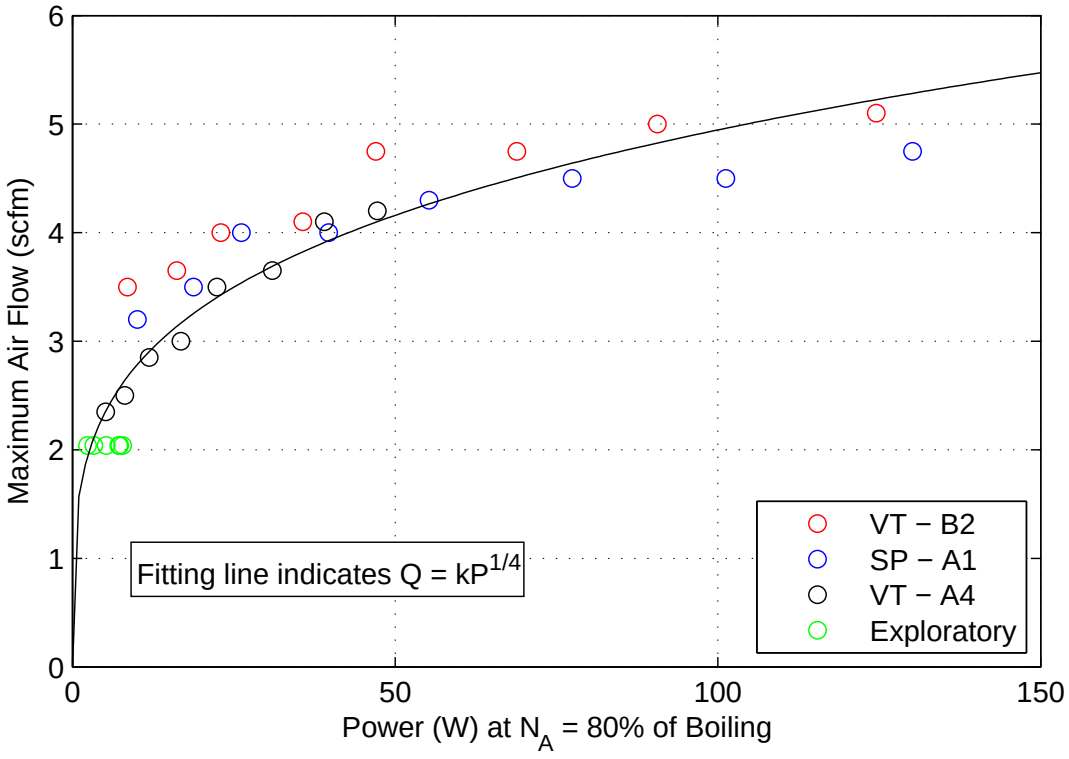

Figure 4.13: Maximum dispersible air flow as a function of supplied power.

Table 4.5: Detailed Testing: Sanding Condition Measurement Parameters

Parameter Type	**Parameter**	**Value**
Equipment	Rotor Diameter	2.75 in.
	Tank Diameter	14 in.
	Tank Volume	31.5 L
Material	Solids Material	Silica Beads
	% Solids	5.1%
	Particle Size	203 micron
	Material SG	2.44
Chemical	Frother Type	None
	Collector type	None
Operational	Superficial Gas Velocity	0 to 1.9 cm/s
	Tip Speed	3.38 to 6.58 m/s

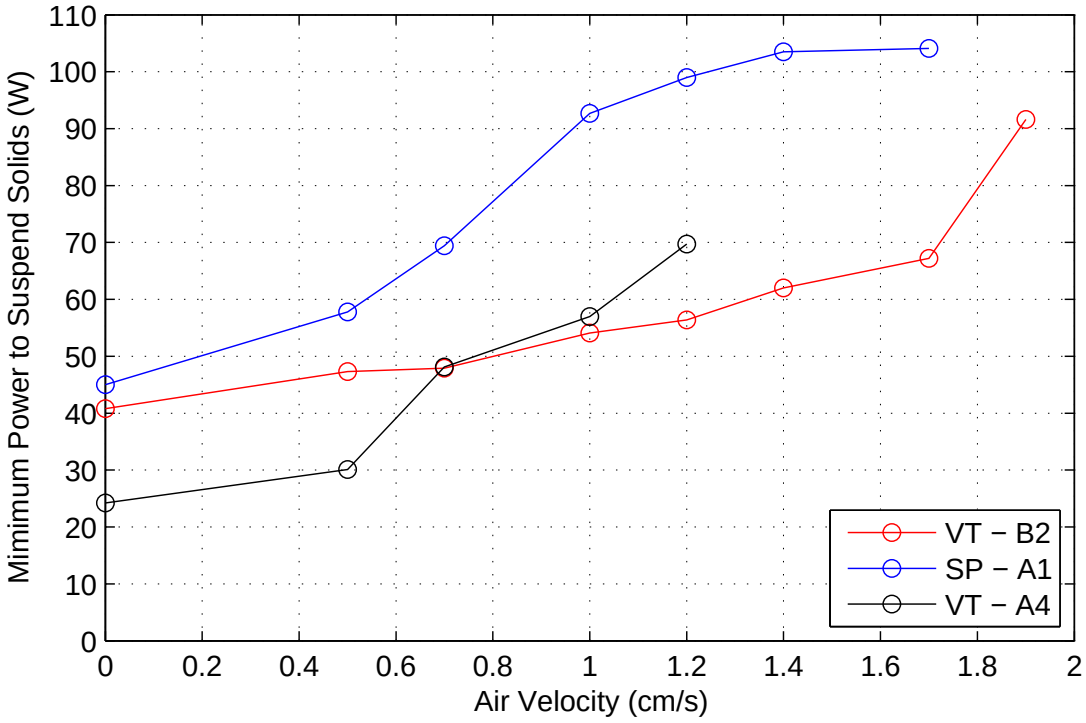

Figure 4.14: Minimum power to suspend solids plotted as a function of forced air velocity for each rotor included in detailed testing. Tests were conducted in a 31.5 liter tank in the absence of reagents.

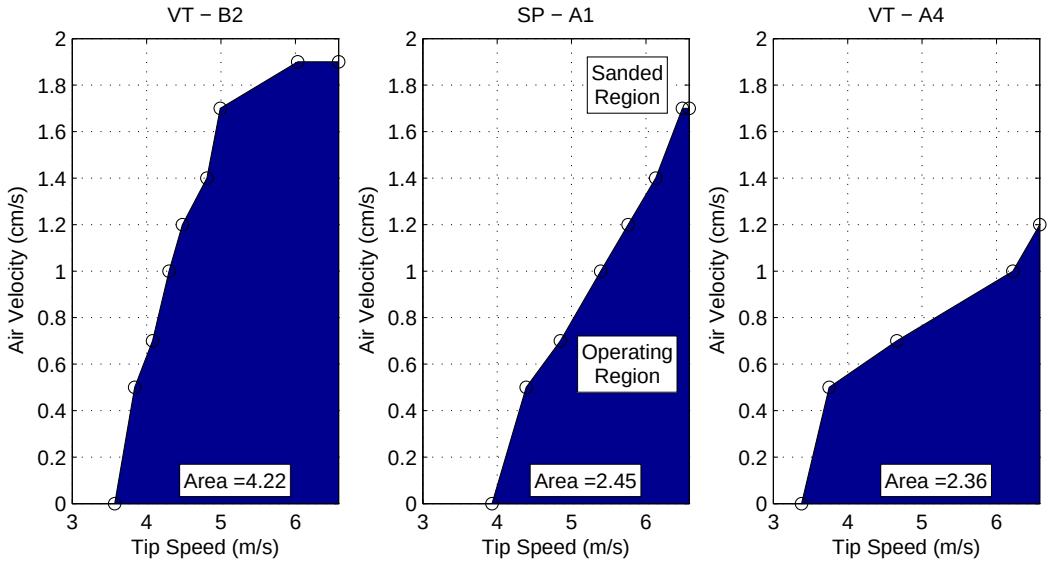

Figure 4.15: Operational limits determination for detailed testing: silica sanding test area plots. The blue region indicates the combination of tip speed and air velocities required for stable operation. Areas outside of the blue region indicate the sanded region. All rotors were 2.75 inches in diameter. Tests were conducted in a 31.5 liter tank in the absence of reagents.

requires more power to suspend solids.

Figure 4.15 shows the sanding data as area of stable operation plots. Similar to Figure 4.11, these plots depict stable operation as blue regions and inoperable (sanded) regions as white. Comparisons between the rotors can be made by evaluating the overall area of the blue regions. A larger area indicates that the rotor can operate stably over a larger range of operational conditions. By this means of comparison, the VT - B2 significantly outperforms its counterparts, nearly doubling the nominal area of the SP - A1 and VT - A4 rotors (nominal areas of 4.22, 2.45, and 2.36 for the VT - B2, SP - A1, and VT - A4 rotors, respectively).

Each plot in Figure 4.15 shows areas of linearity (tip speeds of 3.5 to 5.0 m/s for VT - B2; 4.2 to 6.5 m/s for SP - A1; and 3.8 to 6.2 m/s for VT - A4). By the orientation of this plot, a greater slope indicates that the rotor is less sensitive to air addition (a high slope is marked by a large increase in air and a small increase in tip speed). According to this comparison, the suspension capacity VT - B2 is very insensitive to air addition, since the linear portion of the graph is much steeper than the linear portion of the other graphs.

Together, Figure 4.14 and Figure 4.15 show that the VT - B2 is the better rotor in terms of solid suspension, regardless of the means of analysis. In general, the VT - B2 is

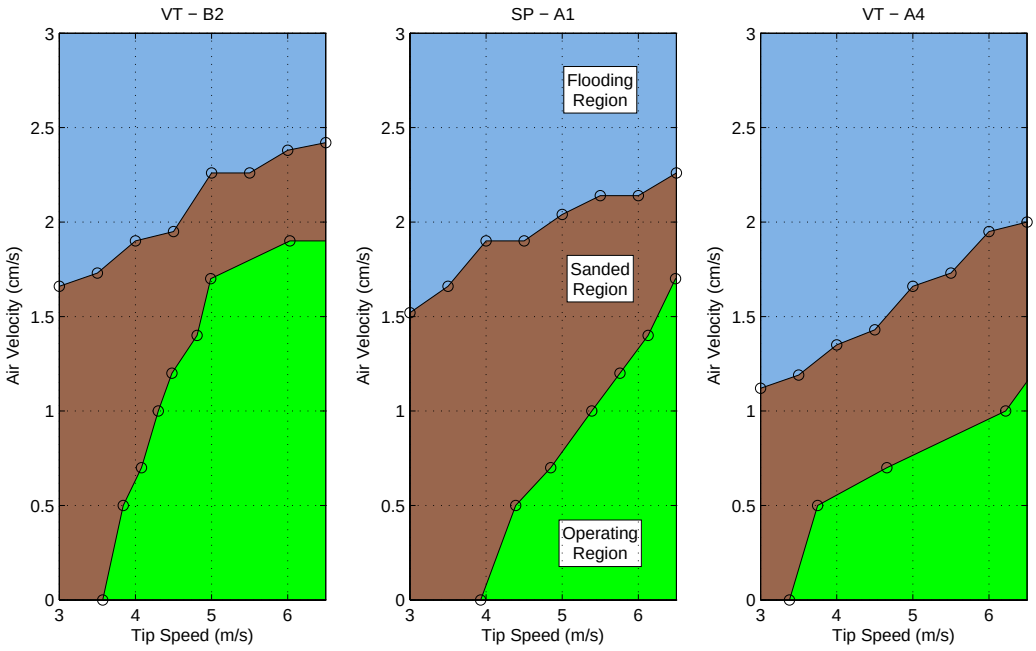

Figure 4.16: Operational limits determination for detailed testing: silica sanding and flooding area plots. The green region indicates the combination of tip speed and air velocities required for stable operation. The brown region indicates the operational conditions which will induce sanding, and the blue region indicates the flooding condition. All rotors were 2.75 inches in diameter. Tests were conducted in a 31.5 liter tank in the absence of reagents

very insensitive to air addition, given the relative slopes of both plots. This result is justified, since the VT - B2 contains additional blades and dedicated bottom-side suction. The specific components of this rotor do entail a higher power requirement (Figure 4.2 and Figure 4.3), but these suspension tests show one benefit of such a system.

To summarize the results of the flooding test and the solid suspension test, a final area of stable operation graph was generated (Figure 4.16). This plot combines the data from Figure 4.11 and Figure 4.15 to consistently and conveniently depict the relative areas of sanding, flooding, and stable operation. From this plot, the relative susceptibility to each operational limit is shown for the three rotors. This plot further supports the VT - B2 as the most operationally robust rotor, while highlighting the SP - A1's increased susceptibility to sanding the VT - A4's enhanced susceptibility to flooding.

Table 4.6: Continuous Flotation Test Matrix

Test Run	**Tip Speed (m/s)**	J_g **(cm/s)**
1	5.25	1.25
2	6.00	1.00
3	6.31	1.25
4	4.50	1.50
5	5.25	0.90
6	5.25	1.25
7	6.00	1.50
8	4.20	1.25
9	4.50	1.00
10	5.25	1.60
11	5.25	1.25

4.3.4 Continuous Flotation Performance

During the detailed campaign, flotation performance for each rotor was determined by a series of continuous flotation tests. In the tests, the experimental conditions were rigidly controlled in order to form a reliable comparison between the various rotors. Each rotor was tested in identical chemical conditions and in a consistent test matrix of tip speeds and air velocities. Table 4.6 shows this central composite experimental design. In this matrix, runs 1, 6, and 11 are repeat conditions used to assess the uncertainty of independent measurements. Overall, this experimental design was chosen to meet three primary objectives: (1) populate the flotation rate versus specific power plot at multiple air rates, (2) fully populate the flotation rate versus bubble surface area flux graph at a variety of conditions, and (3) test the rotors at extreme "corner" conditions.

Two materials were used throughout the continuous tests: 35 micron silica beads and 71 micron silica beads. The results of these tests are presented separately. Both materials were hydrophobized by dodecylamine at neutral pH. Due to their purely spherical shape and small size range, this material minimizes the effects of inconsistent collector absorption. Furthermore, since the pure flotation rate is the desired response, the tests were conducted with only a single, floatable species. The absence of a hydrophilic species eliminated the

Table 4.7: Continuous Flotation Test Parameters

Parameter Type	Parameter	Value
Equipment	Rotor Diameter	2.75 in.
	Tank Diameter	14 in.
	Tank Volume	35.3 L
	System Volume	86 L
	Launder Lip Length	44 in.
Material	Solids Material	Silica Beads
	% Solids	0.5%
	Mean Particle Size	35, 71, 203 micron
Chemical	Frother Type	PPG
	Frother Dosage	6.0 ppm
	Collector Type	Dodecylamine
	Collector Dosage	30 g/tonne (9.4×10^{-7} M)
Operational	Froth Depth	2 in.
	Superficial Gas Velocity	0.9 to 1.6 cm/s
	Tip Speed	4.2 to 6.4 m/s
	Flotation Time	2 to 4.5 min

need to assay the test results, hastening the data collection phase.

For the rotor comparisons, true flotation, rather than effects from the froth, was desired. Consequently, the weight percent solids was kept intentionally low (0.5%) to reduce the risk of froth overloading. Specific experimental details are listed in Table 4.7.

Data collected from the tests (mass flow rates and weight percent solids for the feed, concentrate, and tailings streams) was first subjected to a mass balance routine to reconcile redundancies. Mass and water recovery were then determined by comparing the concentrate flow rates to the reconciled feed flow rate.

Bubble images were collected and analyzed for each individual test run. Bubble samples were taken from the region approximately one inch below the froth, using the technique described by Hernandez-Aguilar, Gomez, and Finch (2002). Image analysis was conducted using an ellipse fitting routine presented by Fitzgibbon, Pilu, and Fisher (1999).

From the measured air velocity and bubble size, the air holdup was determined by the drift flux model presented by Banisi and Finch (1994). The reconciled tailings flow rate and the tank volume, less the air holdup were used to calculate the mean residence time. Finally, the mean residence time and the flotation recovery were used to calculate the flotation rate constant.

To complement the exploratory batch testing (Section 3.3.4), the data is presented by two means: rate constant as a function of specific power input and rate constant as a function of bubble surface area flux. Figure 4.17 shows the rate constant plotted against the specific power input for each rotor for a range of air velocities and mean particle sizes. This plot can be interpreted as an energy efficiency plot. The abscissa (power input) represents a cost, while the ordinate (the flotation rate constant) represents a benefit. More efficient curves produce a higher flotation rate at a lower power cost. The uncertainty bars in this plot indicate the relative standard deviation of each point, as determined from the repeat runs of the center point.

While the individual trends vary, the data in Figure 4.17 generally shows that the flotation rate constant increases with increasing power input. Also, in each of the six plots, the VT - A4 is capable of producing the highest flotation rates at the lowest power requirement. Conversely, the VT - B2 consistently produces the lowest flotation rate constants at relatively high specific power inputs. These results coincide with those found in exploratory testing (Figure).

Figure 4.18 shows the flotation rate constant as a function of bubble surface area flux. This plot may be interpreted as a hydrodynamic efficiency plot. Theoretically, the flotation rate constant is proportional to the bubble surface area flux via a proportionality constant (P) which accounts for ore floatability and collision frequency. Rotors which produce a greater slope are capable of inducing a hydrodynamic environment which is more favorable for collisions. The uncertainty bars in this plot indicate the relative standard deviation of each point, as determined from the repeat runs of the center point.

Figure 4.18 presents results comparable to those found in exploratory testing (Figure 3.13). While the relative magnitudes are dissimilar, both the batch testing and both instances of continuous testing show that the VT - A4 has an increased P value when compared to the other rotors. Once again, this data indicates that the VT - A4 is capable of producing hydrodynamic conditions (i.e. fluid velocities, turbulent kinetic energies) which are more conducive for bubble-particle collisions and flotation.

Unfortunately, though, the scatter of the data presented in Figure 4.18 should warrant

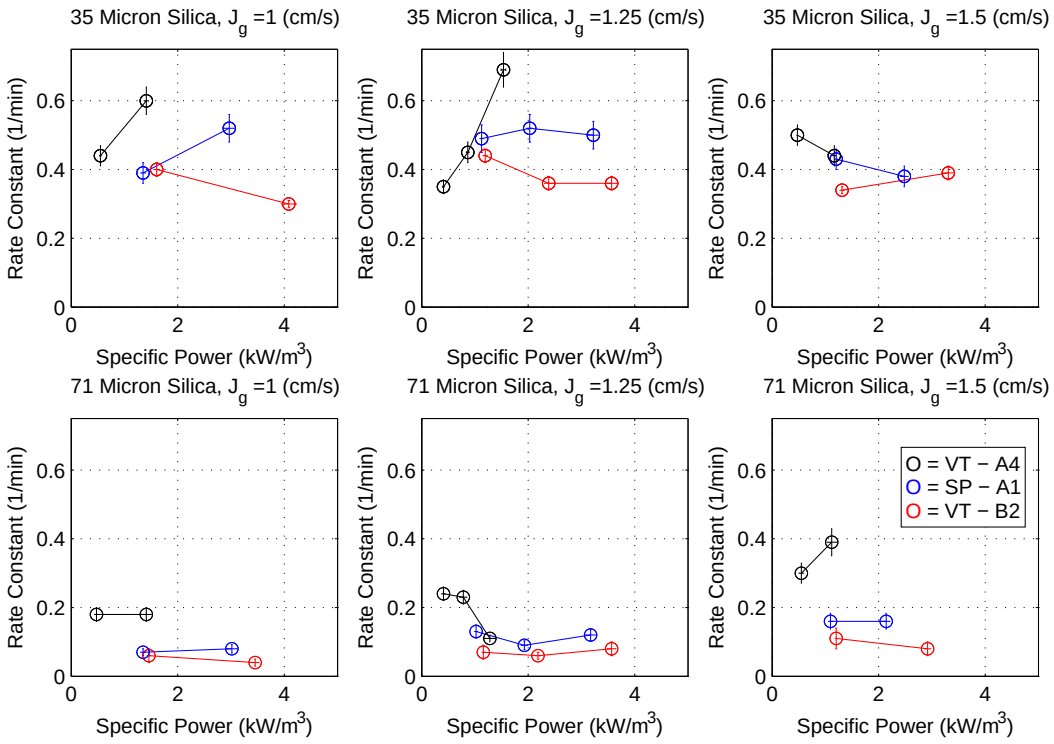

Figure 4.17: Flotation rate constant plotted against specific power for continuous flotation test. Columns represent air velocities of 1, 1.25, and 1.5 cm/s. Rows represent tests conducted with different materials: 35 and 71 micron monosized silica. Data shown for rotors included in detailed testing campaign. Uncertainty bars indicate one standard deviation as determined from the repeat center points.

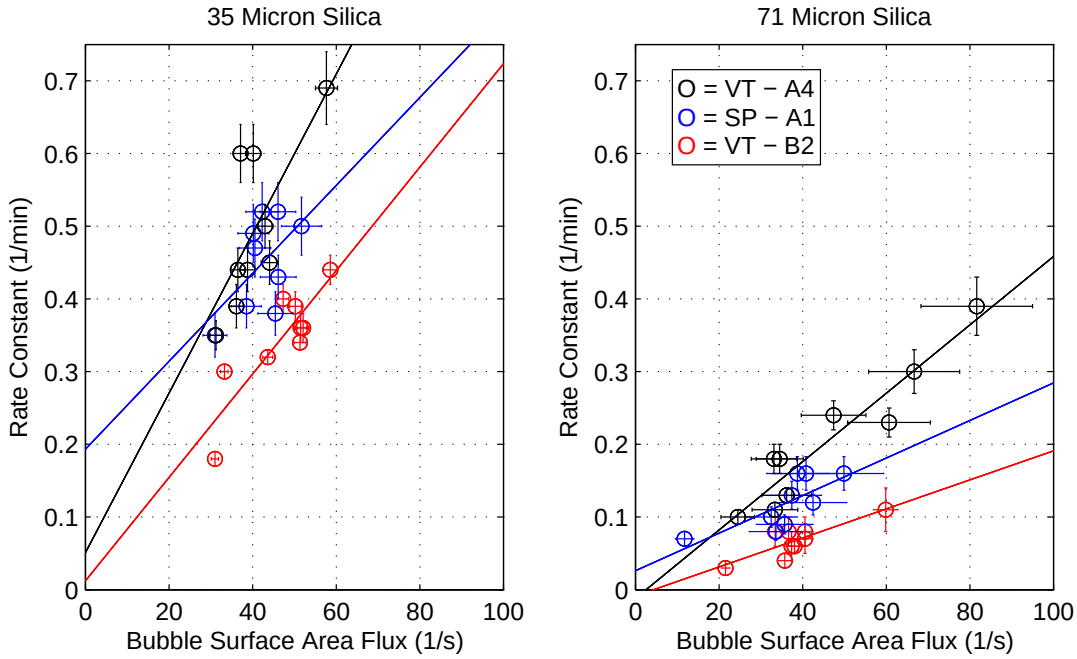

Figure 4.18: Flotation rate constant plotted against bubble surface area flux for continuous flotation test (rotors included in detailed testing campaign). Various air velocities. Solids = 35 and 71 micron monosized silica. Uncertainty bars indicate one relative standard deviation as determined from the repeat center points.

caution in determining conclusive results. For example, in the 35 micron silica data, most of the central points for each rotor reside around a common bubble surface area flux value. Consequently, the slope of the fitting line is then very sensitive to the few points at the extreme values. This phenomenon is also present in the SP - A1 and VT - B2 data for the 71 micron silica tests. Furthermore, given the scatter in the data, the varying slopes may be insignificant, since most of the data tends to fall in a narrow range and roughly around a single line. Depending on the scale that the data is presented at, the difference in slope values may or may not be as pronounced as depicted in Figure 4.18. In light of these cautions, the $k - S_b$ data should merely stand as another piece of evidence in the larger context of the overall rotor comparison conclusions.

As a supplementary analytical exercise, the air holdup measurements were qualitatively compared to the flotation rate data to test the hypothesis that air holdup is a suitable surrogate test for flotation performance. In this bulk comparison, the full data set of air holdup versus power data was holistically compared to the full data set of flotation rate constant versus power. In both data sets, the operational conditions (tip speed and air velocity) covered a similar range, with the range of the flotation data set falling completely within the range of the air holdup data set.

Figure 4.19 shows the air holdup data set for each rotor. These plots include data at all air velocities. To assist in visualizing the data sets, an "ellipse-of-best-fit" was superimposed on the plot. This ellipse was determined by an optimization routine which minimized the ellipse area while covering a designated percentage of the total points. In these cases, the target coverage was set to 75% of the data set. By this ellipse fit, the general locus of holdup as a function of power input for the test conditions is conveniently summarized. Figure 4.20 shows each ellipse on the same axis.

Figure 4.21 and Figure 4.22 show a similar analysis conducted for rate constant values determined from continuous flotation tests. Here the 35 and 71 micron tests are presented independently. Since these data sets contain significantly fewer points, the target coverage was set to 100% of the data set. Once again, the locus of values can be easily determined by the shape and orientation of the ellipse. Figure 4.21 shows the data points and ellipses for each rotor independently, and Figure 4.22 shows all ellipses on the same axes.

Visual comparison of Figure 4.20 and Figure 4.22 show that the same general trends exist for both air holdup and flotation rate constant for both particle sizes tested. In all three cases, the VT - A4 occupies the high measured value (holdup or rate constant) at low power inputs, while the SP - A1 shows moderate to high measured values at moderate power inputs. Finally, the VT - B2 generally shows low measured values at moderate to high

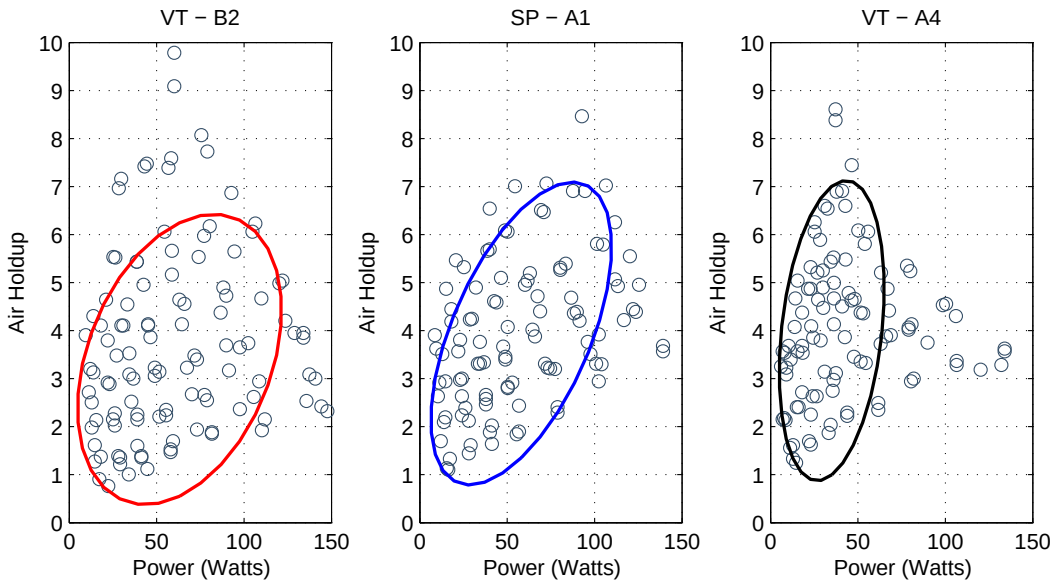

Figure 4.19: Air holdup plotted against power for each rotor included in the detailed testing. Data is presented for gas velocities ranging from 0.48 to 1.9 cm/s. Grey markers indicate the values of individual test points, and the red ellipse indicates the minimum-area locus which covers 75% of the test points. Tests were conducted in a 35.3 liter tank in the absence of solids and reagents. All rotors were 2.75 inches in diameter.

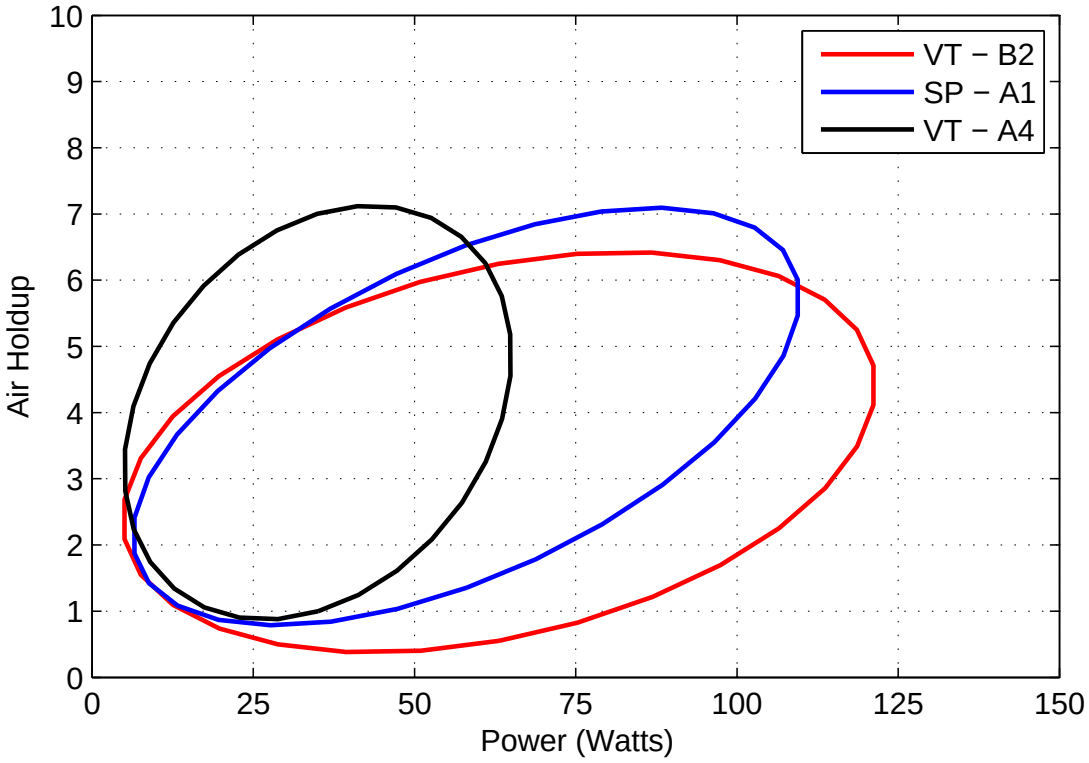

Figure 4.20: Air holdup plotted against power for all rotors included in the detailed testing. This plot compares the individual loci presented in Figure 4.19.

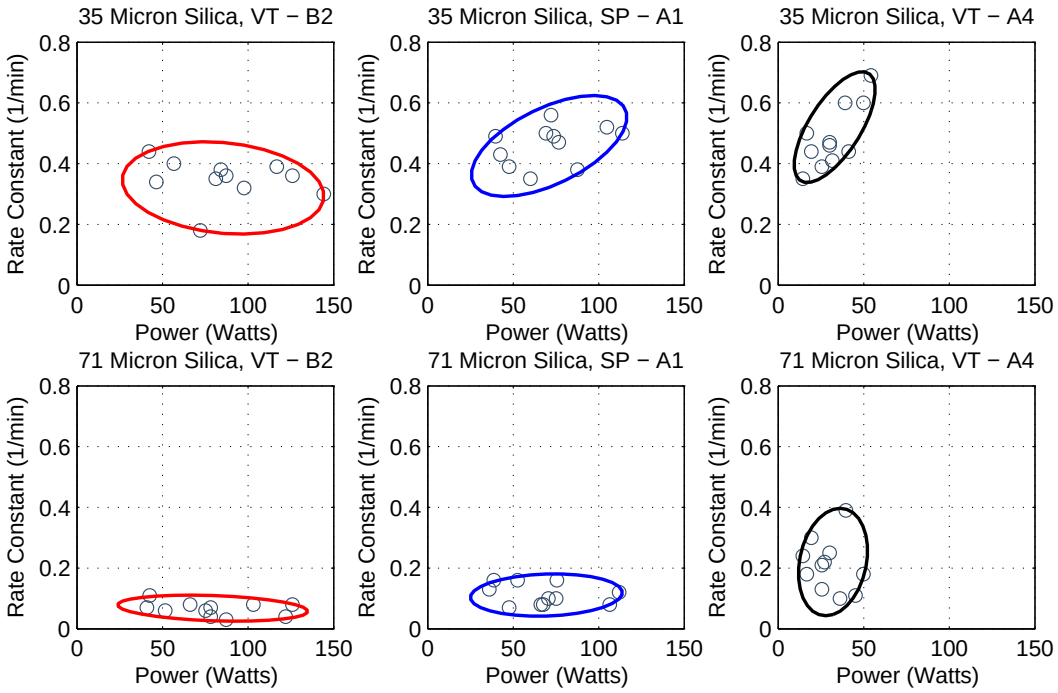

Figure 4.21: Flotation rate constant plotted against power for each rotor included in the detailed testing. Data is presented for 35 and 71 micron flotation tests. Grey markers indicate the values of individual test points, and the red ellipse indicates the minimum-area locus which covers 100% of the test points. Tests were conducted in a 35.3 liter tank in the absence of solids and reagents. All rotors were 2.75 inches in diameter.

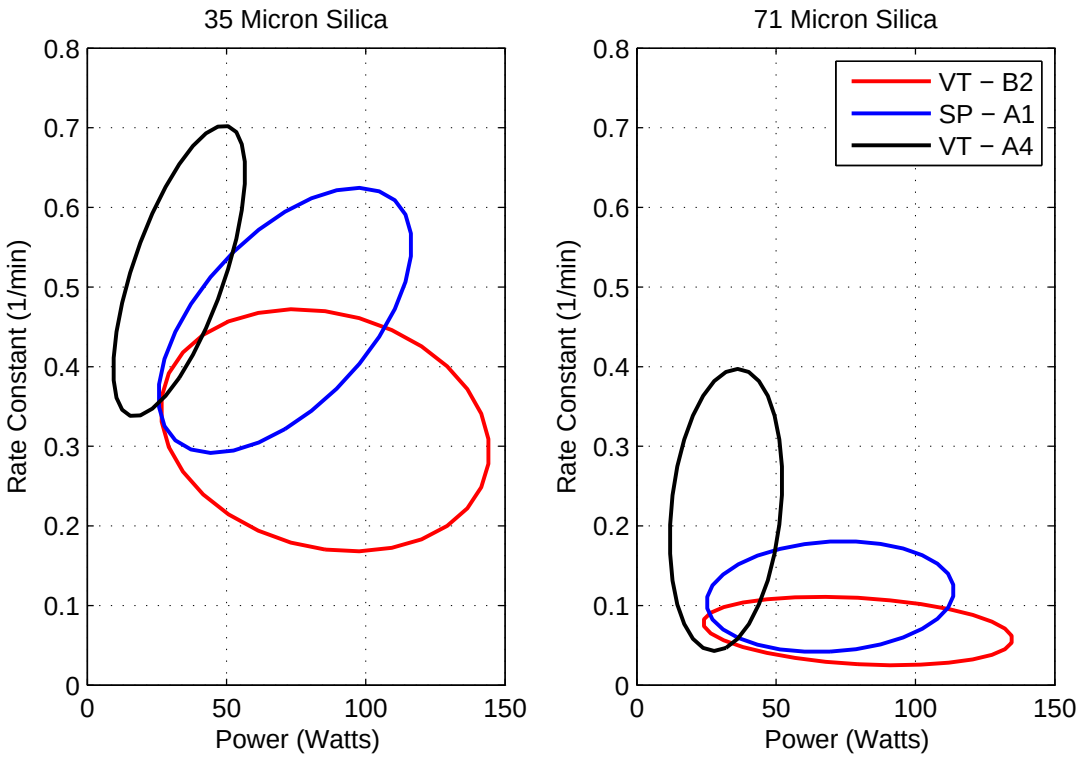

Figure 4.22: Flotation rate constant plotted against power for all rotors included in the detailed testing. This plot compares the individual loci presented in Figure 4.21.

power inputs. While this analysis certainly does not indicate a one-to-one relationship, the trends compare favorably, and similar results would be found if either test were presented independently.

4.3.5 Comparison of Batch and Continuous Data

Since this research has included batch and continuous flotation tests in similar experimental conditions, a single experiment was used to test the validity of the plug flow and perfectly mixed reactor models used to fit flotation rate constants. These experiments were performed with a single material (35 micron silica) under similar chemical conditions (15 g/t dodecylamine and 8.1 ppm MIBC). Figure 4.23 shows the experimental data and model fits for the kinetics tests. In this plot, the batch data was used to fit a fast and slow rate constant (and proportion), using a plug flow reactor model. These kinetic parameters and a perfectly mixed reactor model were then used to predict the flotation performance of the continuous unit. Since the tests were run at different air rates, an S_b adjustment factor was used to scale the rate constants between the tests.

While this single plot is not ultimately conclusive, it does indicate the predictive power of the perfectly mixed and plug flow reactor models as well as the substantial loss in flotation recovery in moving from a high S_b batch machine to a lower S_b continuous machine.

4.4 Summary and Conclusions

Laboratory-scale tests were performed to assess the operational capabilities of various rotors in four performance areas: power consumption, air holdup, operational robustness, and flotation performance. In total, the VT - A4, VT - B2, and SP - A1 were subjected to detailed laboratory experiments and numerous modes of analysis. In forming a more concise evaluation, both quantitative and qualitative evaluation matrices was generated (Table 4.8 and Table 4.9).

These tables summarize the data in this chapter by integrating at least one indicative measurement from the evaluation of each of the four performance criteria. These measurements include: average power number, interpolation from the holdup versus power graph, flooding test area of operation, sanding test area of operation, interpolation from the rate constant versus power graph, and average P. The presented measurements were selected for this summary since they efficiently convey the most useful data, retain the general conclu-

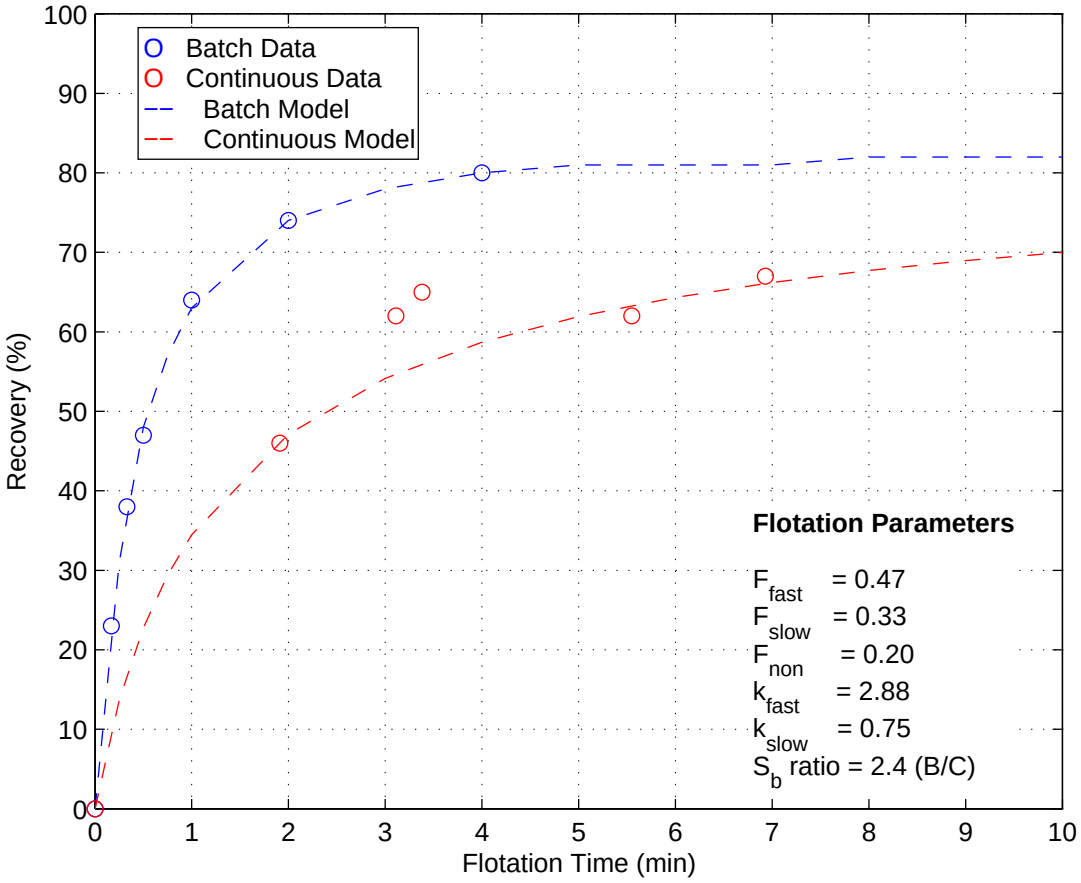

Figure 4.23: Comparison of data collected from batch and continuous testing. Batch test was fit by data regression and used to predict continuous model. Parameters of the model fit are shown.

Table 4.8: Summary of Selected Detailed Testing Results - Raw Data

Parameter	**SP - A1**	**VT - A4**	**VT - B2**
Power Number	4.63	3.93	4.86
Power (W) to achieve 3.5% Holdup $J_g = 0.95$ cm/s	44.3	11.8	78.0
Flooding Area of Operation	6.83	5.44	7.26
Sanding Area of Operation	2.45	2.36	4.22
k **(1/min)** $J_g = 1.25$ cm/s 35 micron silica Power=1.5 kW/m^3	0.5	0.68	0.42
Average P **(x10^{-3})** 71 micron silica	2.59	4.70	2.00

sions found in the full data set, and generally preserve the paradigm of power-normalization as a basis for a fair comparison. Table 4.9 provides another level of simplification by providing ordinal rankings for each evaluation parameter.

From the data set collected during the detailed testing campaign, six key conclusions are ascertained:

1. The results of the detailed testing campaign generally bolster those of the exploratory campaign. The modes of analysis of the four operating criteria have provided consistent comparisons. Furthermore, using the SP - A1 as the benchmark, both prototype rotors showed strengths and weaknesses in the various criteria.

2. The degree of uncertainty for several measurements has been quantified by replicate testing. In general, the measured performance differences exceed the uncertainty.

3. In terms of power draw, air dispersion, flotation energy efficiency, and flotation hydrodynamic efficiency, the VT - A4 substantially outperforms its counterparts. Similar results were first presented in the exploratory testing, and further support has been provided in the detailed testing. Much of this rotors strength lies in its ability to operate

Table 4.9: Summary of Selected Detailed Testing Results - Comparative Analysis

Parameter	**SP - A1**	**VT - A4**	**VT - B2**
Power Number	◐	●	○
Power (W) to achiever 3.5% Holdup $J_g = 0.95$ cm/s	◐	●	○
Flooding Area of Operation	◐	○	●
Sanding Area of Operation	◐	○	●
k **(1/min)** $J_g = 1.25$ cm/s; 35 micron silica; Power=1.5 kW/m^3]	◐	●	○
Average P **(x10^{-3})** [71 micron silica]	◐	●	○

●= First; ◐= Second; ○= Third

at high tip speeds while drawing low power. Furthermore, the drastic phenomenological difference in power reduction and gas dispersion (Figure 5.9) may provide insight on the operational advantages present in this rotor.

4. In terms of flooding limit, solid suspension, and overall area of stable operation, the VT - B2 substantially outperforms its counterparts. This rotor is capable of suspending solids at a relatively low power draw, and this suspension capacity is not as sensitive to air addition as the other rotors. The two additional blades of the VT - B2 provide additional area for gas dispersion. This mechanical feature necessitates an increased power number, but it also provided additional capacity to overcome the flooding condition.

5. Bulk comparisons of the air holdup versus power data and the rate constant versus power data show strikingly similar trends. While a one-to-one correlation is not necessarily suggested, the same results are determined from test. Theoretically, this result is justified since air holdup is related to the available surface area which is related to flotation performance.

6. Factors such as S_b and other dimensionless parameters (Reynolds number, Power Number, and Aeration Number) are capable of producing consistent relationships to performance criteria for each rotor. The magnitude of the laboratory values generally match those reported for industrial machines. The continued use of these values in scaling studies is recommended.

4.5 Bibliography

Banisi, S., & Finch, J. (1994). Technical note reconciliation of bubble size estimation methods using drift flux analysis. *Minerals Engineering*, *7*(12), 1555–1559.

Fitzgibbon, A., Pilu, M., & Fisher, R. (1999). Direct least square fitting of ellipses. *Pattern Analysis and Machine Intelligence, IEEE Transactions on*, *21*(5), 476–480.

Hernandez-Aguilar, J., Gomez, C., & Finch, J. (2002). A technique for the direct measurement of bubble size distributions in industrial flotation cells. In *Proceedings of the 34th annual meeting of the canadian mineral processors* (pp. 389–402).

Silva, R., Echeverri, L., Olson, T., Foreman, D., Yang, Y., & Caldwell, K. (2012). The effect of laboratory cell design on flotation machine hydrodynamics, solid suspension and particle recovery. In *2012 sme annual meeting and exhibit preprints* (pp. 452–457). SME.

Chapter 5

Conclusions and Recommendations

The primary objective of this research was to characterize and compare small-scale flotation rotors while developing scaling relationships and future design criteria. In order to complete this task, several experimental setups were initially constructed to measure various flotation performance parameters. In choosing the appropriate parameters to measure, theoretical factors, practical limitations, and industrial experience were equally acknowledged. As a result, most testing focused on four distinct evaluation criteria: power draw, gas dispersion, operational robustness, and flotation performance. The measurement and analytical approach to these criteria needed to provide reliable data which retains significance as the rotors are scaled to the industrial size. Furthermore, the data must provide a basis for fair comparison among the alternative rotor designs, and the experimental techniques must coincide with the expected paradigms and costs of a typical flotation laboratory.

This report extensively described the experimental techniques used to evaluate the four performance criteria. The theoretical background was first established, and the required equipment and analytical means were explained. When applicable, measurements were normalized by or compared against power input. In the laboratory setting, power input is the most easily determined cost associated with flotation equipment, and this measurement may be scaled to the full-size by dimensionless relationships. Furthermore, when comparing alternative rotors, differences in power draw measured at the laboratory scale will retain relative relationships as the scale is increased (although the absolute magnitude of the difference may radically change).

Testing for this project task was primarily conducted in two campaigns. The original, exploratory campaign focused on the analysis of 14 rotors in a select range of operating conditions. The second, detailed campaign included on a more rigorous analysis of three

select rotors in several operating conditions. All tests were performed with 2.75 inch diameter rotors in tanks 10 and 14 inch diameter tanks (9 - 35 liters). The goals of the exploratory campaign were to establish and refine the experimental procedures, verify the existence of performance difference between rotors, and narrow the field of potentially viable prototypes by eliminating underperforming or "fatally-flawed" alternatives. From this campaign, the SP - A1, VT - A4, and VT - B2 were selected for further experimentation. The goals of the detailed campaign were to implement standard modes of evaluation and analysis, examine uncertainty and repeatability in the measurements, thoroughly characterize the remaining rotor prototypes, and establish insight on the causes of performance differences.

Following the successful completion of both laboratory campaigns, the following observations and design criteria are derived:

1. Given the strengths of the VT - A4 in the areas of power-normalized gas dispersion and flotation performance, flotation systems desiring these characteristics should design rotors to exhibit low inherent power numbers and operate near the boiling condition (see Figure 4.3, Figure 4.12, Table 4.6, and Figure 4.22. Unfortunately, these attributes general realize a reduction in operational robustness, especially with regard to the sanding condition (see Figure 4.15, and Figure 4.16).

2. Alternatively, the strengths of the VT - B2 rotor in the areas of operational robustness should entice high power numbers and operational away from the boiling condition with solid suspension is problematic (see Figure 4.3, Figure 4.14, Figure 4.15, and Figure 4.16).

3. Given the measured linear relationship between k and S_b, rotors desiring high flotation rates should seek to maximize S_b (see Figure 3.13, Figure 3.14, and Figure 4.18).

4. Plots showing global air holdup plotted against power show striking general similarity to plots showing flotation rate constant plotted against power. Consequently, air holdup can be used as an acceptably surrogate to flotation testing when comparing machine designs (see Figure 4.20 and Figure 4.22).

5. Care should be taken when comparing batch and continuous data. S_b ratios should be used to scale the measured flotation rates, and appropriate plug-flow or perfectly-mixed models should be selected. Note that in order to achieve the same recovery up to a seven-fold increase may be necessary in residence time when changing from batch to a continuous reactor (see Figure 4.23, compare residence time at 65% recovery).

Finally, the author of this thesis recommends the following three topics for further and continued study:

1. Additional quantification of scale factors and verification of lab-scale to full-scale applicability. While the tested rotors consistently show variations in performance criteria on the lab scale, the absolute magnitude of these differences is not expected to remain proportional as the scale is increased. Testing and characterization at the larger scales may assist in identifying scale-factor which can reliably predict the magnitude of these differences as the scale is increased.

2. Larger scale implementation of the prototype rotors. Given the strengths each rotor has consistently manifested at the laboratory scale, further development and implementation at a larger scale is recommended.

3. Additional refinement of laboratory testing and analytical techniques. While the methods described in this report have fulfilled the goals of obtaining a fair and consistent basis of comparison between the rotor alternatives, further development and revision may provide additional insight to the fundamental difference between each rotor. Also, by incorporating automation (level controls, air holdup measurements, solid suspension determination), the degree of testing reliability and reproducibility will be enhanced.